UNIVERSITY OF OKLAHOMA

GRADUATE COLLEGE

INTERACTIONS OF NITRIC OXIDE AND NITROSAMINES WITH GROUP 8 METALLOPORPHYRINS

A DISSERTATION

SUBMITTED TO THE GRADUATE FACULTY

in partial fulfillment of the requirements for the

degree of

Doctor of Philosophy

By
NAN XU
Norman, Oklahoma
2007

Downloaded from SHAREOK. Persistent Handle URL: https://hdl.handle.net/11244/1314

UMI Number: 3294671



UMI Microform 3294671

Copyright 2008 by ProQuest Information and Learning Company.
All rights reserved. This microform edition is protected against unauthorized copying under Title 17, United States Code.

ProQuest Information and Learning Company
300 North Zeeb Road
P.O. Box 1346
Ann Arbor, MI 48106-1346

INTERACTIONS OF NITRIC OXIDE AND NITROSAMINES WITH GROUP 8 METALLOPORPHYRINS

A DISSERTATION APPROVED FOR THE
DEPARTMENT OF CHEMISTRY AND BIOCHEMISTRY

BY

_____
George B. Richter-Addo

_____
Robert P. Houser

_____
David P. Nagle, Jr.

_____
Ralph A. Wheeler

_____
Richard W. Taylor

© Copyright by NAN XU 2007
All Rights Reserved.

Acknowledgments

Firstly, I would like to express my tremendous gratitude to my research advisor, Dr. George B. Richter–Addo. Without his guidance, support, encouragement, and patience I would never have finished my Ph.D. studies at OU. I would also like to thank Drs. David Nagle, Robert Houser, Ralph Wheeler, Richard Taylor, and Rudolf (Rudi) Wehmschulte for serving as my advisory committee members. I have greatly benefited from your friendly help and guidance. Special thanks to Drs. Douglas Powell and Masood Khan for providing X-ray crystallographic analyses on my many compounds.

I would like to thank all my coworkers present and past in Dr. Richter–Addo's group: Dr. Jonghyuk Lee, Dr. Shawn Carter, Myron Jones, Zaki Zahran, Yi Jun, Adam Warhausen, Christal Sohl, Dr. Lillian Chooback, Dr. Daniel Copeland and Carolina Salazar. I would also like to thank other fellow Inorganic Division graduate students: Lei Yang, Ruibo Li, Jason Wickham, Bheki Xulu (Alex), Tim Dowd, Garry Chapman, Zhaodong Wang, and Penghe Qiu.

I appreciate the financial support provided by the Department of Chemistry and Biochemistry at OU. In addition, I would like to thank the National Institutes of Health (NIH) and National Science Foundation (NSF) for the funding which made the completion of this dissertation possible.

I would like to thank my parents and my sister for their love and support during my graduate study. Finally, I would like to dedicate this dissertation to my lovely wife, Jian Huang for her love, support, and sacrifices made to help me to complete this dissertation. I am so lucky to have you in my life.

Table of Contents

		Page
List of Tables		vii
List of Figures		ix
Abstract		xii
Chapter 1	Introduction	1
	My thesis research	7
	References	11
Chapter 2	Synthesis, characterization, and redox behavior of six-coordinate (por)Ru(NO)Cl compounds	
	Introduction	14
	Experimental section	16
	Results and discussion	20
	Synthesis and structural characterization	20
	Electrochemistry	26
	Conclusion	32
	References	32
Chapter 3	Synthesis and characterization of organometallic nitrosyl complexes of ruthenium porphyrins	
	Introduction	34
	Experimental section	36
	Results and discussion	41
	Synthesis and characterization	41
	Molecular structure	45
	Cyclic voltammetry and infrared spectroelectrochemistry	54
	Conclusion	59
	References	60

Chapter 4	Interactions of nitrosamines with iron porphyrins	
	Introduction	63
	Experimental section	66
	Results and discussion	70
	Synthesis and characterization	70
	Molecular structures	76
	Conclusion	82
	References	83
Chapter 5	Synthesis, characterization, and structures of nitrosyl heme (III) model complexes for thiolate and alkoxide heme proteins	
	Introduction	86
	Experimental section	90
	Results and discussion	100
	Conclusion	122
	References	123

List of Tables

		Page
Table 2.1	Infrared nitrosyl stretching frequencies of (por)Ru(NO)X and (por)Ru(NO)(O-*i*-C_5H_{11}) (por = TPP, TTP, OEP, T(*p*-OMe)PP, T(*p*-CF_3)PP; X =Cl, Br).	23
Table 2.2	Selected bond lengths (Å) and angles (°) for (OEP)Ru(NO)Cl.	25
Table 2.3	Formal potentials for oxidations of (por)Ru-(NO)Cl in CH_2Cl_2, 0.1 M NBu_4PF_6.	29
Table 3.1	Infrared nitrosyl stretching frequencies of selected nitrosyl organoruthenium porphyrins and their precursors.	43
Table 3.2	Selected bond lengths (Å) and angles (°) for (T(*p*-OMe)PP)Ru(NO)Et.	47
Table 3.3	Axial ligand tilts (°) in organometallic porphyrins (por)M(NO)R, (por)M(R) and (por)M$(R)_2$.	49
Table 3.4	Ru-N(nitrosyl) bond lengths in nitrosyl ruthenium porphyrin compounds.	52
Table 3.5	Ru-C bond lengths in ruthenium porphyrin compounds with axial alkyl/aryl (non-carbonyl) ligands.	53
Table 3.6	Half-wave and anodic potentials in volts for the first oxidations of selected six-coordinate nitrosyl ruthenium porphyrins vs Ag/AgCl in CH_2Cl_2, 0.1 M NBu_4PF_6.	58
Table 4.1	IR data for ν_{NO} and ν_{NN} in nitrosamine iron porphyrin complexes.	72
Table 4.2	Selected bond lengths (Å), angles (°) and torsion angles (°) for nitrosamine metal complexes.	80

Table 5.1	Bond angles for Ru(Os)-N-O (°) in six-coordinate nitrosyl thiolate metalloporphyrins.	88
Table 5.2	Infrared spectral data for six-coordinate nitrosyl thiolate iron porphyrins.	106
Table 5.3	Selected structural data (in Å and °) for (OEP)Fe[S-2,6-$(CF_3CONH)_2C_6H_3$] (**1)** and (OEP)Fe(NO)[S-2,6-$(CF_3CONH)_2C_6H_3$] (**6)**.	110
Table 5.4	Selected structural data (in Å and °) for (TPC)Fe-($OCOCF_3$) **(5)** and (TPC)Fe(NO)($OCOCF_3$) **(10)**.	114

List of Figures

		Page
Figure 1.1	Synthetic metalloporphyrins and -chlorins.	5
Figure 1.2	Four binding modes of monometallic nitrosyl compounds.	6
Figure 1.3	Molecular structure of the cation of $[(TPP)Fe(Et_2NNO)_2]^+ClO_4^-$.	9
Figure 2.1	(a) Molecular structure of (OEP)Ru(NO)Cl. Hydrogen atoms have been omitted for clarity. (b) Perpendicular atom displacements (in units of 0.01 Å) of the porphyrin core from the 24-atom mean porphyrin plane.	24
Figure 2.2	Cyclic voltammograms of the (por)Ru(NO)Cl compounds in CH_2Cl_2 containing 0.1 M NBu_4PF_6 and at a scan rate of 200 mV/s. The solubility of (TPP)Ru(NO)Cl in CH_2Cl_2 is very low relative to the other compounds.	27
Figure 2.3	Plot of E°' vs the Hammett substituent constants for the first oxidation of (por)Ru(NO)Cl in CH_2Cl_2. Half-wave potentials are listed in Table 2.3.	30
Figure 3.1	(a) Molecular structure of (T(*p*-OMe)PP)Ru(NO)Et. Hydrogen atoms have been omitted for clarity. (b) Perpendicular atom displacements (in units of 0.01 Å) of the porphyrin core from the 24-atom mean porphyrin plane.	46
Figure 3.2	Crystal packing diagram of (T(*p*-OMe)PP)Ru(NO)Et showing the closest intermolecular distance involving the NO group. Most parts of the porphyrin molecule B have been omitted for clarity. Closest intermolecular contacts in Å: O1···O2A = 3.47, O1···C23A = 3.59, N5···C41B = 3.51.	48
Figure 3.3	Tilting and bending nitrosyl conformation on the right has better bonding interaction between the NO π* orbital and metal (mixed) orbital than tilting and linear conformation on the left in the model (porphine)Fe(NO)(*p*-C_6H_4F). (Reference 28)	50

Figure 3.4	Cyclic voltammograms of (T(*p*-OMe)PP)Ru(NO)Me and (T(*p*-OMe)PP)Ru(NO)Et in CH_2Cl_2 containing 0.1 M NBu_4PF_6 and at a scan rate of 200 mV/s. Potentials are referenced to the Ag/AgCl couple. (a) Complete cyclic voltammogram of (T(*p*-OMe)PP)Ru(NO)Me. (b) Complete cyclic voltammogram of (T(*p*-OMe)PP)Ru(NO)Et. (c) Partial cyclic voltammogram of (T(*p*-OMe)PP)Ru(NO)Et showing only the first oxidation.	54
Figure 3.5	Difference FTIR spectra after controlled-potential oxidation of (a) (T(*p*-OMe)PP)Ru(NO)Me and (b) (T(*p*-OMe)PP)Ru(NO)Et.	56
Figure 4.1	Proposed interactions of nitrosamine with the heme site of cytochrome P450.	64
Figure 4.2	Four binding modes in metal-nitrosamine complexes.	65
Figure 4.3	Resonance structures of nitrosamines.	71
Figure 4.4	Structural diagrams of alkyl nitrites, alkyl thionitrites, Diazald and NONOate compounds.	76
Figure 4.5	Molecular structure of the cation of $[(TPP)Fe(Me_2NNO)_2]^+ ClO_4^-$.	77
Figure 4.6	Molecular structure of the cation of $[(TPP)Fe((PhCH_2)_2NNO)_2]^+ClO_4^-$.	78
Figure 4.7	Molecular structure of the cation of $[(TPP)Fe((cyclo\text{-}CH_2)_4NNO)_2]^+ClO_4^-$.	79
Figure 4.8	Molecular structure of the cation of $[(TPP)Fe((cyclo\text{-}CH_2)_5NNO)_2]^+ClO_4^-$.	79
Figure 5.1	Proposed mechanism for the nitrosation of heme and axial thiolate in P450.	87
Figure 5.2	Structural diagrams of porphine and chlorin.	90
Figure 5.3	Synthesis of bis[2,6-bis(trifluoroacetylamino)phenyl]-disulfide.	101
Figure 5.4	Structural diagrams of compounds **1-10**.	103

Figure 5.5	Infrared spectral monitoring of the reaction of **1** with NO in CH_2Cl_2; Intervals are 0 s, 10 s, 20 s, 35 s, 60 s, and 120 s.	105
Figure 5.6	Structural diagram of $SR(Fe^{III})$-NO (R = $NHCOC(CH_3)_3$).	107
Figure 5.7	Molecular structure of (OEP)Fe[S-2,6-$(CF_3CONH)_2C_6H_3$] **(1)**.	108
Figure 5.8	Molecular structure of (OEP)Fe(NO)[S-2,6-$(CF_3CONH)_2C_6H_3$] **(6)**.	109
Figure 5.9	Molecular structure of (TPC)Fe($OCOCF_3$) **(5)**.	111
Figure 5.10	Molecular structure of (TPC)Fe(NO)($OCOCF_3$) **(10)**.	113
Figure 5.11	Selected bond angles and tilting angles of (OEP)Fe(NO)[S-2,6-$(CF_3CONH)_2C_6H_3$] **(6)**, and (TPC)Fe(NO)($OCOCF_3$) **(10)**.	115
Figure 5.12	Perpendicular atom displacements (in units of 0.01 Å) of the porphyrin core from the 24-atom mean porphyrin planes of (a) (OEP)Fe[S-2,6-$(CF_3CONH)_2C_6H_3$] **(1)** and (b) (OEP)Fe(NO)[S-2,6-$(CF_3CONH)_2C_6H_3$] **(6)**.	116
Figure 5.13	Perpendicular atom displacements (in units of 0.01 Å) of the porphyrin core from the 24-atom mean porphyrin planes of (a) (TPC)Fe($OCOCF_3$) **(5)** and (b) (TPC)Fe(NO)-($OCOCF_3$) **(10)**.	116
Figure 5.14	(a) Side view and (b) top view of two neighboring porphyrin molecules of **1** in a unit cell. The thiolate ligands in the two molecules have been omitted for clarity in the bottom figure.	119
Figure 5.15	(a) Side view and (b) top view of two neighboring porphyrin molecules of **2** in a unit cell. The thiolate ligands in the two molecules have been omitted for clarity in the bottom figure.	120

Abstract

This dissertation describes the interactions of nitric oxide and nitrosamines with group 8 metalloporphyrins.

Chapter 1 of this dissertation introduces the importance of nitric oxide in biological systems.

Chapter 2 describes the syntheses of the (por)Ru(NO)X complexes (por = TPP, TTP, T(*p*-OMe)PP, T(*p*-CF_3)PP, OEP; X = Cl, Br) from the reaction of corresponding (por)Ru(NO)(OR) precursors with boron trichloride or tribromide. These nitrosyl halide derivatives were characterized by IR and ^{1}H NMR spectroscopy, and ESI mass spectrometry. The IR spectrum of electron rich octaethyl *β*-substituted porphyrin (OEP)Ru(NO)Cl shows the nitrosyl stretch at 1842 cm^{-1} in CH_2Cl_2 which is significantly lower than those of other aryl *meso*-substituted porphyrin derivatives (TTP, T(*p*-OMe)PP, T(*p*-CF_3)PP). This is due to the stronger metal-nitrosyl π back-bonding in the OEP derivative. A crystal structure of (OEP)Ru(NO)Cl was obtained and exhibits a linear Ru-NO geometry. The redox behavior of the (por)Ru(NO)Cl compounds has been determined by cyclic voltammetry. Analysis of the electrochemical data reveals that the first oxidations of the (por)Ru(NO)Cl compounds are porphyrin-ring centered.

Chapter 3 describes the syntheses of new nitrosyl organoruthenium porphyrin complexes (T(*p*-X)PP)Ru(NO)R (X = OMe, CF_3; R = Me, Et) by the reactions of their nitrosyl chloro precursors with alkylating agents $Al(R)_3$ and RMgBr. These (T(*p*-X)PP)Ru(NO)R complexes were characterized by elemental analyses, IR and ^{1}H NMR spectroscopy. The ν_{NO} of these nitrosyl organoruthenium complexes and their chloro

precursors support the increasing electron donating ability of chloro < aryl < alkyl groups. The (T(*p*-OMe)PP)Ru(OS(O)Me) compound was obtained by the reaction of SO_2 with (T(*p*-OMe)PP)Ru(NO)Me. Judging by the lack of reaction between SO_2 and (T(*p*-OMe)PP)Ru(Me)$_2$, we believe that the nitrosyl group in the (T(*p*-OMe)PP)Ru(NO)Me imparts a strong *trans* effect on the ruthenium-carbon bond in (T(*p*-OMe)PP)Ru(NO)Me weakening the metal-carbon bond. The solid-state structure of (T(*p*-OMe)PP)Ru(NO)Et was obtained. An unusual bent ruthenium-nitrosyl linkage with the angle of 153.0(3)º was observed. The structure reported here is the first organometallic nitrosyl porphyrin with an alkyl group as the axial ligand. The redox behavior of (T(*p*-OMe)PP)Ru(NO)R (R = Me, Et) has also been examined by cyclic voltammetry and infrared spectroelectrochemistry. Both of the (T(*p*-OMe)PP)Ru(NO)R compounds display a chemically and electrochemically reversible first oxidation. Infrared spectroelectrochemistry studies indicate a porphyrin-centered first oxidation for both (T(*p*-OMe)PP)Ru(NO)Et and (T(*p*-OMe)PP)Ru(NO)Me.

Chapter 4 describes the syntheses of new bis-nitrosamine iron porphyrin complexes via the reactions of precursor [(por)Fe(THF)$_2$](ClO$_4$) with nitrosamines (Me_2NNO, Et_2NNO, (*cyclo*-CH_2)$_4$NNO, (*cyclo*-CH_2)$_5$NNO, ($PhCH_2$)$_2$NNO). These iron nitrosamine complexes have been characterized by Infrared spectroscopy and X-ray structure determination. Interestingly, a sole η^1-O binding mode for nitrosamine iron(III) complexes has been determined by single-crystal X-ray crystallography. In addition, the interactions of three aryl nitrosamines (Ph_2NNO, PhMeNNO, PhEtNNO) with four-coordinate iron(II) porphyrin compound resulted in five-coordinate nitrosyl iron porphyrins and the corresponding amines.

Chapter 5 describes the syntheses of a series of iron porphyrin/chlorin complexes containing axial *S*-bound and *O*-bound ligands *trans* to nitric oxide using a unique heterogenous solid-gas method which allows the NO gas to diffuse into the crystals and coordinate to the iron center in a solvent-free environment. This method overcomes synthetic difficulties of $\{FeNO\}^6$ complexes such as the lability of the Fe-NO linkage, the easy reduction of $\{FeNO\}^6$ complexes and fast decomposition in organic solvents. This new method could be used in preparations and structure determinations of many other previously inaccessible complexes. Solid-state structures were obtained for the six-coordinate (OEP)Fe(NO)[S-2,6-$(CF_3CONH)_2C_6H_3$] and (TPC)Fe(NO)($OCOCF_3$) compounds. Interestingly, the (OEP)Fe(NO)[S-2,6-$(CF_3CONH)_2C_6H_3$] compound displays an unusual bent metal-nitrosyl linkage (159.6(8)°), while the (TPC)Fe(NO)($OCOCF_3$) compound exhibit the typical linear metal-nitrosyl linkage of $\{FeNO\}^6$ complexes. No significant *trans* effect of NO was observed in (OEP)Fe(NO)[S-2,6-$(CF_3CONH)_2C_6H_3$] based on the Fe-S bond length change from the five-coordinate precursor to the six-coordinate nitrosyl compounds. In the case of (TPC)Fe(NO)($OCOCF_3$), a small *trans* effect of NO was observed. Additionally, both of the Fe atoms in these two-phase reactions were pulled upwards to nitrosyl groups with remarkable movements of ~0.46 Å and ~0.55 Å in solid state respectively. The structure of (OEP)Fe(NO)[S-2,6-$(CF_3CONH)_2C_6H_3$] is the first reported structure of model complexes of nitrosyl cysteinate heme proteins. The bent FeNO geometry in (OEP)Fe(NO)[S-2,6-$(CF_3CONH)_2C_6H_3$] suggests that the bending of the NO group may be a common feature in the NO adducts of ferric heme thiolate proteins. The (TPC)Fe(NO)($OCOCF_3$) compound is also the first

structurally characterized neutral model complex of nitrosyl tyrosinate heme proteins. The structure displays a typical linear Fe-NO linkage of $\{FeNO\}^6$ complexes.

Chapter 1. Introduction

Nitric oxide (NO) is a simple diatomic radical. It was first recognized as an atmospheric pollutant.[1] More recently, it was discovered as a crucial physiological signaling molecule, playing key roles in vascular regulation[2,3], the immune defense system[4,5], and in the central and peripheral nervous systems[6]. These important physiological functions result from the interaction of NO with various heme-containing proteins.

Nitric oxide is produced by a heme-containing enzyme called nitric oxide synthase (NOS). NOS catalyzes the oxidation of L-arginine to NO and citrulline (Eq. 1.1).[7] When NO reacts with ferrous NOS, the formation of the resulting NOS-NO

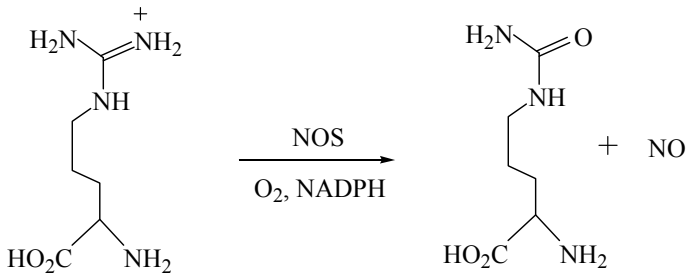

L-arginine citrulline (1.1)

adduct inhibits the catalytic activity of NOS.[8] Protein crystal structures of NOS derivatives with an Fe-NO moiety have been obtained, showing bent conformations of both ferrous-NO and ferric-NO moieties with the angles ranging from 126°-160° and 101°-161°, respectively.[9,10] However, these FeNO derivatives also contain bound

substrates in the protein distal pocket. NO interacts with other heme-thiolate proteins and heme-alkoxide proteins such as cytochrome P450 and catalase, inhibiting the function of the enzymes.[11-15] However, no protein crystal structures of cytochrome P450-NO and catalase-NO have been reported. NO also binds to imidazole-ligated heme proteins. For example, ferric-NO adducts occur in the salivary glands of blood-sucking insects, and NO can be either stored in the bug's salivary glands or released in their victim's tissue under altered pH conditions.[16,17] Additionally, the protein crystal structures of the NO adducts of cyt cd_1 nitrite reductase from *Thiosphaera pantotropha* and *Pseudomonas aeruginosa* reveal bent Fe-NO angles of 131° and 135° respectively, and the bending FeNO geometry has been proposed to result from the interaction of the amino acids in distal pocket of the protein and the NO ligand.[18,19]

Interactions of organic substrates with heme proteins are also very important. For example, reactions of phenylhydrazine ($PhNHNH_2$) with hemoglobin, myoglobin, and cytochrome P450 result in the formation of σ-bonded aryl-iron(III) porphyrin species (Eq. 1.2) and the subsequent aryl group migration from the iron to the porphyrin nitrogen atoms inactivates these hemeproteins.[20-24] Additionally, an unstable σ-bonded alkyl-iron(III) complex was proposed during the metabolism of alkylhydrazines by cytochrome P450 (Eq. 1.2).[25-27] In addition, carcinogenic nitrosamine compounds

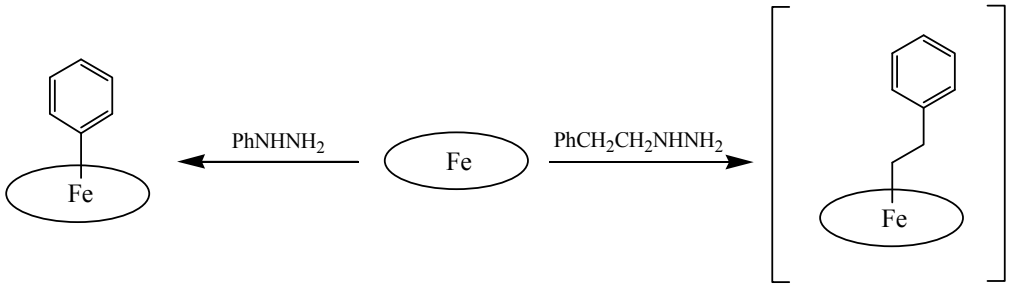

(1.2)

require metabolic activation by cytochrome P450 to exert their physiological effects.[28,29] Nitrosamines (*N*-nitroso compounds) are one of the four main types of organic nitroso compounds and they can be written in two main forms (Eq. 1.3).[30] The form B

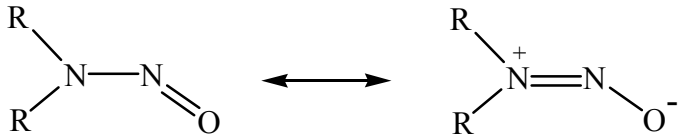

(1.3)

A B

represents the commonly used 1,3-dipolar contribution with a formal N=N double bond. Oxidative dealkylation and reductive denitrosation are the two major pathways for the metabolic activation of nitrosamines (Scheme 1.1).[31,32] Oxidative dealkylation begins with the P450-catalyzed hydroxylation of the α-carbon, resulting eventually in the production of an aldehyde and an alkyldiazonium ion which could then alkylate DNA. Reductive denitrosation produces nitric oxide and a secondary amine which may represent a detoxification process. Both metabolic pathways are initiated by the interactions of nitrosamines with cytochrome P450.

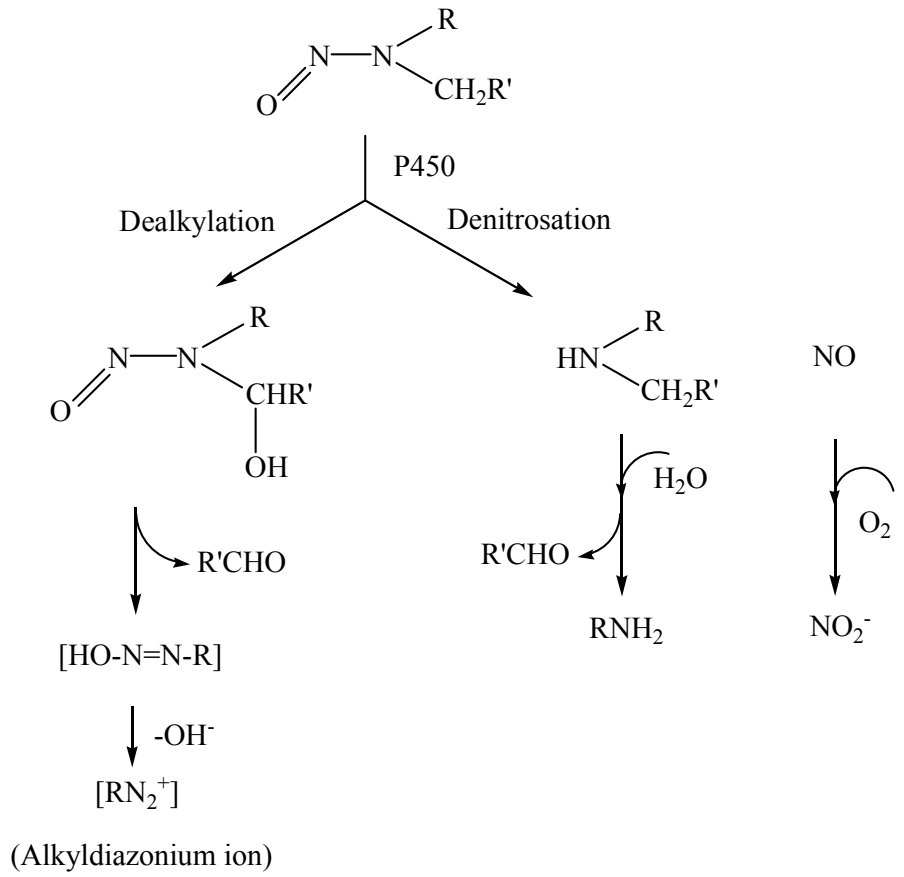

Scheme 1.1. Metabolic activation of a typical *N*-nitrosodialkylamine.

Our group is interested in using biomimetic systems to model the interactions of NO and related organic nitroso compounds with heme-containing proteins. A heme unit is basically an iron porphyrin or chlorin compound; thus, synthetic iron porphyrin and chlorin complexes have been used in the model chemistry of heme proteins. Figure 1.1 shows four commonly used synthetic metalloporphyrin and chlorin compounds in the

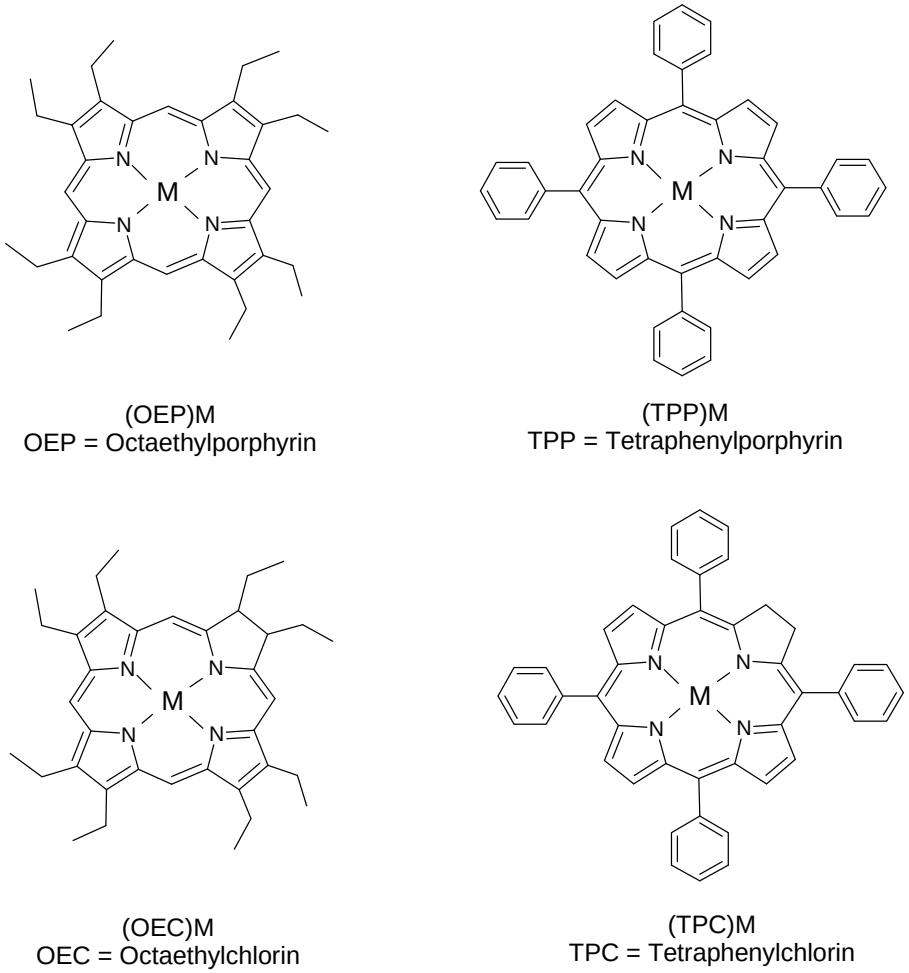

Figure 1.1. Synthetic metalloporphyrins and -chlorins.

study. Ru and Os porphyrin complexes, due to their electronic (low spin) similarity to the (group 8) low spin Fe porphyrin analogues, have also been employed by synthetic chemists as potential model complexes. The valence d orbitals of Ru and Os are more diffuse than the 3d orbitals of Fe which makes the bonding interactions between the metals and axial ligands stronger. Consequently, Ru and Os porphyrin complexes are generally more stable and easier to isolate than the corresponding iron derivatives.

Additionally, the low spin configurations of Ru and Os porphyrin complexes also make spectroscopic characterization easier compared to corresponding iron porphyrin complexes.

Nitric oxide may bind to metalloporphyrin complexes in one of four binding modes which are shown in Figure 1.2. Prior to 1999, the description of heme-NO

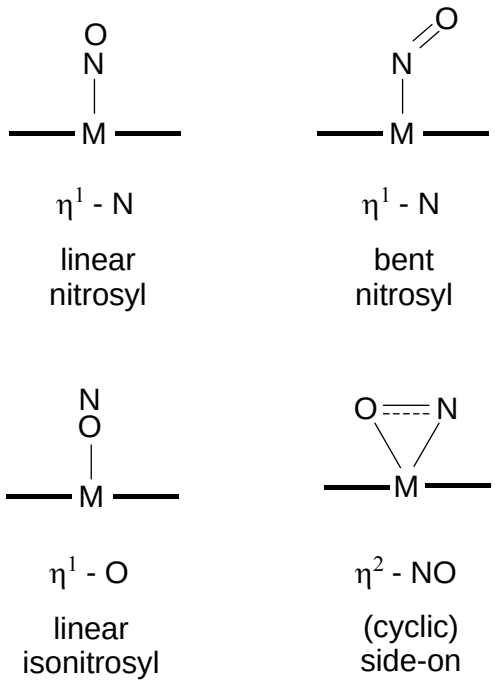

Figure 1.2. Four binding modes of monometallic nitrosyl compounds.

compounds were limited to linear nitrosyl and bent nitrosyl forms. However, together with Coppens' group, our group has shown that the linear isonitrosyl and side-on forms can exist as metastable states in synthetic nitrosyl heme models.[33] Linear and bent nitrosyl forms are still the most common binding modes observed in metal-nitrosyl complexes. Enemark and Feltham formulated a notation system which can be used to

predict the geometries of metal-nitrosyl groups.[34] In this system, metal nitrosyl complexes are considered as $\{MNO\}^n$ species, where n represents the total number of electrons from the d orbital of the metal and the π^* orbital of the NO in the MNO unit. In general, six-coordinate $\{MNO\}^6$ mononitrosyl metal complexes are expected to have a linear or near linear MNO group, while $\{MNO\}^7$ complexes should have a bent MNO group. The Enemark and Feltham notation is used throughout this dissertation.

My thesis research

My research is focused on modeling the interaction of nitric oxide and nitrosamines with heme proteins using synthetic metalloporphyrins with Ru and Fe.

By the time I joined our group, the group had reported the preparation of the nitrosyl alkoxide/thiolate ruthenium porphyrins by the *trans* addition reaction of alkyl nitrites (RONO) or alkyl thionitrites (RSNO) with a ruthenium porphyrin carbonyl compound (Eq. 1.4).[35-40] Also, we had reported the preparation of the *N*-binding

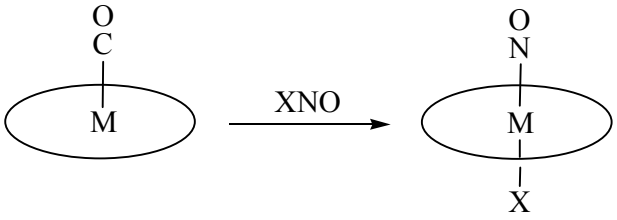

X = OR, SR (1.4)

nitrosoarene ferrous porphyrin complex, $(TPP)Fe(PhNO)_2$ by the reaction of $(TPP)Fe^{II}$ with excess PhNO (Eq. 1.5).[41] We were particularly interested in products resulting

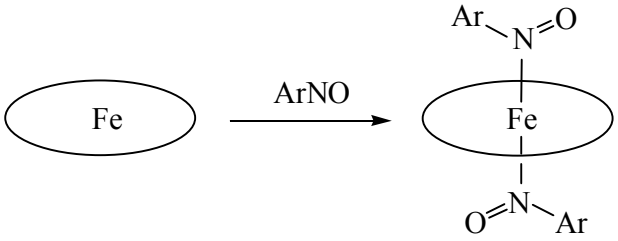

(1.5)

from the "hypothetical" C-N cleavage of *C*-nitroso compounds (Eq. 1.6). However, such products proved difficult to isolate for Ru. Therefore, the preparation and characterization of organoruthenium nitrosyl porphyrin complexes form the basis for my first project.

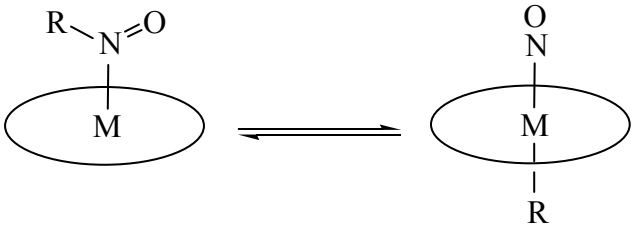

(1.6)

The second part of my work concerns about the interactions of nitrosamines with iron porphyrins. Our group reported the preparation of the first bis-nitrosamine iron heme model complex $[(TPP)Fe^{III}(Et_2NNO)_2]ClO_4$.[42] The crystal structure shows that the nitrosamine ligand is coordinated to the ferric center of the porphyrin in a σ-O binding mode (Figure 1.3). We extended such nitrosamine binding to ruthenium and

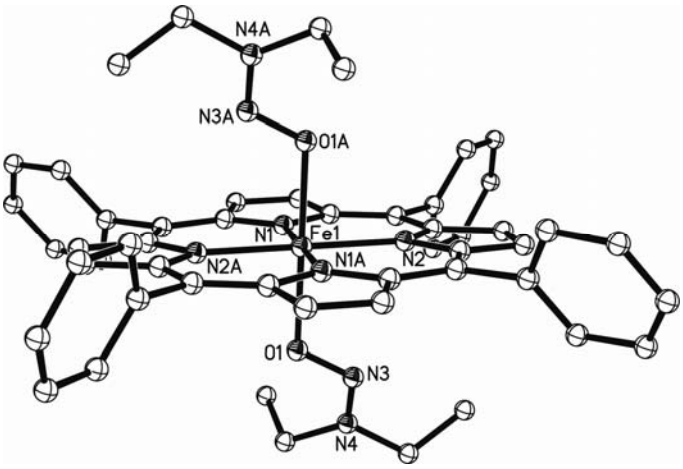

Figure 1.3. Molecular structure of the cation of $[(TPP)Fe(Et_2NNO)_2]^+ClO_4^-$.

osmium heme model complexes.[43,44] Despite repeated efforts, earlier workers in our group could only obtain crystals of these metalloporphyrin-nitrosamine compounds for the case of Et_2NNO. Thus, we embarked on investigating whether other nitrosamines would interact with iron porphyrins in the same σ-O binding mode or in other modes. In this work, we extended the study of interaction of nitrosamines with iron heme models to other nitrosamines. In addition, reactions involving nitrosamine N-N(O) bond cleavage were also explored.

The last part of my work was to prepare structurally unknown nitrosyl heme model complexes with thiolate/alkoxide ligands. Despite the importance of the nitrosyl thiolate heme proteins in biology, only one synthetic six-coordinate nitrosyl thiolate iron porphyrin compound was reported[45,46] prior to our study because of the extreme instability of the nitrosyl iron thiolate porphyrin compounds. Although NO has been

shown to bind reversibly to the synthetic ferric thiolate porphyrin (Eq. 1.7), no X-ray

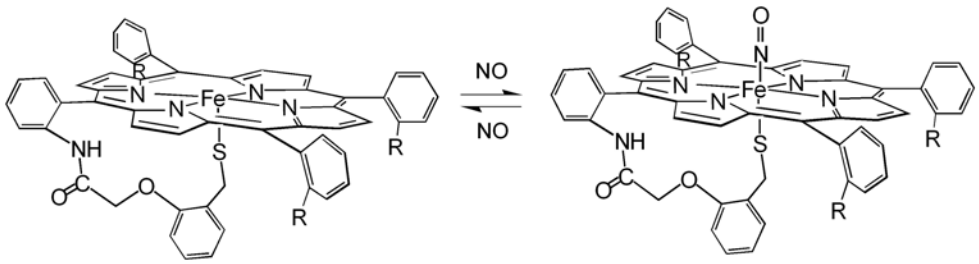

(1.7)

R = $NHCOC(CH_3)_3$

structural studies of synthetic iron nitrosyl heme thiolate compounds had been reported. In addition, our group reported the preparation of nitrosyl thiolate porphyrins of Ru and Os by the *trans* addition reaction of alkyl thionitrites (RSNO) with a metalloporphyrin carbonyl compound.[35-38,47,48] Several of these were characterized by X-ray crystallography and the near linear Ru(Os)-N-O bond angles are dominant in these complexes. Surprisingly, the Fe-N-O angles in the two structural reports on the NO adducts of ferric heme thiolate proteins range from 100° to 165°. In the case of the model chemistry of nitrosyl alkoxide heme proteins, the only structurally characterized synthetic ferric porphyrin model complex with a *O*-bound ligand (other than water) *trans* to the nitrosyl was prepared in our group by the reaction of $[(TPP)Fe(THF)_2]ClO_4$ with *i*-$C_5H_{11}ONO$.[49] The crystal structure of the resulting cationic $[(TPP)Fe(NO)(HO\text{-}i\text{-}C_5H_{11})]^+$ compound reveals a linear FeNO geometry.

In this work, we prepared ferric heme model complexes containing mutually *trans* NO and *S*-bound or *O*-bound ligands using a unique two-phase gas diffusion

method. In addition, the first structurally characterized model complexes of nitrosyl cysteinate and tyrosinate heme proteins were obtained.

References

(1) Ainscough, E. W.; Brodie, A. M. *J. Chem. Ed.* **1995**, *72*, 686-692.
(2) Ignarro, L. J.; Adams, J. B.; Horwitz, P. M.; Wood, K. S. *J. Biol. Chem.* **1986**, *261*, 1997-5002.
(3) Radomski, M. W.; Palmer, R. M. J.; Moncada, S. *Proc. Natl. Acad. Sci. USA* **1990**, *87*, 5193-5197.
(4) J. B. Hibbs, J.; Taintor, R. R.; Vavrin, Z. *Science* **1987**, *235*, 473-476.
(5) Nathan, C. *The FASEB J.* **1992**, *6*, 3051-3064.
(6) Gally, J. A.; Montague, P. R.; G. N. Reeke, J.; Edelman, G. M. *Proc. Natl. Acad. Sci. USA* **1990**, *87*, 3547-3551.
(7) Marletta, M. A. *J. Biol. Chem.* **1993**, *17*, 12231-12234.
(8) Rousseau, D. L.; Li, D.; Couture, M.; Yeh, S.-R. *J. Inorg. Biochem.* **2005**, *99*, 306-323.
(9) Li, H.; Raman, C. S.; Martasek, P.; Masters, B. S. S.; Poulos, T. L. *Biochemistry* **2001**, *40*, 5399-5406.
(10) Pant, K.; Crane, B. R. *Biochemistry* **2006**, *45*, 2537-2544.
(11) Abu-Soud, H. M.; Ichimori, K.; Nakazawa, H.; Stuehr, D. J. *Biochemistry* **2001**, *40*, 6876-6881.
(12) Stadler, J.; Trockfeld, J.; Schmalix, W. A.; Brill, T.; Siewert, J. R.; Greim, H.; Doehmer, J. *Proc. Natl. Acad. Sci. USA* **1994**, *91*, 3559-3563.
(13) Hu, S.; James, R. K. *J. Am. Chem. Soc.* **1991**, *113*, 2843-2850.
(14) Brown, G. C. *Eur. J. Biochem.* **1995**, *232*, 181-191.
(15) Hoshino, M.; Ozawa, K.; Seki, H.; Ford, P. C. *J. Am. Chem. Soc.* **1993**, *115*, 9568-9575.
(16) Ribeiro, J. M.; Hazzard, J. M.; Nussenzveig, R. H.; Champagne, D. E.; Walker, F. A. *Science* **1993**, *260*, 539-541.
(17) Andersen, J. F.; Champagne, D. E.; Weichsel, A.; Ribeiro, J. M. C.; Balfour, C. A.; Dress, V.; Montfort, W. R. *Biochemistry* **1997**, *36*, 4423-4428.
(18) Nurizzo, D.; Cutruzzola, F.; Arese, M.; Bourgeois, D.; Brunori, M.; Cambillau, C.; Tegoni, M. *Biochemistry* **1998**, *37*, 13987-13996.
(19) Williams, P. A.; Fülöp, V.; Garman, E. F.; Saunders, N. F. W.; Ferguson, S. J.; Hajdu, J. *Nature* **1997**, *389*, 406-412.

(20) Ortiz de Montellano, P. R.; Correia, M. A. In *Cytochrome P450 Structure, Mechanism, and Biochemistry*; Montellano, P. R. O. d., Ed.; Plenum Press: New York and London, 2005; Vol. 9.
(21) Augusto, O.; Kunze, K. L.; Ortiz de Montellano, P. R. *J. Biol. Chem.* **1982**, *257*, 6231-6241.
(22) Ortiz de Montellano, P. R.; Kerr, D. E. *Biochemistry* **1985**, *24*, 1147-1152.
(23) Ortiz de Montellano, P. R.; Kunze, K. L. *J. Am. Chem. Soc.* **1981**, *103*, 6534-6536.
(24) Saito, S.; Itano, H. A. *PNAS* **1981**, *78*, 5508-5512.
(25) Ortiz de Montellano, P. R.; Augusto, O.; Viola, F.; Kunze, K. L. *J. Biol. Chem.* **1983**, *258*, 8623-8629.
(26) Ortiz de Montellano, P. R.; Watanabe, M. D. *Mol. Pharmacol* **1987**, *31*, 213-219.
(27) *Cytochrome P450 Structure, Mechanism, and Biochemistry*; Ortiz de Montellano, P. R., Ed.; Plenum Press: New York and London, 2005.
(28) Gutternplan, J. B. *Nutat. Res.* **1987**, *186*, 81-134.
(29) Magee, P. N.; Barnes, J. M. *Cancer Res.* **1967**, *10*, 136-246.
(30) Lee, J.; Chen, L.; West, A. H.; Richter-Addo, G. B. *Chem. Rev.* **2002**, *102*, 1019-1065.
(31) Okochi, E.; Mochizuki, M. *Chem. Pharm. Bull.* **1995**, *43*, 2173-2176.
(32) Appel, K. E.; Gorsdorf, S.; Scheper, T.; Spiegelhalder, B.; Wiessler, M.; Schoepke, M.; Engeholm, C.; Kramer, R. *IARC Sci. Pub.* **1991**, *105*, 351-357.
(33) Fomitchev, D. V.; Coppens, P.; Li, T.; Bagley, K. A.; Chen, L.; Richter-Addo, G. B. *Chem. Commun.* **1999**, 2013-2014.
(34) Feltham, R. D.; Enemark, J. H. *Coord. Chem. Rev.* **1974**, *13*, 339-406.
(35) Yi, G.-B.; Chen, L.; Khan, M. A.; Richter-Addo, G. B. *Inorg. Chem.* **1997**, *36*, 3876-3885.
(36) Yi, G.-B.; Khan, M. A.; Richter-Addo, G. B. *Chem. Commun.* **1996**, 2045-2046.
(37) Lee, J.; Yi, G.-B.; Khan, M. A.; Richter-Addo, G. B. *Inorg. Chem.* **1999**, *38*, 4578-4584.
(38) Yi, G.-B.; Khan, M. A.; Powell, D. R.; Richter-Addo, G. B. *Inorg. Chem.* **1998**, *37*, 208-204.
(39) Carter, S. M.; Lee, J.; Hixson, C. A.; Powell, D. R.; Wheeler, R. A.; Shaw, M. J.; Richter-Addo, G. B. *Dalton Trans.* **2006**, *10*, 1338-1346.
(40) Andreasen, L. V.; Lorkovic, I. M.; Richter-Addo, G. B.; Ford, P. C. *Nitric Oxide* **2002**, *6*, 228-235.
(41) Wang, L.-S.; Chen, L.; Khan, M. A.; Richter-Addo, G. B. *Chem. Commun.* **1996**, 323-324.
(42) Yi, G.-B.; Khan, M. A.; Richter-Addo, G. B. *J. Am. Chem. Soc.* **1995**, *117*, 7850-7851.
(43) Chen, L.; Yi, G.-B.; Wang, L.-S.; Dharmawardana, U. R.; Dart, A. C.; Khan, M. A.; Richter-Addo, G. B. *Inorg. Chem.* **1998**, *37*, 4677-4688.
(44) Yi, G.-B.; Khan, M. A.; Richter-Addo, G. B. *Inorg. Chem.* **1996**, *35*, 3453-3454.

(45) Franke, A.; Stochel, G.; Suzuki, N.; Higuchi, T.; Okuzono, K.; Van Eldik, R. *J. Am. Chem. Soc.* **2005**, *127*, 5360-5375.
(46) Suzuki, N.; Higuchi, T.; Urano, Y.; Kikuchi, K.; Uchida, T.; Mukai, M.; Kitagawa, T.; Nagano, T. *J. Am. Chem. Soc.* **2000**, *122*, 12059-12060.
(47) Lee, J.; Yi, G.-B.; Powell, D. R.; Khan, M. A.; Richter-Addo, G. B. *Can. J. Chem.* **2001**, *79*, 830-840.
(48) Carter, S. M. Ph.D. Thesis, *Syntheses, Molecular Structures, and fiber-optic infrared spectroelectrochemistry of nitrosyl metalloporphyrins containing axially bound alkoxide thiolate, imidazole, and imidazolate.* **2006**, *University of Oklahoma*.
(49) Yi, G.-B.; Chen, L.; Khan, M. A.; Richter-Addo, G. B. *Inorg. Chem.* **1997**, *36*, 3876-3885.

Chapter 2. Synthesis, characterization, and redox behavior of six-coordinate (por)Ru(NO)Cl compounds*

Introduction

The renewed interest in the interaction of nitric oxide (NO) and the iron porphyrin cofactor in the heme-containing guanylyl cyclase enzyme is due, in a large part, to the observation that the heme-NO interaction is important in many biological events such as vascular smooth muscle relaxation, platelet aggregation, and neuronal communication.[1,2] NO is now known to interact with many other heme proteins, and some of these interactions have physiological significance.[3] It is well known that the isolation and characterization of iron nitrosyl porphyrins are sometimes difficult. Ruthenium, in the same group 8 as iron, is one of the most used substitutions for iron in biomimetic metalloporphyrin complexes because of its tendency to form strong metal-ligand bonds. Thus, ruthenium derivatives have been used as models for low-spin iron porphyrins. For example, we reported the syntheses of stable six-coordinate nitrosyl thiolate complexes (OEP)Ru(NO)(SR) (SR = SCH_2CF_3, SC_6F_4H)[4] and the X-ray crystal structure of (OEP)Ru(NO)(*S*-NACysMe) (NACysMe = *N*-acetyl-L-cysteinate methyl ester)[5] as a structural model of the NO adduct of ferric cytochrome P450 whose X-ray structure has not been reported. Other nitrosyl thiolate compounds of ruthenium porphyrins have been prepared successfully, by us[6-9] and others.[10] We have also shown the preparation of the

* Reproduced in part with permission from "Synthesis, Characterization, and and Redox behavior of Six-coordinate (por)Ru(NO)Cl compounds." Xu, N.; Lee, J.; Powell, D. R.; Richter-Addo, G. B. *Inorg. Chim. Acta.* **2005***, 258,* 2855-2860. *Copyright © Elsevier B.V.*. http://www.elsevier.com/wps/find/supportfaq.cws_home/rightsasanauthor

organometallic compounds (por)Ru(NO)R (R = alkyl, aryl)[11,12] from the chloride precursors by reaction with alkylating agents (See Chapter 3).

Importantly, the (por)Ru(NO)Cl compounds are useful starting reagents for the preparation of other ruthenium nitrosyl porphyrin derivatives.[10,12,13] Preparative methods for generating (por)Ru(NO)Cl are shown in equations 2.1-2.4. (TPP = tetraphenylporphyrinato dianion; TTP = tetratolylporphyrinato dianion; OEP = octaethylporphyrinato dianion).[10,13-16]

$$(por)Ru(CO) + ClNO \longrightarrow (por)Ru(NO)Cl + CO \quad (2.1)$$

(por = TPP, TTP, OEP)

$$(TTP)Ru(NO)(OMe) + HCl \longrightarrow (TTP)Ru(NO)Cl + HOMe \quad (2.2)$$

$$(por)Ru(NO)(OH) + HCl \longrightarrow (por)Ru(NO)Cl + H_2O \quad (2.3)$$

(por = TPP, OEP)

$$(OEP)Ru(NO)(ONO) + HCl \longrightarrow (OEP)Ru(NO)Cl + HNO_2 \quad (2.4)$$

Our research group has previously shown that the nitrosyl alkoxides (por)Ru(NO)(OR) can be prepared in high yields from the reaction of alkyl nitrites (RONO) with the precursor (por)Ru(CO) compounds via a formal *trans* addition reaction.[6,17] In this chapter, we show that the (por)Ru(NO)Cl compounds can be obtained in quantitative yield (as determined by IR and NMR spectroscopy) by the reaction of corresponding (por)Ru(NO)(OR) compounds with boron trichloride. Furthermore, the

redox properties of the (por)Ru(NO)Cl compounds have been investigated by cyclic voltammetry.

Experimental section

All reactions were performed under an atmosphere of prepurified nitrogen using standard Schlenk glassware and/or in an Innovative Technology Labmaster 100 Dry Box. Solutions for spectral studies were also prepared under a nitrogen atmosphere. Solvents were distilled from appropriate drying agents under nitrogen just prior to use: CH_2Cl_2 (CaH_2), hexane (CaH_2).

Chemicals. The (por)Ru(NO)(O-*i*-C_5H_{11}) (por = TPP[6], TTP[8], OEP[6]) compounds were prepared by literature methods. (T(*p*-OMe)PP)Ru(NO)(O-*i*-C_5H_{11}) and (T(*p*-CF_3)PP)Ru(NO)(O-*i*-C_5H_{11}) were also prepared as described for the TTP analogue. BCl_3 (1.0 M in CH_2Cl_2), BBr_3 (1.0 M in CH_2Cl_2), ferrocene (Cp_2Fe; Cp = η^5-cyclopentadienyl anion, 98%) were purchased from Aldrich Chemical Company and used as received. NBu_4PF_6 (98%; Aldrich Chemical Company) was recrystallized from hot ethanol. Chloroform–*d* (99.8%) was obtained from Cambridge Isotope Laboratories, purified by three freeze-pump-thaw cycles, and stored over Linde 4 Å molecular sieves.

Instrumentation. Infrared spectra were recorded on a Bio-Rad FT-155 FTIR spectrometer. Proton NMR spectra were obtained on a Varian 300 MHz spectrometer and the signals referenced to the residual signal of the solvent employed ($CHCl_3$ at 7.26 ppm). All coupling constants are in Hz. FAB and ESI mass spectra were obtained on a VG-ZAB-E or a Micromass Q-TOF mass spectrometer, respectively. UV-vis spectra were recorded on a Hewlett-Packard model 8453 diode array instrument. Wavelengths

are reported with ε (extinction coefficient) values. Elemental analyses were performed by Atlantic Microlab, Norcross, Georgia, U.S.A..

Cyclic voltammetric measurements were performed using a BAS CV50W instrument (Bioanalytical Systems, West Lafayette, IN, USA). A three-electrode cell was utilized and consisted of a 3.0 mm diameter Pt disk working electrode, a Pt wire counter electrode and a Ag/AgCl reference electrode. Deaeration of all solutions was accomplished by passing a stream of high purity nitrogen through the solution for 10 min and maintaining a blanket of nitrogen over the solution while performing the measurements. All experiments were performed on CH_2Cl_2 solutions containing 0.1 M NBu_4PF_6 at room temperature; under our conditions, 1.0 mM ferrocene displayed a redox couple at 0.37 V.

Preparation of (por)Ru(NO)Cl (por = TPP, TTP, T(*p*-OMe)PP, T(*p*-CF_3)PP, OEP). The following reaction is representative:

To a CH_2Cl_2 solution (25 mL) of (T(*p*-CF_3)PP)Ru(NO)(O-*i*-C_5H_{11}) (0.10 g, 0.091 mmol) was added BCl_3 (0.12 mL, 1.0 M in CH_2Cl_2, 0.12 mmol). The color of the solution changed from red to dark red-purple over a 1 h period. The volume of the solution was reduced to *ca.* 5 mL, and hexane (25 mL) was added to precipitate a dark red-purple solid. The supernatant solution was discarded, and the solid was washed with hexane (3 x 25 mL) and dried in vacuo to give (T(*p*-CF_3)PP)Ru(NO)Cl (0.088 g, 0.084 mmol, 92% isolated yield). IR (CH_2Cl_2, cm^{-1}): ν_{NO} = 1855; (KBr, cm^{-1}): ν_{NO} = 1847; also 3216 s, 1617 m, 1406 m, 1324 s, 1169 m, 1128 s, 1108 m, 1069 s, 1016 s, 858 w, 815 m, 798 m, 714 w. ^{1}H NMR ($CDCl_3$, ppm): δ 8.99 (s, 8H, *pyrrole*-H of T(*p*-CF_3)PP), 8.42 (d, 8H, *J* = 8 Hz, *o*-H of T(*p*-CF_3)PP), 8.09 (m, 8H, *m*-H of T(*p*-CF_3)PP). ESI mass

spectrum: *m/z* 1050 [(T(*p*-CF_3)PP)Ru(NO)Cl - H]$^+$ (100%), 1016 [(T(*p*-CF_3)PP)Ru(NO)]$^+$ (29%). UV-vis spectrum (λ (ε, mM^{-1} cm^{-1}), 4.88 x 10^{-6} M in CH_2Cl_2): 331 (19), 412 (203), 465 (19) (sh), 563 (12), 573 (10) nm.

The new (T(*p*-OMe)PP)Ru(NO)Cl compound and the previously reported compounds (por)Ru(NO)Cl (por = TPP,[14,15] TTP,[10,11,13,18] and OEP[14]) were generated similarly.

(T(*p*-OMe)PP)Ru(NO)Cl. 90% isolated yield. IR (CH_2Cl_2, cm^{-1}): ν_{NO} = 1851 (KBr, cm^{-1}): ν_{NO} = 1844; also 1605 m, 1511 m, 1350 m, 1287 m, 1244 s, 1175 s, 1071 w, 1018 s, 860 w, 851 m, 611 w. ^{1}H NMR ($CDCl_3$, ppm): δ 9.06 (s, 8H, *pyrrole*-H of T(*p*-OMe)PP), 8.21 (m, 8H, *o*-H of T(*p*-OMe)PP), 7.33 (m, 8H, *m*-H of T(*p*-OMe)PP), 4.13 (s, 12H, OC*H*$_3$ of T(*p*-OMe)PP). ESI mass spectrum: *m/z* 834 [(T(*p*-OMe)Ru]$^+$ (100%). UV-vis spectrum (λ (ε, mM^{-1} cm^{-1}), 2.67 x 10^{-6} M in CH_2Cl_2): 319 (32), 417 (283), 571 (12) nm.

(TPP)Ru(NO)Cl. 92% isolated yield. IR (KBr, cm^{-1}): ν_{NO} = 1848；also 1596 m, 1484 w, 1440 m, 1351 m, 1308 w, 1209 w, 1176 m, 1071 m, 1016 s, 799 w, 752 m, 714 w, 704 m, 667 w, 531 w. ^{1}H NMR ($CDCl_3$, ppm): δ 9.01 (s, 8H, *pyrrole*-H of TPP), 8.28 (m, 8H, *o*-H of TPP), 7.79 (m, 12H, *m,p*-H of TPP).

(TTP)Ru(NO)Cl. 85% isolated yield. IR (CH_2Cl_2, cm^{-1}): ν_{NO} = 1851; (KBr, cm^{-1}): ν_{NO} = 1845; also 3230 m, 1441 m, 1350 m, 1306 w, 1212 w, 1179 m, 1070 m, 1016 s, 797 s, 714 m, 525 w. ^{1}H NMR ($CDCl_3$, ppm): δ 9.03 (s, 8H, *pyrrole*-H of TTP), 8.16 (m, 8H, *o*-H of TTP), 7.58 (m, 8H, *m*-H of TTP), 2.73 (s, 12H, C*H*$_3$ of TTP).

(OEP)Ru(NO)Cl. 82% isolated yield. IR (CH_2Cl_2, cm^{-1}): ν_{NO} = 1842; (KBr, cm^{-1}): ν_{NO} = 1829; also 3215 m, 1459 s, 1196 m, 1057 w, 1153 w, 1020 w, 963 w. ^1H NMR ($CDCl_3$, ppm): δ 10.38 (s, 4H, *meso*-H of OEP), 4.18 (m, 16H, CH_2CH_3 of OEP), 2.03 (m, 24H, CH_2CH_3 of OEP).

Preparation of (TTP)Ru(NO)Br. To a CH_2Cl_2 solution (20 mL) of (TTP)Ru(NO)(O-*i*-C_5H_{11}) (0.050 g, 0.056 mmol) was added BBr_3 (0.08 mL, 1.0 M in CH_2Cl_2, 0.08 mmol). The color of the solution changed from dark purple to dark green-purple over a 1 h period. The volume of the solution was reduced to *ca.* 5 mL, and hexane (25 mL) was added to precipitate a dark green-purple solid. The supernatant solution was discarded, and the solid was then washed with hexane (3 x 25 mL) and dried in vacuo to give (TTP)Ru(NO)Br·0.9CH_2Cl_2 (0.040 g, 0.042 mmol, 74% isolated yield). Anal. Calcd for $C_{48}H_{36}N_5O_1Br_1Ru_1$·0.9$CH_2Cl_2$: C, 61.42; H, 3.98; N, 7.32. Found: C, 61.53; H, 4.13; N, 7.04. IR (CH_2Cl_2, cm^{-1}): ν_{NO} = 1847, (KBr, cm^{-1}): ν_{NO} = 1838; also 1442 w, 1350 m, 1306 w, 1212 w, 1179 m, 1070 s, 1016 s, 797 w, 714 w, 525 w. ^1H NMR ($CDCl_3$, ppm): δ 9.04 (s, 8H, *pyrrole*-H of TTP), 8.16 (m, 8H, *o*-H of TTP), 7.59 (m, 8H, *m*-H of TTP), 5.28 (s, CH_2Cl_2), 2.73 (s, 12H, CH_3 of TTP). Low-resolution mass spectrum (FAB): *m/z* 879 $[(TTP)Ru(NO)Br]^+$ (28%), 849 $[(TTP)RuBr]^+$ (20%), 800 $[(TTP)Ru(NO)]^+$ (100%), 770 $[(TTP)Ru]^+$ (94%). UV-vis spectrum (λ (ε, mM^{-1} cm^{-1}), 4.08 x 10^{-6} M in CH_2Cl_2): 338 (21), 417 (247), 465 (21) (sh), 486 (19), 578 (11) nm.

Results and discussion

Synthesis and structural characterization. The (por)Ru(NO)Cl compounds were prepared by the reactions of the (por)Ru(NO)(alkoxide) complexes with boron trichloride. For example, the reaction of (por)Ru(NO)(O-*i*-C_5H_{11}) (por = TPP, TTP, T(*p*-OMe)PP, T(*p*-CF_3)PP, OEP) with the Lewis acid BCl_3 in CH_2Cl_2 produces, after work-up, the (por)Ru(NO)Cl complexes in 82-92% isolated yields as shown in equation 2.5 (where X = Cl). Two of these compounds (por = T(*p*-OMe)PP, T(*p*-CF_3)PP) had not been reported previously. The progress of the reaction was monitored by IR spectroscopy. The disappearance of the ν_{NO} bands of the starting (por)Ru(NO)(alkoxide) complexes at 1800-1813 cm^{-1} in CH_2Cl_2 and the appearance of the new ν_{NO} bands in the range 1842-1855 cm^{-1} suggested the reactions were complete. We also successfully extended this methodology to the preparation of the analogous (TTP)Ru(NO)Br complex. Thus, (TTP)Ru(NO)Br was formed from the reaction of (TTP)Ru(NO)(O-*i*-C_5H_{11}) with BBr_3 in CH_2Cl_2 in 74% isolated yield.

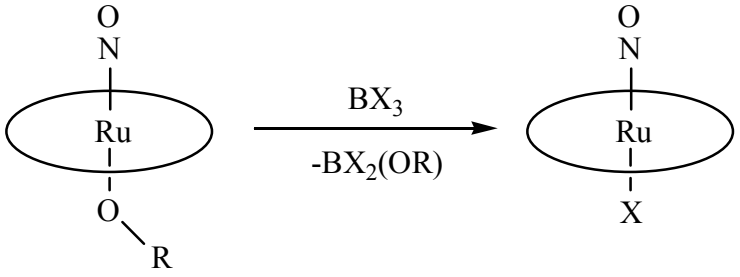

(2.5)

Por = TPP, TTP, T(*p*-OMe)PP, T(*p*-CF_3)PP, OEP
R = *i*-C_5H_{11}
X = Cl, Br

Compared with previously reported synthetic methods, the method described by equation 2.5 is more straightforward and the products are easier to isolate from the reaction mixtures. Furthermore, the use of alkyl nitrites (RONO) to prepare the precursor (por)Ru(NO)(OR) compounds is a much cheaper alternative when compared with previous methods employing NO gas.

The IR spectral data for (por)Ru(NO)X (por = TPP, TTP, OEP, T(*p*-OMe)PP, T(*p*-CF_3)PP; X = Cl, Br) and their precursors (por)Ru(NO)(O-*i*-C_5H_{11}) are listed in Table 2.1. In the case of (TPP)Ru(NO)Cl, the IR spectrum in CH_2Cl_2 is not available because of its poor solubility in dichloromethane. The IR spectra of (por)Ru(NO)X as KBr pellets show strong bands in the range 1829-1848 cm^{-1} due to ν_{NO}, and these values are significantly higher than those of the (por)Ru(NO)(O-*i*-C_5H_{11}) precursors (1788-1809 cm^{-1}). This observation is consistent with the fact that halides are more electron-withdrawing than alkoxide ligands. Also, the lower ν_{NO} of (OEP)Ru(NO)Cl (1829 cm^{-1}) in KBr compared to those of the tetraaryl-based porphyrin derivatives (1844-1848 cm^{-1}) indicates that the octaalkyl-based porphyrins are more electron-rich than the tetraaryl-based porphyrins. Further, the infrared data of (TTP)Ru(NO)Cl (1845 cm^{-1}) and (TTP)Ru(NO)Br (1838 cm^{-1}) suggests better electron donating ability of Br compared to Cl when placed *trans* to NO, a result that is consistent with their relative electronegativities.

A suitable brown prism-shaped crystal of (OEP)Ru(NO)Cl·CH_2Cl_2 was adventitiously grown from the light-induced decomposition of (OEP)Ru(NO)(*i*Bu) in methylene chloride. The molecular structure and the porphyrin atom displacements for (OEP)Ru(NO)Cl are shown in Figure 2.1a and 2.1b, respectively. To the best of our

knowledge, this is the first reported crystal structure of a nitrosyl porphyrin chloride of any metal. Selected bond lengths and angles are listed in Table 2.2.

Both linear and bent RuNO geometries have been observed in ruthenium nitrosyl porphyrins. While majority of the structurally characterized ruthenium nitrosyl porphyrins display linear Ru–N–O bond linkages,[3] it is not always certain that the {RuNO}^{6} derivatives contain linear RuNO groups (this is discussed more fully in the next Chapter). For example, moderately bent geometries of RuNO groups have been determined for (TTP)Ru(NO)(*p*-C_6H_4F) (152°),[11] (OEP)Ru(NO)(*p*-C_6H_4F) (155°),[12] (OEP)Ru(NO)(SCH_2CF_3) (161° and 157°)[3,19] and (TTP)Ru(NO)($NOsO_3$) (153°).[20] We were thus interested in determining the structure of the axial NO group in (por)Ru(NO)Cl.

Table 2.1. Infrared nitrosyl stretching frequencies of (por)Ru(NO)X and (por)Ru(NO)(O-*i*-C_5H_{11}) (por = TPP, TTP, OEP, T(*p*-OMe)PP, T(*p*-CF_3)PP; X = Cl, Br).

Compound	ν_{NO} (KBr, cm^{-1})	ν_{NO} (CH_2Cl_2, cm^{-1})	Reference
(TPP)Ru(NO)Cl	1848		This work
(TTP)Ru(NO)Cl	1845	1851	This work
(T(*p*-CF_3)PP)Ru(NO)Cl	1847	1855	This work
(T(*p*-OMe)PP)Ru(NO)Cl	1844	1851	This work
(OEP)Ru(NO)Cl	1829	1842	This work
(TTP)Ru(NO)Br	1838	1847	This work
(TPP)Ru(NO)(O-*i*-C_5H_{11})	1800	1809	6
(TTP)Ru(NO)(O-*i*-C_5H_{11})	1809	1810	8
(T(*p*-CF_3)PP)Ru(NO)(O-*i*-C_5H_{11})	1805	1813	This work
(T(*p*-OMe)PP)Ru(NO)(O-*i*-C_5H_{11})	1801	1808	This work
(OEP)Ru(NO)(O-*i*-C_5H_{11})	1788	1800	6

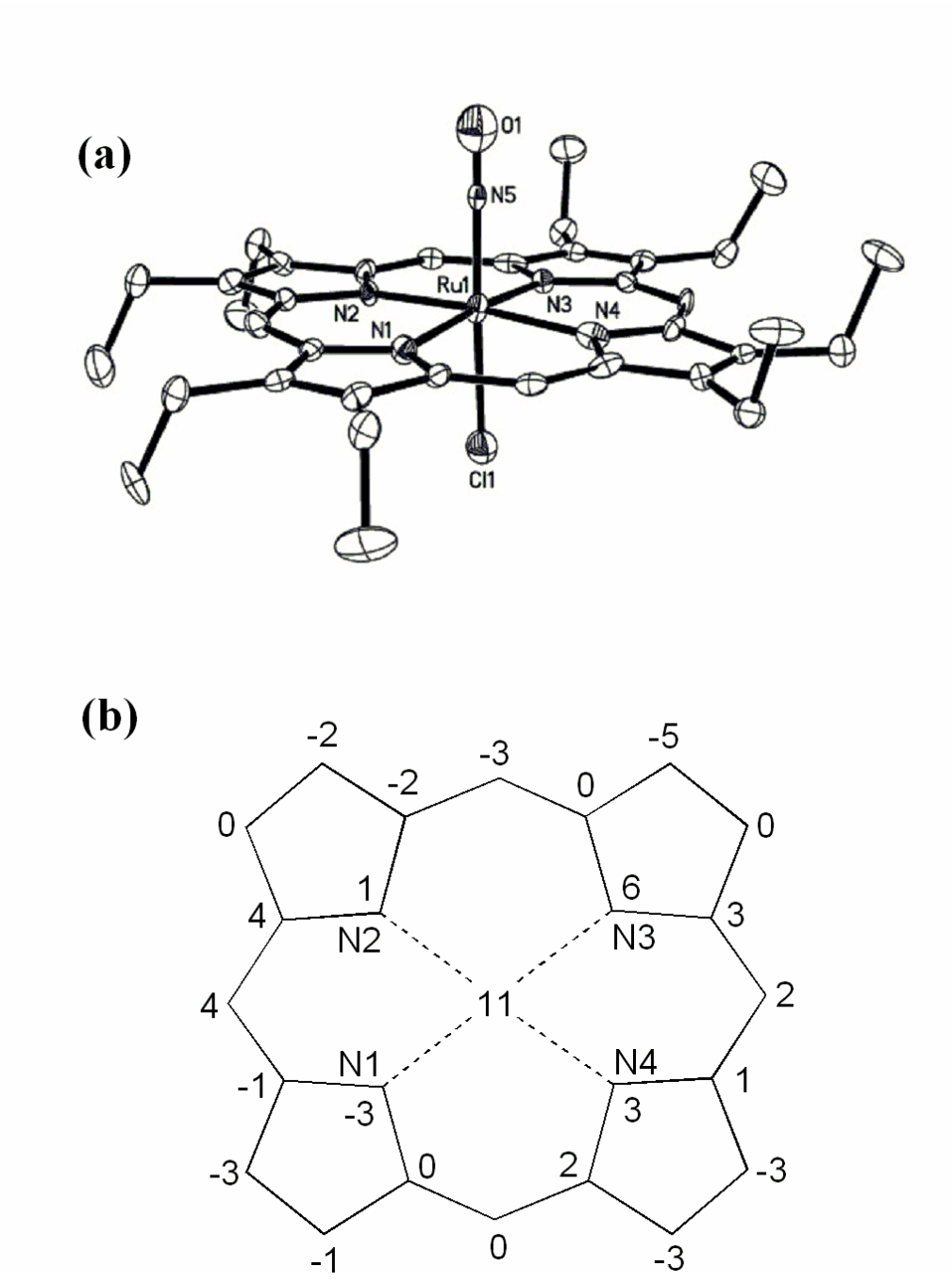

Figure 2.1 (a) Molecular structure of (OEP)Ru(NO)Cl. Hydrogen atoms have been omitted for clarity. (b) Perpendicular atom displacements (in units of 0.01 Å) of the porphyrin core from the 24-atom mean porphyrin plane.

Table 2.2. Selected bond lengths (Å) and angles (°) for (OEP)Ru(NO)Cl.

Bond Lengths (Å)			
N(5)-O(1)	1.093(9)	Ru(1)-N(3)	2.048(5)
Ru(1)-N(5)	1.803(7)	Ru(1)-N(4)	2.055(7)
Ru(1)-N(1)	2.064(5)	Ru(1)-Cl(1)	2.331(2)
Ru(1)-N(2)	2.039(6)		
Bond Angles (°)			
O(1)-N(5)-Ru(1)	176.6(6)	N(2)-Ru(1)-N(1)	90.0(2)
N(5)-Ru(1)-N(2)	92.8(2)	N(3)-Ru(1)-N(1)	174.8(2)
N(5)-Ru(1)-N(3)	93.2(2)	N(4)-Ru(1)-N(1)	89.8(2)
N(2)-Ru(1)-N(3)	89.6(2)	N(5)-Ru(1)-Cl(1)	178.2(2)
N(5)-Ru(1)-N(4)	92.4(3)	N(2)-Ru(1)-Cl(1)	88.6(2)
N(2)-Ru(1)-N(4)	174.9(3)	N(3)-Ru(1)-Cl(1)	85.73(16)
N(3)-Ru(1)-N(4)	90.2(2)	N(4)-Ru(1)-Cl(1)	86.26(18)
N(5)-Ru(1)-N(1)	92.1(2)	N(1)-Ru(1)-Cl(1)	89.04(17)

The Ru–N(O) and N–O bond lengths are 1.803(7) and 1.093(9) Å, respectively, and the RuNO group is essentially linear with a bond angle of 176.6(6)°. The axial (O)N–Ru–Cl bond angle is 178.2(2)°. The Ru–N(por) bond lengths in (OEP)Ru(NO)Cl range from 2.039(6) to 2.064(5) Å, and the Ru atom is displaced by 0.11 Å from the 24-atom mean porphyrin plane toward the π-acid NO. The porphyrin moiety exhibits a slightly *ruffled* distortion.[21] The axial Ru–Cl bond length of 2.331(2) Å is similar to the Ru–Cl length of 2.320(6) Å in $[(OEP)RuCl]_2(\mu\text{-}O)$,[22] but is slightly shorter than the reported Ru–Cl length of 2.356(2) Å in (TTP)Ru(NS)Cl.[18]

Electrochemistry. The redox behavior of the (por)Ru(NO)Cl compounds (por = TPP, TTP, T(*p*-OMe)PP, T(*p*-CF_3)PP, OEP) in CH_2Cl_2 was examined at room temperature using cyclic voltammetry. The resulting cyclic voltammograms are shown in Figure 2.2 and the electrochemical data are summarized in Table 2.3.

The (OEP)Ru(NO)Cl compound undergoes two reversible oxidations at +0.86 V and +1.38 V vs Ag/AgCl within the solvent potential limit (Figure 2.2a). The separations in peak potentials, $\Delta E_p = |E_{pa} - E_{pc}|$ are both 78 mV for the first and second oxidations, and this value is similar to that determined for the ferrocene-ferrocinium couple (80 mV) under identical conditions. In addition, these two oxidations are chemically reversible processes, with anodic to cathodic peak current ratios (i_{pa}/i_{pc}) of ~1.0. Furthermore, the plots of i_{pa} vs $\nu^{1/2}$ for the first and second oxidations show linear relationships, indicating that these processes are diffusion-controlled. We thus ascribed the first two oxidations to electrochemically and chemically reversible, single-electron processes as shown in equations 2.6 and 2.7.

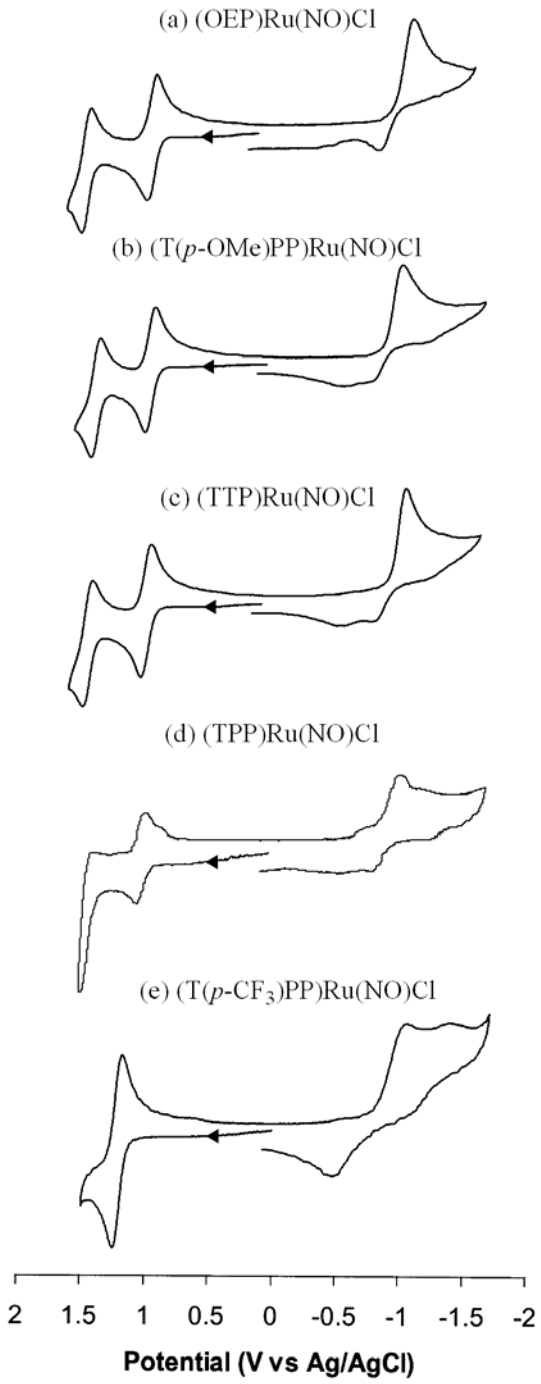

Figure 2.2. Cyclic voltammograms of the (por)Ru(NO)Cl compounds in CH_2Cl_2 containing 0.1 M NBu_4PF_6 and at a scan rate of 200 mV/s. The solubility of (TPP)Ru(NO)Cl in CH_2Cl_2 is very low relative to the other compounds.

$$(OEP)Ru(NO)Cl - e^- \rightleftharpoons [(OEP)Ru(NO)Cl]^+ \quad (2.6)$$

$$[(OEP)Ru(NO)Cl]^+ - e^- \rightleftharpoons [(OEP)Ru(NO)Cl]^{2+} \quad (2.7)$$

Electrochemical reversibility occurs when the rate of electron transfer between the complex and the working electrode is rapid enough to establish an equilibrium between the redox species.[23] Chemically reversibility occurs when the product of the redox reaction is stable enough to be returned to the original species by the reverse electron transfer.[23] The criterion for diffusion control is that i_{pa} vs $\upsilon^{1/2}$ must be constant, which indicates the current is controlled by the rate of diffusion of the sample electrolyte through the depleting layer to the working electrode surface.[24]

Returning to the electrochemistry of (OEP)Ru(NO)Cl, this compound displays a partially-reversible reduction peak at $E_{pc} = -1.18$ V that is coupled to a weak return peak E_{pa} at –0.92 V. This reduction process is likely due to initial reduction of the complex followed by fast loss of chloride ion (i.e., an E_rC_i process) as judged by analysis of the shape of the redox couple as a function of scan rate.[10]

The cyclic voltammograms of the other compounds are also shown in Figure 2.2. In general, all the (por)Ru(NO)Cl compounds undergo similar redox processes to that of the OEP derivative, however, the complexes containing less electron-rich porphyrin macrocycles are harder to oxidize, and this is not unexpected. For example, the first oxidations of the (por)Ru(NO)Cl compounds occur at $E°' = 0.86$ V (for OEP), 0.93 V (for T(*p*-OMe)PP), 0.97 V (for TTP), 1.04 V (for TPP), and 1.21 V (for T(*p*-CF_3)PP), reflecting the decreasing donor ability of the different porphyrins (Table 2.3). The $E°'$

for the first oxidation of (OEP)Ru(NO)Cl is lower than those of the four *para*-substituted TPP type compounds, consistent with the easier oxidation of the more electron-rich OEP macrocycle relative to the TPP type macrocycles. The same trend was also observed based on the ν_{NO} in infrared spectra. The increasing difficulty of oxidation with decreasing donor ability of the porphyrin macrocycles makes the second oxidations of the TPP and T(*p*-CF_3)PP derivatives inaccessible within the experimental solvent system range employed.

Table 2.3. Formal potentials for oxidations and reductions of (por)Ru(NO)Cl in CH_2Cl_2, 0.1 M NBu_4PF_6.

Compound	σ^a	$E°'$		E_{pc}
		1st oxidn	2nd oxidn	reduction
(OEP)Ru(NO)Cl		0.86	1.38	–1.18
(T(*p*-OMe)PP)Ru(NO)Cl	–0.27	0.93	1.35	–1.03
(TTP)Ru(NO)Cl	–0.17	0.97	1.43	–1.05
(TPP)Ru(NO)Cl	0.00	1.04		–1.00
(T(*p*-CF_3)PP)Ru(NO)Cl	0.54	1.21		–1.05

[a] Hammett parameters taken from reference 24.

The examination of substituent effects on redox potentials in tetraaryl-substituted porphyrins provides very useful information regarding redox-active sites in metalloporphyrins. Thus, the correlation between half-wave potentials and the Hammett

parameters (σ) of the substituents can serve to infer the site of oxidation processes in metalloporphyrins.[25] In general, substituent effects on redox potentials are larger for porphyrin-ring centered redox reactions than for metal centered redox reactions in the case of substituted tetraarylporphyrins, and the average value of ρ for ring-centered redox processes has been determined to be 70±10 mV.[25] The plot of $E^{\circ\prime}$ vs Hammett parameter[26] (actually the sum of (4)σ for the four phenyl groups) for the first oxidation of the four *para*-substituted tetraarylporphyrin compounds is shown in Figure 2.3.

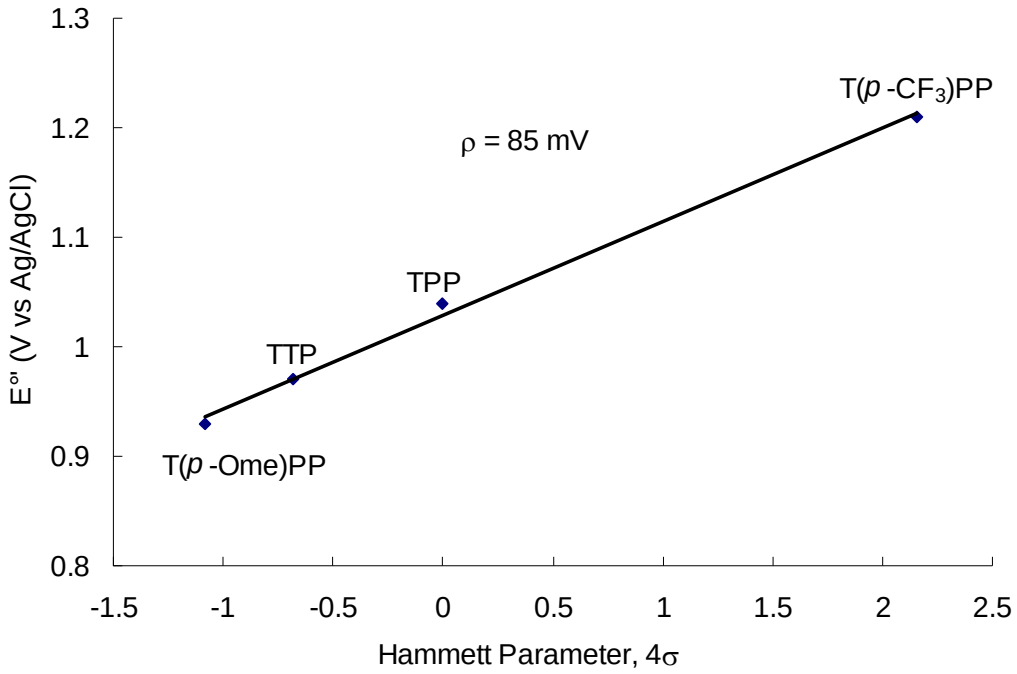

Figure 2.3. Plot of E°' vs the Hammett substituent constants for the first oxidation of (por)Ru(NO)Cl in CH_2Cl_2. Half-wave potentials are listed in Table 2.3.

A linear relationship is obtained for the first oxidations of the compounds, with a calculated slope (ρ) of 85 mV. Due to this relatively strong effect of substituents on

redox potentials, we thus assign the first oxidations of the (por)Ru(NO)Cl compounds as porphyrin ring-centered oxidations. In related published work with several substituted tetraarylporphyrin (por)Co(NO) compounds, we showed that the related slope for the first oxidation of (por)Co(NO) was 76 mV which also corresponded to ring-centered oxidations.[27] Due to the limitations of accessible ranges in the solvent system employed, we are not able to assign the site of redox activity for the second oxidations (since the second oxidations of the TPP and T(*p*-CF_3)PP complexes do not occur within the solvent potential limits).

To the best of our knowledge, there are only three other reports on the electrochemistry of ruthenium nitrosyl porphyrins.[10,20,28,29] The only previously published electrochemistry of a ruthenium porphyrin nitrosyl chloride was that of (TTP)Ru(NO)Cl,[10] and our results are similar to those obtained in the previous study. Most (por)Ru(NO)-containing compounds display similar redox behavior to those reported here for the (por)Ru(NO)Cl compounds. Thus, they undergo one or two reversible oxidations, and generally irreversible or quasi-reversible reductions, except for (TPP)Ru(NO)(ONO) and $[(TPP)Ru(NO)(H_2O)]^+$.[28] In the latter study, a perchlorate salt was used as supporting electrolyte. Interestingly, the oxidation of $[(TPP)Ru(NO)(H_2O)]^+$ was observed to be reversible to quasi-reversible, and (TPP)Ru(NO)(ONO) underwent replacement of the nitrito ligand by the perchlorate anion (from the supporting electrolyte) after oxidation.

Conclusion

A new high-yield preparative route to (por)Ru(NO)Cl compounds (por = porphyrinato dianion) from reactions of (por)Ru(NO)(alkoxide) precursors with boron trichloride is reported. The method is much easier and safer compared to the previous reported synthetic methods. The diamagnetic ruthenium nitrosyl chloride complexes have been characterized by IR and ^{1}H NMR spectroscopy. The IR spectrum of electron rich octaethyl β-substituted porphyrin shows the nitrosyl stretch at 1842 cm^{-1} in CH_2Cl_2 which is significant lower than those of other aryl *meso*-substituted porphyrin derivatives (TTP, T(*p*-OMe)PP, T(*p*-CF_3)PP). This is due to the stronger metal-nitrosyl π back-bonding in the OEP derivative. A crystal structure of (OEP)Ru(NO)Cl was obtained and exhibits a linear Ru-NO geometry. The redox behavior of the (por)Ru(NO)Cl compounds has been determined by cyclic voltammetry. Analysis of the data reveals that the first oxidations of the (por)Ru(NO)Cl compounds are porphyrin-ring centered. These ruthenium nitrosyl chloride complexes were used as precursors to prepare organometallic (por)Ru(NO)(R) derivatives described in the next Chapter.

References

(1) Stuehr, D. J.; Griffith, O. W. *Adv. Enzymol. Relat. Areas Mol. Biol.* **1992**, *65*, 287-386.
(2) Bredt, D. S.; Snyder, S. H. *Ann. Rev. Biochem.* **1994**, *63*, 175-195.
(3) Cheng, L.; Richter-Addo, G. B. In *Binding and Activation of Nitric Oxide by Metalloporphyrins and Heme, The Porphyrin Handbook*; Guilard, R., Smith, K., Kadish, K. M., Eds.; Academic Press: San Diego, CA, 2000; Vol. 4.
(4) Yi, G.-B.; Khan, M. A.; Richter-Addo, G. B. *Inorg. Chem.* **1996**, *35*, 3453-3454.
(5) Yi, G.-B.; Khan, M. A.; Richter-Addo, G. B. *Chem. Commun.* **1996**, 2045-2046.

(6) Lee, J.; Yi, G.-B.; Khan, M. A.; Ricther-Addo, G. B. *Inorg. Chem.* **1999**, *38*, 4578-4584.
(7) Lee, J.; Yi, G.-B.; Powell, D. R.; Khan, M. A.; Richter-Addo, G. B. *Can. J. Chem.* **2001**, *79*, 830-840.
(8) Yi, G.-B.; Chen, L.; Khan, M. A.; Richter-Addo, G. B. *Inorg. Chem.* **1997**, *36*, 3876-3885.
(9) Yi, G.-B.; Khan, M. A.; Powell, D. R.; Richter-Addo, G. B. *Inorg. Chem.* **1998**, *37*, 208-214.
(10) Bohle, D. S.; Hung, C.-H.; Smith, B. D. *Inorg. Chem.* **1998**, *37*, 5798-5806.
(11) Hodge, S. J.; Wang, L.-S.; Khan, M. A.; V. G. Young, J.; Richter-Addo, G. B. *Chem. Commun.* **1996**, 2283-2284.
(12) Richter-Addo, G. B.; Wheeler, R. A.; Hixon, C. A.; Chen, L.; Khan, M. A.; Ellison, M. K.; Schulz, C. E.; Scheidt, W. R. *J. Am. Chem. Soc.* **2001**, *123*, 6314-6326.
(13) Bohle, D. S.; Goodson, P. A.; Smith, B. D. *Polyhedron* **1996**, *15*, 3147-3150.
(14) Lorkovic, I. M.; Miranda, K. M.; Lee, B.; Bernhard, S.; Schoonover, J. R.; Ford, P. C. *J. Am. Chem. Soc.* **1998**, *120*, 11674-11683.
(15) Massoudipour, M.; Pandey, K. K. *Inorg. Chim. Acta* **1989**, *160*, 115-118.
(16) Miranda, K. M.; Bu, X.; Lorkovic, I.; Ford, P. C. *Inorg. Chem.* **1997**, *36*.
(17) Richter-Addo, G. B. *Acc. Chem. Res.* **1999**, *32*, 529-536.
(18) Bohle, D. S.; Hung, C.-H.; Powell, A. K.; Smith, B. D.; Wocadlo, S. *Inorg. Chem.* **1997**, *36*, 1992-1993.
(19) Fomitchev, D. V.; Coppens, P.; Li, T.; Bagley, K. A.; Chen, L.; Richter-Addo, G. B. *Chem. Commun.* **1999**, 2013-2014.
(20) Leung, W.-H.; Chim, J. L. C.; Lai, W.; Lam, L.; Wong, W.-T.; Chan, W. H.; Yeung, C.-H. *Inorg. Chim. Acta* **1999**, *290*, 28-35.
(21) Scheidt, W. R. In *The Porphyrin Handbook*; Guilard, R., K., S., Kadish, K. M., Eds., Eds.; Academic Press: New York, 2000; Vol. 3.
(22) Masuda, H.; Taga, T.; Osaki, K.; Sugimoto, H.; Mori, M.; Ogoshi, H. *Bull. Chem. Soc. Jpn.* **1982**, *55*, 3887-3890.
(23) Kissinger, P. T.; Heineman, W. R. *J. Chem. Ed.* **1983**, *60*, 702-706.
(24) Evans, D. H.; O'Connell, K. M.; Petersen, R. A.; Kelly, M. J. *J. Chem. Ed.* **1983**, *60*, 290-293.
(25) Kadish, K. M.; Caemelbecke, E. V.; Royal, G. *Electrochemistry of Metalloporphyrins in Nonaqueous Media* San Diego, CA, 2000.
(26) Hansch, C.; Leo, A.; Taft, R. W. *Chem. Rev.* **1991**, *91*, 165-195.
(27) Richter-Addo, G. B.; Hodge, S. J.; Yi, G.-B.; Khan, M. A.; Ma, T.; Caemelbecke, E. V.; Guo, N.; Kadish, K. M. *Inorg. Chem.* **1996**, *35*, 6530-6538, and 1997, p2693[erratum].
(28) Kadish, K. M.; Adamian, V. A.; Caemelbecke, E. V.; Tan, Z.; Tagliatesta, P.; Bianco, P.; Boschi, T.; Yi, G.-B.; Khan, M. A.; Richter-Addo, G. B. *Inorg. Chem.* **1996**, *35*, 1343-1348.
(29) Carter, S. M.; Lee, J.; Hixson, C. A.; Powell, D. R.; Wheeler, R. A.; Shaw, M. J.; Richter-Addo, G. B. *Dalton Trans.* **2006**, *10*, 1338-1346.

Chapter 3. Synthesis and characterization of organometallic nitrosyl complexes of ruthenium porphyrins

Introduction

The continuous interest in the studies of organometallic porphyrins and related macrocycles is largely due to the distinct roles that metal-carbon bonds play in the natural and model chemistry of coenzyme B_{12} and cytochrome P450.[1-5] The discovery of cobalt-carbon bonds in coenzyme B_{12} sparked the extensive study in the chemistry of organometallic macrocycles. The formation of σ-bonded aryl-iron(III) porphyrin species from the reaction of phenylhydrazines ($PhNHNH_2$) with hemoglobin, myoglobin, and cytochrome P450 has also been reported.[6-9] Additionally, an unstable σ-bonded alkyl-iron(III) complex was proposed during the metabolism of alkylhydrazines by cytochrome P450.[10-12] Many organometallic porphyrin complexes, especially those of iron and cobalt [13-19], have been synthesized as models of these biological systems. However, the general instability of organoiron(III) porphyrin complexes makes it difficult to characterize and isolate these compounds.[20] As mentioned in Chapter 2, ruthenium-substituted heme model complexes are generally more stable than their iron counterparts. Thus, organoruthenium porphyrins become important synthetic targets in this research field.[21,22]

It is known that nitric oxide (NO) binds to metal centers of heme proteins such as guanylate cyclase, hemoglobin, myoglobin and cytochrome P450.[23,24] NO gas binds to some (por)Fe(R) complexes to form organometallic nitrosyl adducts (por)Fe(NO)(R) (Eq. 3.1).[25,26] Our group reported the synthesis and characterization of the organoruthenium nitrosyl porphyrins (TTP)Ru(NO)R via the reaction of the (TTP)Ru(NO)Cl precursor

with Grignard reagents (Eq. 3.2).[27,28] The single-crystal X-ray structures of

$$(por)FeR + NO \longrightarrow (por)Fe(NO)R \qquad (3.1)$$

por = TPP, OEP; R = alkyl, aryl

$$(por)Ru(NO)Cl + RMgX \longrightarrow (por)Ru(NO)R \qquad (3.2)$$

por = TTP, OEP; R = *p*-C_6H_4F, Me

(TTP)Ru(NO)(*p*-C_6H_4F) and (OEP)Ru(NO)(*p*-C_6H_4F) reveal unexpectedly bent Ru-N-O moieties with the bond angles of 152° and 157°, respectively. Also, our group successfully extended the study to nitrosyl organoosmium complexes, (por)Os(NO)R (por = OEP, TTP; R = ^{t}Bu, ^{i}Pr, Et, Me, *p*-C_6H_4F) using the same procedure for the synthesis of (TTP)Ru(NO)R.[29] The osmium OEP derivatives were also obtained in much higher yields from the two-step reaction of (OEP)Os(CO) with $NOPF_6$ and then RMgX (Eq. 3.3).[29]

$$(OEP)Os(CO) \xrightarrow[(ii)\ RMgX/THF]{(i)\ NOPF_6/CH_2Cl_2} (OEP)Os(NO)R \qquad (3.3)$$

R = Me, Et, ^{i}Pr, ^{t}Bu, *p*-C_6H_4F; X = Cl, Br

In this chapter, we report the preparation of the (T(*p*-X)PP)Ru(NO)R (X = OMe, CF_3; R=Me, Et) complexes. The crystal structure of (T(*p*-OMe)PP)Ru(NO)Et was obtained. To the best of our knowledge, this is the first report on the structural study of nitrosyl organometallic porphyrin complexes containing an alkyl group. Additionally,

the electrochemistry and infrared spectroelectrochemistry of the (T(*p*-OMe)PP)Ru(NO)Me and (T(*p*-OMe)PP)Ru(NO)Et compounds were investigated.

Experimental section

All reactions were performed under an atmosphere of prepurified nitrogen using standard Schlenk glassware and/or in an Innovative Technology Labmaster 100 Dry Box. Solutions for spectral studies were also prepared under a nitrogen atmosphere. Solvents were distilled from appropriate drying agents under nitrogen just prior to use: CH_2Cl_2 (CaH_2), THF (CaH_2), hexane (CaH_2), benzene (Na), toluene (Na).

Chemicals. (T(*p*-OMe)PP)Ru(NO)Cl and (T(*p*-CF_3)PP)Ru(NO)Cl were prepared according to a newly developed method as described in Chapter 2.[30] SO_2 (99%), $Al(Me)_3$ (2.0 M in toluene), $Al(Et)_3$ (1.9 M in toluene), MeMgBr (1.0M in toluene/THF(75:25)) and EtMgBr (1.0M in THF) were purchased from Aldrich Chemical Company and used as received. Ferrocene (Cp_2Fe; Cp = η^5-cyclopentadienyl anion, 98%) was purchased from Aldrich Chemical Co. and sublimed prior to use. NBu_4PF_6 (98%; Aldrich Chemical Company) was recrystallized from hot ethanol. Chloroform–*d* (99.8%) was obtained from Cambridge Isotope Laboratories, and purified by three freeze-pump-thaw cycles, and stored over Linde 4 Å molecular sieves. Elemental analyses were performed by Atlantic Microlab, Norcross, Georgia.

Instrumentation. Electrochemical measurements were performed using a BAS CV-50W instrument (Bioanalytical Systems, West Lafayette, IN). For all cyclic voltammetric measurements, a three-electrode cell with a 3 mm diameter Pt disk working electrode, a Pt wire counter electrode, and a Ag/AgCl reference electrode was utilized. The solutions for all electrochemical experiments were prepared by adding 0.5-1.0 mM

analyte in 10 mL CH_2Cl_2 solution of 0.1M NBu_4PF_6. The solutions were deaerated by bubbling prepurified nitrogen for 10 min before each set of measurements and then the nitrogen atmosphere was maintained during the measurements.

Infrared spectra for the synthetic work were performed on a Bio–Rad FT–155 FTIR spectrometer. For the spectroelectrochemical experiments, the infrared spectra were recorded using a Bruker Vector 22 FTIR spectrometer equipped with a mid-IR fiber-optic dip probe and liquid nitrogen cooled MCT detector (Remspec Corporation, Sturbridge, Ma, USA). Proton NMR spectra were obtained on Varian 300 MHz spectrometers and the signals referenced to the residual signal of the solvent employed ($CHCl_3$ at 7.26 ppm). All coupling constants are in Hz. ESI mass spectra were obtained on a Micromass Q-TOF mass spectrometer.

Preparation of (T(*p*-X)PP)Ru(NO)R compounds (X = OMe, CF_3; R = Me, Et).

Method I. All compounds were synthesized at room temperature under reduced laboratory lighting. The following reaction is representative:

(T(*p*-OMe)PP)Ru(NO)Me. To a toluene solution (20 mL) of (T(*p*-OMe)PP)Ru(NO)Cl (0.050 g, 0.056 mmol) was added $Al(Me)_3$ (0.11 mL, 2.0 M in toluene, 0.22 mmol). The mixture was left to stir under reduced lighting for 30 min, during which time the color changed from brownish green to dark green. The solvent was removed in vacuo, the residue was dissolved in benzene (10 mL), and the solution was transferred to the top of a neutral alumina column (1 x 15 cm) prepared in hexane. Elution with a benzene/hexane (1:1) mixture under nitrogen yielded a green band. The green band was collected and taken to dryness in vacuo. The residue was dissolved in a $CHCl_3$/hexane (5 mL, 4:1), and slow evaporation of the solvent mixture under inert atmosphere gave microcrystals of the product (0.023 g, 47% isolated yield). IR (CH_2Cl_2,

cm^{-1}): ν_{NO} = 1742. IR (KBr, cm^{-1}): ν_{NO} = 1735; also 1606 m, 1528 m, 1510 m, 1286 m, 1243 s, 1174 s, 1070 w, 1015 s, 849 w, 809 m, 715 w, 609 w. ^{1}H NMR ($CDCl_3$, ppm): δ 8.89 (s, 8H, *pyrrole*-H of T(*p*-OMe)PP), 8.15 (m, 8H, *o*-H of T(*p*-OMe)PP), 7.30 (t, 8H, *J* = 6 Hz, *m*-H of T-(*p*-OMe)PP), 4.11 (s, 12H, OC*H*$_3$ of T(*p*-OMe)PP), -6.72 (s, 3H, C*H*$_3$). ESI mass spectrum: *m/z* 879 [(T(*p*-OMe)PP)Ru(NO)Me]$^+$ (28%), 864 [(T(*p*-OMe)PP)Ru(NO)]$^+$ (12%).

(T(*p*-CF_3)PP)Ru(NO)Me. The (T(*p*-CF_3)PP)Ru(NO)Me compound was generated similarly (using 2-fold excess $Al(Me)_3$) in 28% isolated yield. Anal. Calcd for $C_{49}H_{27}F_{12}N_5ORu \cdot 0.03CHCl_3$: C, 56.93; H, 2.63; N, 6.77; Cl, 0.31. Found: C, 56.55; H, 2.98; N, 6.32; Cl, 0.28. IR (CH_2Cl_2, cm^{-1}): ν_{NO} = 1748. IR (KBr, cm^{-1}): ν_{NO} = 1735; also 1616 m, 1404 m, 1324 s, 1168 m, 1129 s, 1068 m, 1013 s, 814 m, 797 m, 717 w. ^{1}H NMR ($CDCl_3$, ppm): δ 8.82 (s, 8H, *pyrrole*-H of T(*p*-CF_3)PP), 8.41 (d, 4H, *J* = 7 Hz, *o*-H of T(*p*-CF_3)PP), 8.33 (d, 4H, *J* = 7 Hz, *o′*-H of T(*p*-CF_3)PP), 8.06 (app t (overlapping d's), 8H, *J* = 6, *m/ m′*-H of T(*p*-CF_3)PP), -6.71 (s, 3H, C*H*$_3$). ESI mass spectrum: *m/z* 1016 [(T(*p*-CF_3)PP)Ru(NO)]$^+$ (39%).

(T(*p*-OMe)PP)Ru(NO)Et. The (T(*p*-OMe)PP)Ru(NO)Et compound was generated similarly (using 2-fold excess $Al(Et)_3$) in 56% isolated yield. Anal. Calcd for $C_{50}H_{41}N_5O_5Ru \cdot 0.1CHCl_3$: C, 66.50; H, 4.58; N, 7.74; Cl, 1.18. Found: C, 66.34; H, 4.53; N, 7.74; Cl, 1.18. IR (CH_2Cl_2, cm^{-1}): ν_{NO} = 1723. IR (KBr, cm^{-1}): ν_{NO} = 1724; also 1606 m, 1527 w, 1510 m, 1349 m, 1245 s, 1174 s, 1070 w, 1015 s, 849 w, 808 m, 715 w, 609 w. ^{1}H NMR ($CDCl_3$, ppm): δ 8.88 (s, 8H, *pyrrole*-H of T(*p*-OMe)PP), 8.15 (m, 8H, *o*-H of T(*p*-OMe)PP), 7.29 (m, 8H, *m*-H of T-(*p*-OMe)PP), 4.11 (s, 12H, OC*H*$_3$ of T(*p*-

OMe)PP), -4.19 (t, 3H, J = 8, CH_2CH_3), -6.00 (q, 2H, J = 8, CH_2CH_3). ESI mass spectrum: *m/z* 893 [(T(*p*-OMe)PP)Ru(NO)Et]$^+$ (30%), 864 [(T(*p*-OMe)PP)Ru(NO)]$^+$ (66%).

A suitable dark green prism-shaped crystal was grown by slow evaporation of CH_2Cl_2/hexane/benzene (2/1/trace) solution of (T(*p*-OMe)PP)Ru(NO)Et at room temperature under inert atmosphere.

Method II. The following reaction is representative of the reactions at room temperature.

(T(*p*-OMe)PP)Ru(NO)Me. To a THF solution (20 mL) of (T(*p*-OMe)PP)Ru(NO)Cl (0.080 g, 0.090 mmol) was added MeMgBr (0.16 mL, 1.4 M in toluene/THF(3:1), 0.22 mmol). The mixture was stirred under reduced lighting for 1 h and all solvent was removed in vacuo. The resulting solid was dissolved in minimum amount of benzene (7 mL), and filtered through a neutral alumina column (1 x 15 cm) with benzene as eluent. The green fraction was collected and taken to dryness in vacuo. The residue was dissolved in a $CHCl_3$/hexane (5 mL, 4:1), and slow evaporation of the solvent mixture under inert atmosphere gave (T(*p*-OMe)PP)Ru(NO)Me (0.018g, 0.020 mmol, 23% isolated yield).

(T(*p*-CF_3)PP)Ru(NO)Me. The (T(*p*-CF_3)PP)Ru(NO)Me compound was generated similarly (2-fold excess using MeMgBr, 5 h reaction time) in 18% isolated yield.

(T(*p*-CF_3)PP)Ru(Me)$_2$. The (T(*p*-CF_3)PP)Ru(Me)$_2$ compound was generated similarly (using 9 fold excess MeMgBr, 1 hour reaction time). ^{1}H NMR ($CDCl_3$, ppm):

δ 8.25 (s, 8H, *pyrrole*-H of T(*p*-CF_3)PP), 8.19 (d, 8H, *J* = 8.4 Hz, *o*-H of T(*p*-CF_3)PP), 7.98 (d, 8H, *J* = 8 Hz, *m*-H of T(*p*-CF_3)PP), -2.71 (s, 6H, CH_3).

(T(*p*-OMe)PP)Ru(NO)Et. The (T(*p*-OMe)PP)Ru(NO)Et compound was generated similarly (using EtMgBr, 1.0 M in THF, 2-fold excess, 80 min reaction time) in 26% isolated yield.

(T(*p*-CF_3)PP)Ru(NO)Et. The (T(*p*-CF_3)PP)Ru(NO)Et compound was generated similarly (using EtMgBr, 1.0 M in THF, 2-fold excess, 1 h reaction time) in 17% isolated yield. IR (CH_2Cl_2, cm^{-1}): ν_{NO} = 1735. IR (KBr, cm^{-1}): ν_{NO} = 1735; also 1617 m, 1405 m, 1324 s, 1169 s, 1128 s, 1069 s, 1013 s, 858 m, 814 m, 716 w, 684 w. ^{1}H NMR ($CDCl_3$, ppm): δ 8.81 (s, 8H, *pyrrole*-H of T(*p*-CF_3)PP), 8.42 (d, 4H, *J* = 8 Hz, *o*-H of T(*p*-CF_3)PP), 8.33 (d, 4H, *J* = 8 Hz, *o′*-H of T(*p*-CF_3)PP), 8.06 (app t (overlapping d's), 8H, *J* = 7, *m/m′*-H of T(*p*-CF_3)PP), -4.17 (t, 3H, *J* = 8, CH_2CH_3), -5.96 (q, 2H, *J* = 8, CH_2CH_3). ESI mass spectrum: *m/z* 1016 $[(T(p\text{-}CF_3)PP)Ru(NO)]^+$ (39%).

Preparation of (T(*p*-OMe)PP)Ru(NO)(SO_2Me). (T(*p*-OMe)PP)Ru(NO)Me (0.023 g, 0.026 mmol) was dissolved in CH_2Cl_2 (20 mL) and SO_2 (g) was bubbled through the solution at -14°C for 20 min, at room temperature for 30 min, and then at -14°C for another 20 min. The solution was sealed under SO_2 pressure, and stirred at room temperature for an additional 30 min. During this time, the color of the solution changed from green to red. Removal of the solvent and excess SO_2 (g) gave (T(*p*-OMe)PP)Ru(NO)(SO_2Me) in 80% yield as judged by NMR spectroscopy. IR (CH_2Cl_2, cm^{-1}): ν_{NO} = 1853. IR (KBr, cm^{-1}): ν_{NO} = 1840 m; also 1606 m, 1511 m, 1349 w, 1288 m, 1245 s, 1175 s, 1019 m, 848 w, 799 m, 713 w, 607 w, 539 w. ^{1}H NMR ($CDCl_3$, ppm):

δ 9.06 (s, 8H, *pyrrole*-H of T(*p*-OMe)PP), 8.19 (m, 8H, *o*-H of T(*p*-OMe)PP), 7.34 (m, 8H, *m*-H of T(*p*-OMe)PP), 4.13 (s, 12, OCH_3 of T(*p*-OMe)PP), -1.35 (s, 3H, CH_3).

Results and discussion

Synthesis and characterization. Two methods were used to prepare the organometallic (T(*p*-X)PP)Ru(NO)R (X = OMe, CF_3; R = Me, Et) complexes. Both of them are based on the synthesis of related species, (TTP)Ru(NO)(*p*-C_6H_4F)[27] and (OEP)Ru(NO)(*p*-C_6H_4F)[28], involving the reaction of (T(*p*-X)PP)Ru(NO)Cl with corresponding trialkyl aluminum reagents or Grignard reagents. As mentioned in Chapter 2, the precursors (T(*p*-X)PP)Ru(NO)Cl can be prepared from the reaction of boron trichloride with (T(*p*-X)PP)Ru(NO)(alkoxide) in high yields (Eq. 2.5). Then, the addition of excess trialkyl aluminum reagents or Grignard reagents to (T(*p*-X)PP)Ru(NO)Cl in toluene/THF under reduced laboratory lighting results in the replacement of the chloride with the alkyl groups over a 30 to 60 min period (eg. Eq. 3.4). If large excess Grignard reagents were added, the dialkyl compounds (T(*p*-X)PP)Ru$(R)_2$ were formed (Eq. 3.5). The progress of the reactions was monitored by TLC (silica gel)

$$\text{(por)Ru(NO)Cl} + \text{Al(R)}_3 \xrightarrow[\text{-"Al(R)}_2\text{Cl"}]{} \text{(por)Ru(NO)R} \qquad (3.4)$$

$$\text{(por)Ru(NO)Cl} \xrightarrow{\text{xs. RMgBr}} \text{(por)Ru(NO)R} + \text{(por)Ru(R)}_2 \qquad (3.5)$$

por = T(*p*-OMe)PP, T(*p*-CF_3)PP
R = Me, Et

and IR spectroscopy. For example, in the preparation of (T(*p*-OMe)PP)Ru(NO)Me, the

disappearance of the ν_{NO} band of the starting (T(*p*-OMe)PP)Ru(NO)Cl complex at 1851 cm^{-1} in CH_2Cl_2 and the appearance of the new ν_{NO} band at 1742 cm^{-1} suggested that the reaction was complete. The products were separated by column chromatography on neutral alumina using a 1:1 benzene/hexane mixture as eluent. The first green band was collected and dried under vacuo to give the nitrosyl organometallic compound (T(*p*-OMe)PP)Ru(NO)Me. In order to minimize the decomposition of the nitrosyl alkyl products, the chromatography was performed under nitrogen and reduced lighting. The nitrosyl organometallic compounds have been characterized by IR and ^1H NMR spectroscopy. Table 3.1 lists the infrared nitrosyl stretching frequencies of selected nitrosyl organoruthenium complexes and their chloro precursors. The ν_{NO}s of the (por)Ru(NO)R compounds are much lower than those of their chloro precursors. For example, the IR spectrum of (T(*p*-CF_3)PP)Ru(NO)Me (as a KBr pellet) shows a ν_{NO} band at 1735 cm^{-1}, which is 112 cm^{-1} lower than that of (T(*p*- CF_3)PP)Ru(NO)Cl at 1847 cm^{-1}. This *trans* effect supports the idea that alkyl groups are better electron donors than halides. In addition, the ν_{NO} of (TTP)Ru(NO)(*p*-C_6H_4F) is at 1773 cm^{-1} and is significantly higher than those of the alkyl analogues (T(*p*-X)PP)Ru(NO)R (X = OMe, CF_3; R = Me, Et) (Table 3.1), which is consistent with the better electron donating ability of alkyl groups compared to aryl groups. The ^1H NMR spectra of the (T(*p*-X)PP)Ru(NO)R compounds are similar to those of the chloro precursors with the additional signals of the alkyl ligands. In the case of (T(*p*-OMe)PP)Ru(NO)Me, ^1H NMR spectroscopy showed a new signal at -6.72 ppm due to the protons on the axial methyl group. The large upfield shift of methyl group in the spectrum is caused by the

Table 3.1. Infrared nitrosyl stretching frequencies of selected nitrosyl organoruthenium porphyrins and their precursors.

Compound	ν_{NO} (KBr, cm^{-1})	Reference
(TTP)Ru(NO)Cl	1845	Chapter 2
(OEP)Ru(NO)Cl	1829	Chapter 2
(T(*p*-OMe)PP)Ru(NO)Cl	1844	Chapter 2
(T(*p*-CF_3)PP)Ru(NO)Cl	1847	Chapter 2
(T(*p*-OMe)PP)Ru(NO)Me	1735	This work
(T(*p*-OMe)PP)Ru(NO)Et	1724	This work
(T(*p*-CF_3)PP)Ru(NO)Me	1735	This work
(T(*p*-CF_3)PP)Ru(NO)Et	1735	This work
(TTP)Ru(NO)(*p*-C_6H_4F)	1773	27
(OEP)Ru(NO)(*p*-C_6H_4F)	1759	28

deshielding effect from the porphyrin macrocycle. The same upfield chemical shifts of the protons on the axial groups were observed in (T(*p*-CF_3)PP)Ru(NO)Me at -6.71 ppm (CH_3), (T(*p*-OMe)PP)Ru(NO)Et at -4.19 ppm (CH_2CH_3) and -6.00 ppm (CH_2CH_3), (T(*p*-CF_3)PP)Ru(NO)Et at -4.17 ppm (CH_2CH_3) and -5.96 ppm (CH_2CH_3), and (T(*p*-OMe)PP)Ru(NO)(SO_2Me) at -1.35 ppm (CH_3). The chemical shift data shown above indicates that under the similar environments, the closer the H atoms are to the macrocycle, the more upfield the observed chemical shift. In addition, the (T(*p*-CF_3)PP)Ru$(Me)_2$ compound was probably formed from the further reaction of (T(*p*-CF_3)PP)Ru(NO)Me with MeMgBr. Similar formation of (TTP)Ru(NO)$(Me)_2$[27] and

(OEP)Os(R)$_2$ (R = Me, Et, ^{t}Bu, p-C_6H_4F)[29] have been reported. ^{1}H NMR spectroscopy and density functional theoretical studies on these Ru^{IV} and Os^{IV} dialkyl and diaryl porphyrin complexes have confirmed their +4 oxidation states.[31,32]

As alkyl donors, the trialkyl aluminum reagents performed better than the Grignard reagents in the preparation of (T(p-OMe)PP)Ru(NO)Me, (T(p-OMe)PP)Ru(NO)Et and (T(p-CF_3)PP)Ru(NO)Me. The reactions were fast and clean and no dialkyl byproducts were observed under our conditions. Additionally, the yields were much higher using the trialkyl aluminum reagents than using the Grignard reagents. However, an exception is the case of (T(p-CF_3)PP)Ru(NO)Et, where the use of Al(Et)$_3$ is less efficient than EtMgBr due to the preferred formation of (T(p-CF_3)PP)Ru(Et)$_2$ when triethylaluminum was used.

The nitrosyl ruthenium sulfinato complex, (T(p-OMe)PP)Ru(NO)(SO_2Me), was prepared by bubbling SO_2 gas into a CH_2Cl_2 solution of (T(p-OMe)PP)Ru(NO)Me. The NO stretching frequency shifts from 1742 cm^{-1} to 1853 cm^{-1} because of the presence of the more electron-withdrawing sulfinato group. In the ^{1}H NMR spectrum of the product, a large chemical shift difference from -6.71 ppm to -1.35 ppm of the protons on the methyl group was observed which is consistent with the increased distance between the methyl group and the porphyrin ring. Prior to this work, only two metal nitrosyl sulfinato complexes were prepared from the insertion of SO_2 into a metal-carbon bond.[27,33] Interestingly, the SO_2 insertion reaction did not occur with (T(p-OMe)PP)Ru(Me)$_2$, which indicates the nitrosyl group imparts a *trans* effect which makes the ruthenium-carbon bond weaker in (T(p-OMe)PP)Ru(NO)Me than that in (T(p-OMe)PP)Ru(Me)$_2$.

Molecular structure

A crystal of (T(*p*-OMe)PP)Ru(NO)Et suitable for X-ray crystallography was grown in CH_2Cl_2/hexane (2:1) solution with trace benzene by slow evaporation in the dark. The molecular structure and the porphyrin atom displacements for (T(*p*-OMe)PP)Ru(NO)Et are shown in Figure 3.1a and 3.1b, respectively. Selected bond lengths and angles are listed in Table 3.2. There are several interesting structural features for the (T(*p*-OMe)PP)Ru(NO)Et compound. Unlike most of the $\{MNO\}^6$ ruthenium nitrosyl complexes having linear RuNO geometries, (T(*p*-OMe)PP)Ru(NO)Et has a significantly bent RuNO geometry with an angle of 153.0(3)º. There are only two related $\{RuNO\}^6$ compounds, (TTP)Ru(NO)(*p*-C_6H_4F)[27] and (OEP)Ru(NO)(*p*-C_6H_4F)[28], that contain similar bent RuNO conformation with the angles of 152º and 154.9(3)º respectively. The nitrosyl organoiron analogue, (OEP)Fe(NO)(*p*-C_6H_4F) also shows a bent FeNO group with an angle of 157.4(2)º.[28]

Crystal packing in the (T(*p*-OMe)PP)Ru(NO)Et complex is depicted in Figure 3.2. The closest intermolecular distance involving the nitrosyl group is between the nitrosyl O1 and a nearby methoxyl group on a neighboring molecule at an O1···O2A distance of 3.47 Å. The next closest intermolecular distance (3.51 Å) is between the nitrosyl N5 and a methoxyl group C41B atom on a neighboring molecule. The crystal packing of the known (TTP)Ru(NO)(*p*-C_6H_4F)[28] complex is similar to that of (T(*p*-OMe)PP)Ru(NO)Et reported here. The closest intermolecular distance (3.23 Å) of (TTP)Ru(NO)(*p*-C_6H_4F) involving the NO group is between the nitrosyl oxygen atom and a tolyl group carbon atom.[28] In the case of the Ru and Fe OEP derivatives, (OEP)Ru(NO)(*p*-C_6H_4F) and (OEP)Fe(NO)(*p*-C_6H_4F), the closest intermolecular distances are both between the

(a)

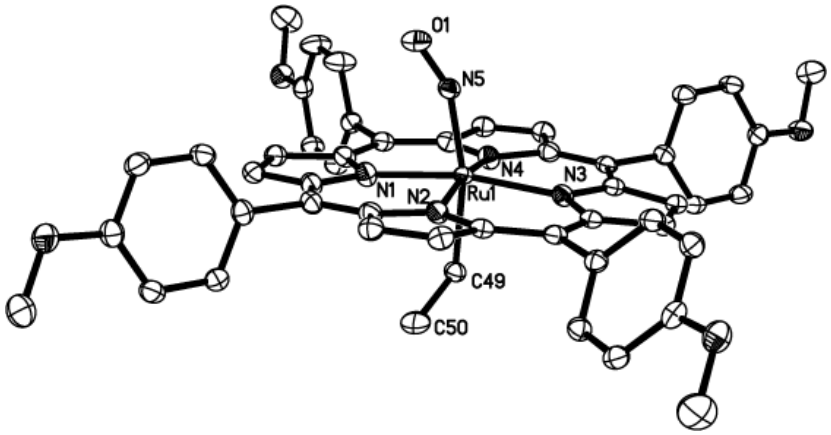

(b)

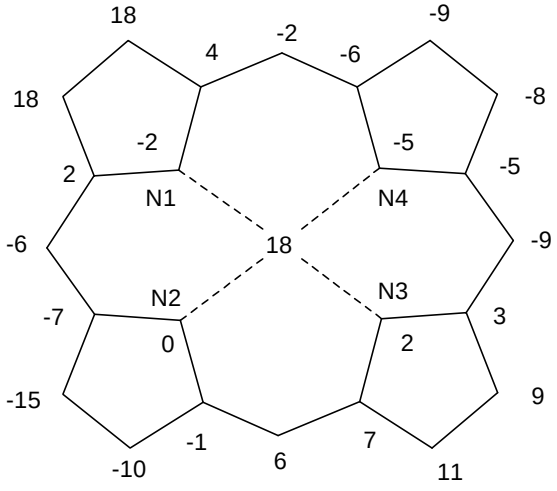

Figure 3.1. (a) Molecular structure of (T(*p*-OMe)PP)Ru(NO)Et. Hydrogen atoms have been omitted for clarity. (b) Perpendicular atom displacements (in units of 0.01 Å) of the porphyrin core from the 24-atom mean porphyrin plane.

Table 3.2. Selected bond lengths (Å) and angles (°) for (T(*p*-OMe)PP)Ru(NO)Et.

Bond Lengths (Å)			
N(5)-O(1)	1.155(3)	Ru(1)-N(3)	2.076(2)
Ru(1)-N(5)	1.826(2)	Ru(1)-N(4)	2.064(2)
Ru(1)-N(1)	2.063(2)	Ru(1)-C(49)	2.120(3)
Ru(1)-N(2)	2.046(2)	C(49-C(50)	1.516(5)
Bond Angles (°)			
O(1)-N(5)-Ru(1)	153.0(3)	N(2)-Ru(1)-N(1)	90.5(1)
N(5)-Ru(1)-N(2)	93.0(1)	N(3)-Ru(1)-N(1)	168.7(1)
N(5)-Ru(1)-N(3)	85.0(1)	N(4)-Ru(1)-N(1)	89.6(1)
N(2)-Ru(1)-N(3)	89.2(6)	N(5)-Ru(1)-C(49)	165.5(1)
N(5)-Ru(1)-N(4)	97.0(1)	N(2)-Ru(1)-C(49)	88.4(1)
N(2)-Ru(1)-N(4)	170.0(1)	N(3)-Ru(1)-C(49)	88.1(1)
N(3)-Ru(1)-N(4)	88.8(1)	N(4)-Ru(1)-C(49)	81.7(1)
N(5)-Ru(1)-N(1)	85.0(1)	N(1)-Ru(1)-C(49)	80.6(1)

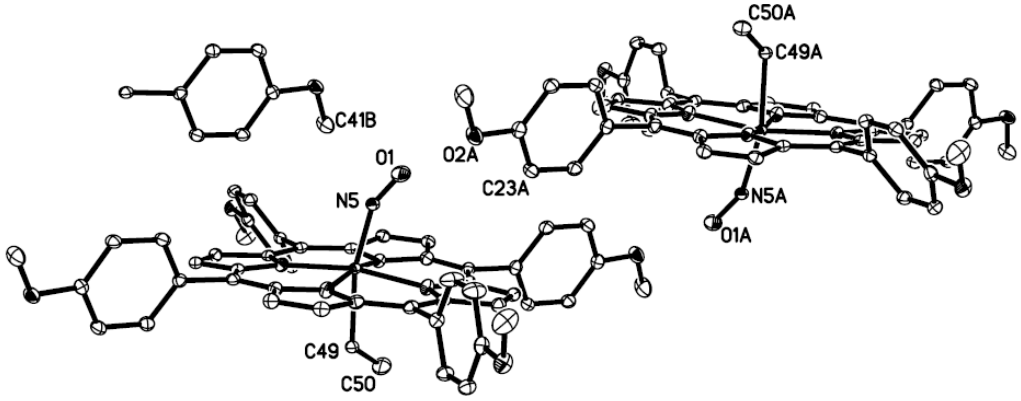

Figure 3.2. Crystal packing diagram of (T(*p*-OMe)PP)Ru(NO)Et showing the closest intermolecular distance involving the NO group. Most parts of the porphyrin molecule B have been omitted for clarity. Closest intermolecular contacts in Å: O1···O2A = 3.47, O1···C23A = 3.59, N5···C41B = 3.51.

two nitrosyl oxygen atoms from adjacent molecules at 2.88 Å and 2.92 Å, respectively.[28] These intermolecular distances indicate that crystal packing does not affect the conformation of the MNO groups significantly.

In addition, the N(O) atom of the nitrosyl group is tilted off the normal to the porphyrin 24-atom plane by 11.7º (α in Table 3.3). The NO group is further tilted 27º (β) from the Ru-N(O) vector in the direction away from the porphyrin normal. The tilting nitrosyl group has also been observed in other nitrosyl metalloporphyrin complexes and is considered a new intrinsic feature of this class of complexes. The C49 atom of the axial ethyl group is also tilted by 5º (γ) in the general direction of the NO tilt and the C-Ru-N angle is 165.5(1)º. The similar tilting of the metal-carbon bonds were reported in (OEP)RuNp (Np = neopentyl)[34] at 12.7º and (TPP)Os($CH_2Si(CH_3)_3)_2$[35] at 18.5º and 21.8º. The angles for these off-axes tilts for the related complexes are shown in Table 3.3.

Table 3.3. Axial ligand tilts (°) in organometallic porphyrins (por)M(NO)R, (por)M(R) and (por)M$(R)_2$.

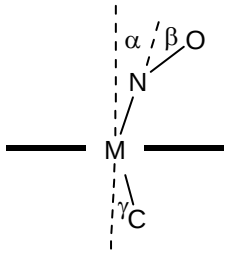

Compound	α*	β	γ*	Reference
(T(*p*-OMe)PP)Ru(NO)Et	11.7	27.0	5.0	This work
(TTP)Ru(NO)(*p*-C_6H_4F)	12.0	27.8	4.3	27
(OEP)Ru(NO)(*p*-C_6H_4F)	10.8	25.1	3.5	28
(OEP)Fe(NO)(*p*-C_6H_4F)	9.2	22.6	3.1	28
(OEP)RuNp			12.7	34
(TPP)Os($CH_2Si(CH_3)_3)_2$			18.5, 21.8	35

*Tilts of the N and C atoms from the normal to the porphyrin 24-atom plane

Although we have not done any calculations on the tilting of the ethyl and nitrosyl ligand and the bending of the NO ligand in (T(*p*-OMe)PP)Ru(NO)Et, extended Hückel molecular orbital (MO) and preliminary hybrid Hartree-Fock density functional calculations (HF/DF) have been performed for the iron analogue (porphine)Fe(NO)(*p*-C_6H_4F) which has a similar tilting and bending revealed in its crystal structure.[28] The related tilting and bending angles of the nitrosyl group are also listed in Table 3.3. Based on the calculations on the (porphine)Fe(NO)(*p*-C_6H_4F) complex, we believe that the unexpected tilting and bending of nitrosyl group of (T(*p*OMe)PP)Ru(NO)Et are due to

electronic factors. The tilt of the nitrosyl group results from the interaction of the NO π* orbital with metal (mixed) orbitals of metal $d_{x^2-y^2}$ and d_{xz} orbitals, and the changes of total energy and individual orbital energies should be small. Further bending of the nitrosyl group also effectively increases the bonding interactions between the NO and metal mixing orbital (Fig. 3.3). In addition, DFT calculations on the (porphine)Ru(NO)Ph complex

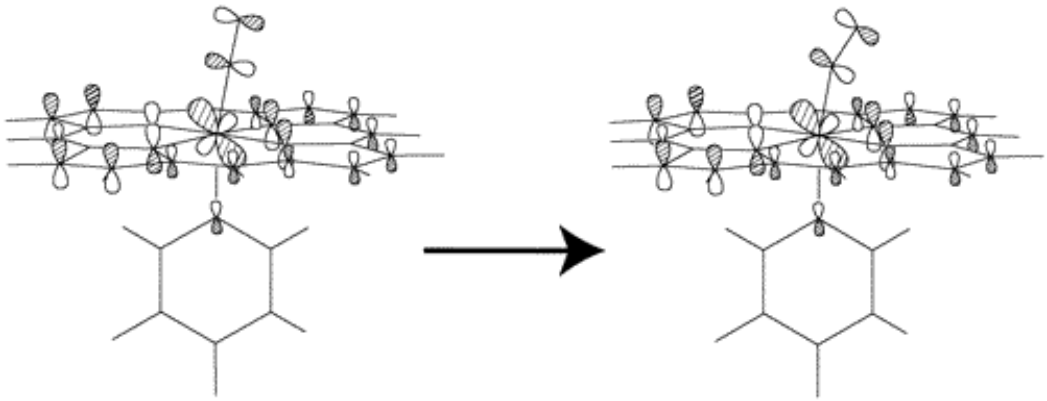

Figure 3.3. Tilting and bending nitrosyl conformation on the right has better bonding interaction between the NO π* orbital and metal (mixed) orbital than tilting and linear conformation on the left in the model (porphine)Fe(NO)(*p*-C_6H_4F). (Reference 28)

also revealed a bending and tilting MNO moiety.[32] Furthermore, according to the data shown in Table 3.3, it appears that the metal-carbon bond tilt is more significant without a nitrosyl group at its *trans* position. Based on the previously reported DFT calculations,[32,36,37] both nitrosyl and alkyl ligands have interactions with the d_{xz} orbital of the metal center. When a strong electron acceptor such as the nitrosyl group presents at the *trans* position of alkyl groups, significant electron density could be drawn towards to

the nitric oxide group, which results in the less interaction between the p orbital of alkyl group and the d orbital of metal center. This may explain the smaller tilting angle of metal-carbon bond in (T(*p*-OMe)PP)Ru(NO)Et.

A question that arises is: what makes these classes of $\{MNO\}^6$ compounds display bent MNO geometries? Are these unique compounds? At this point in time, we do not know the answer. We have considered two possibilities: (1) the improved quality of crystallographic determinations of ordered structures may be the reason why these bending features are observed (not observed previously in highly disordered structures), (2) the presence of electron-donating trans-ligands enable the bending of the MNO moiety. Although the second possibility is an attractive one, we note that the (por)Fe(NO)(NO_2) compound also display a bent FeNO moiety.[38] We are continuing to investigate the generality (or not) of this bending feature in $\{MNO\}^6$ compounds.

Furthermore, the Ru-N(O) bond length in (T(*p*-OMe)PP)Ru(NO)Et is 1.826(2) Å which is 0.09 Å longer than average Ru-N(O) bond length of other $\{RuNO\}^6$ complexes.[28] The significant Ru-N(O) lengthening results from the strong σ-bonding ethyl group *trans* to nitrosyl in (T(*p*-OMe)PP)Ru(NO)Et. The Ru-C(ethyl) bond length is 2.120(3) Å which is expected to be longer than the previously reported Ru-C(Np) bond length in (OEP)Ru(Np)[34] because of the *trans*-effect of the nitrosyl group. However, it is close to the reported Ru-carbon bond length in (OEP)Ru(Np) at 2.069(7) Å and 2.12(1) Å because of the steric effect of the bulky neopentyl group which appears to elongate the Ru-carbon bond in (OEP)Ru(Np).[34] The bond lengths of Ru-N(O) and Ru-C(axial) of related ruthenium porphyrin compounds[21,27,28,30,34,39-51] are listed in Table 3.4 and Table 3.5.

Table 3.4. Ru-N(nitrosyl) bond lengths in nitrosyl ruthenium porphyrin compounds.

Compound	Ru-N(O)	Reference
(TPP)Ru(NO)(ONO)	1.72(2)	47
(TTP)Ru(NO)(ONO)	1.752(6)	41
(OEP)Ru(NO)(ONO)	1.758(7)	47
(TTP)Ru(NO)(OMe)	1.84(4)	39
(TPP)Ru(NO)(OH)	1.726(9)	47
(TTP)Ru(NO)(OH)	1.751(5)	41
(OEP)Ru(NO)(OH)	1.723(11)	47
(OEP)Ru(NO)Cl	1.803(7)	30
$[(OEP)Ru(NO)(H_2O)]^+$	1.888(5)	42
(TTP)Ru(NO)(NSO)	1.737(5)	40
(OEP)Ru(NO)(*S*-NACysMe)[a]	1.790(5)	50,51
$(OEP)Ru(NO)(SCH_2CH_2SH)$	1.802(9)	46
$(OEP)Ru(NO)(SC(Me)_2CH_2NHC(O)Me))$	1.769(3)	50
$(OEP)Ru(NO)(O{=}C(Me)NHCH_2C(Me)_2SH)]^+$	1.708(6)	50
(TTP)Ru(NO)(*p*-C_6H_4F)	1.807	27
(OEP)Ru(NO)(*p*-C_6H_4F)	1.807(3)	28
(T(*p*-OMe)PP)Ru(NO)Et	1.826(2)	This work

[a] *S*-NACysMe = *N*-acetyl-*S*-nitroso-L-cysteinate methyl ester

Table 3.5. Ru-C bond lengths in ruthenium porphyrin compounds with axial alkyl/aryl (non-carbonyl) ligands.

Compound	Ru-C (Å)	Reference
(OEP)Ru(C_6H_5)	2.005(7)	21
(OEP)Ru(Neop)	2.069(7)	34
	2.12(1)	
[(OEP)Ru(Neop)]$_2$(μ-Li)$_2$	2.100(3)	34
[(OEP-*N*-Ph)Ru(C_6H_5)]$_2$$BF_4$	1.999(4)	48
[(TTP)Ru(=CPh_2)(CH_3OH)]	1.845(3)	45
[(TTP)Ru[=C(3-$C_6H_4CF_3$)$_2$](py)	1.868(3)	44
[(TTP)Ru[=C($COPh$)$_2$](py)	1.877(8)	44
(TPP)Ru[=C(CO_2Et)$_2$](MeOH)	1.829(9)	43
(TTP)Ru(NO)(*p*-C_6H_4F)	2.095(6)	27
(OEP)Ru(NO)(*p*-C_6H_4F)	2.111(3)	28
(T(*p*-OMe)PP)Ru(NO)Et	2.120(3)	This work

The Ru-N(porphyrin) bond lengths in (T(*p*-OMe)PP)Ru(NO)Et range from 2.046 (2) to 2.076(2) Å, and the Ru atom is displaced by 0.18 Å from the 24-atom mean porphyrin plane toward the nitrosyl ligand. To the best of our knowledge, this is the first reported crystal structure of a nitrosyl-alkyl porphyrin for any metal.

Cyclic voltammetry and infrared spectroelectrochemistry

The redox behavior of (T(*p*-OMe)PP)Ru(NO)Me and (T(*p*-OMe)PP)Ru(NO)Et in CH_2Cl_2 were examined at room temperature. The cyclic voltammograms are shown in Figure 3.4. Within the solvent limit, the (T(*p*-OMe)PP)Ru(NO)Me compound exhibits

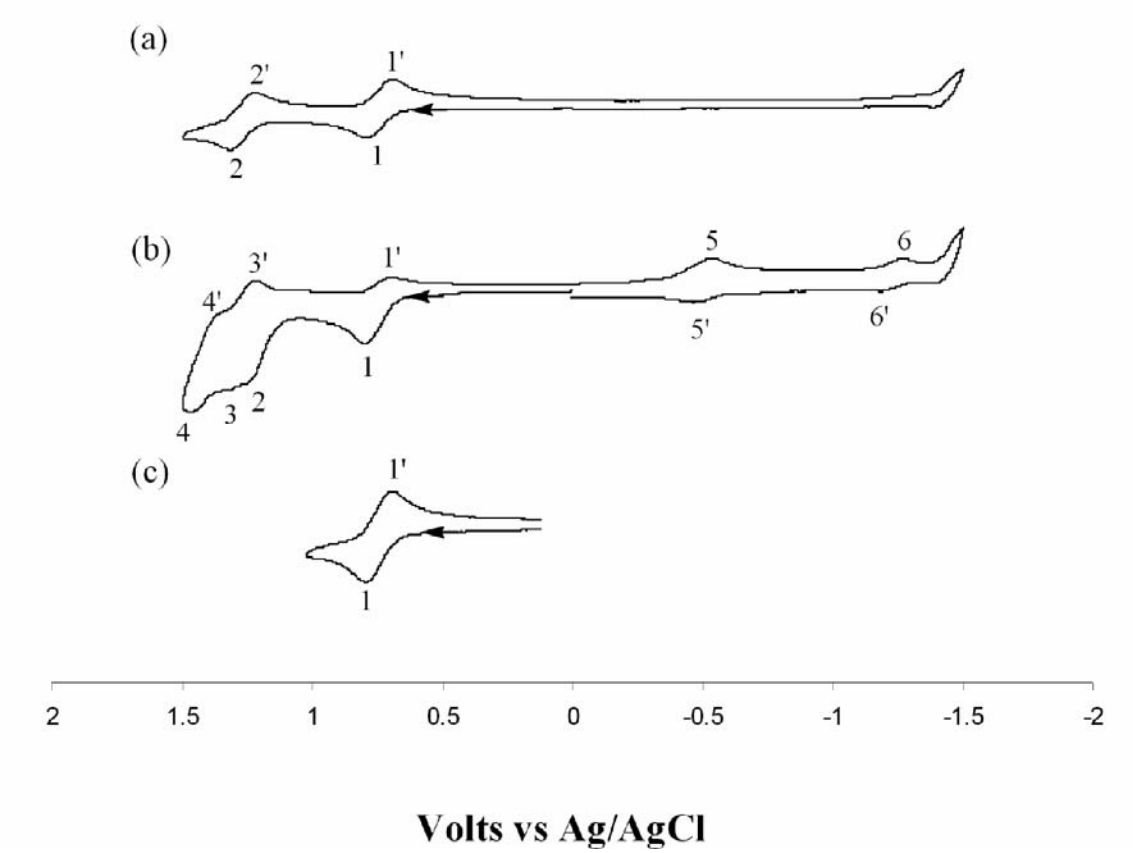

Figure 3.4. Cyclic voltammograms of (T(*p*-OMe)PP)Ru(NO)Me and (T(*p*-OMe)PP)Ru(NO)Et in CH_2Cl_2 containing 0.1 M NBu_4PF_6 and at a scan rate of 200 mV/s. Potentials are referenced to the Ag/AgCl couple. (a) Complete cyclic voltammogram of (T(*p*-OMe)PP)Ru(NO)Me. (b) Complete cyclic voltammogram of (T(*p*-OMe)PP)Ru(NO)Et. (c) Partial cyclic voltammogram of (T(*p*-OMe)PP)Ru(NO)Et showing only the first oxidation.

two reversible oxidations at +0.74 V (couple 1/1' in Figure 3.4a) and +1.23 V (couple 2/2' in Figure 3.4a) vs the Ag/AgCl couple. The peak separations of the first and second oxidations ($\Delta E_p = |E_{pa} - E_{pc}|$) are 147 mV and 150 mV, respectively. These values are similar to that determined for the ferrocene-ferrocinium couple (133 mV) under identical conditions, which indicate that the two oxidations are electrochemically reversible, single-electron processes as shown in equations 3.6 and 3.7.[52] In addition, these two

$$(T(p\text{-OMe})PP)Ru(NO)Me \rightleftharpoons [(T(p\text{-OMe})PP)Ru(NO)Me]^+ + e^- \qquad (3.6)$$

$$[(T(p\text{-OMe})PP)Ru(NO)Me]^+ \rightleftharpoons [(T(p\text{-OMe})PP)Ru(NO)Me]^{2+} + e^- \qquad (3.7)$$

oxidations are chemically reversible processes, with anodic to cathodic peak current ratios (i_{pc}/i_{pa}) of ~1.0. Furthermore, plots of i_{pa} vs. (scan rate)$^{1/2}$ for both the first and the second oxidations show linear relationships that indicates that these two oxidations are diffusion-controlled.[52]

In order to investigate the first oxidation further, difference IR spectra were recorded at room temperature while the electrode was held at the potential just over the first oxidation using a fiber-optic dip probe.[53] The IR spectra, using unoxidized T(*p*-OMe)PP)Ru(NO)Me as the background, showed the changes that occured in the FTIR spectra between 1550 and 2000 cm^{-1} after the first oxidation. As seen in Figure 3.5a, the NO absorbance at 1742 cm^{-1} of starting T(*p*-OMe)PP)Ru(NO)Me disappeared and a new NO absorbance at 1794 cm^{-1} of the first oxidation product formed. The relatively small shift in ν_{NO} ($\Delta\nu_{NO}$ = 52 cm^{-1}) is indicative of the first oxidation that is porphyrin-centered. The oxidized tetraarylporphyrins (π-cation radicals) have a characteristic IR

band in the region of 1270-1295 cm^{-1}. Unfortunately, strong absorption of the support electrolyte in this region does not allow for the identification of this band. Additionally, a band at 1599 cm^{-1} was also observed in IR spectra of both two complexes. In order to assign this band, the same IR spectroelectrochemical experiments of the non-nitrosyl H_2T(*p*-OMe)PP and T(*p*-OMe)PP)Ru(CO) were performed, and similar bands ~1600 cm^{-1} were observed, which indicates that the bands are most likely due to the porphyrin upon oxidation. Similar bands have been assigned to the phenyl rings of other metalloporphyrin complexes.[54]

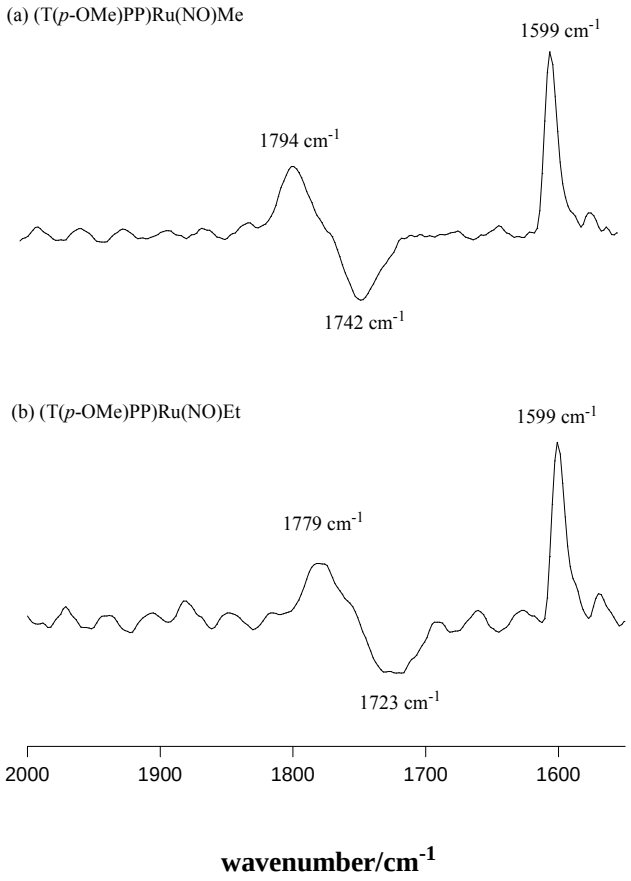

Figure 3.5. Difference FTIR spectra after controlled-potential oxidation of (a) (T(*p*-OMe)PP)Ru(NO)Me and (b) (T(*p*-OMe)PP)Ru(NO)Et.

The cyclic voltammogram of (T(*p*-OMe)PP)Ru(NO)Et compound is shown in Figure 3.4b. The (T(*p*-OMe)PP)Ru(NO)Et compound displayed three partial reversible process, one irreversible oxidation, and two small reduction couples under the full scan within the solvent potential limit. However, when the potential scan was reversed just after the first oxidation, a well-defined reversible first oxidation was observed at +0.74 V, which is shown in Figure 3.4c (couple 1/1'). According to the ΔE_p ($|E_{pa} - E_{pc}|$ = 141 mV), anodic to cathodic peak current ratios (i_{pa}/i_{pc}) and plots of i_{pa} vs. (scan rate)$^{1/2}$, the first oxidation is a chemically and electrochemically reversible, diffusion-controlled, one electron-transfer process (Eq. 3.8).[52,55]

$$(T(p\text{-OMe})PP)Ru(NO)Et \rightleftharpoons [(T(p\text{-OMe})PP)Ru(NO)Et]^+ + e^- \qquad (3.8)$$

The IR spectroelectrochemistry results for the first oxidation of (T(*p*-OMe)PP)Ru(NO)Et are similar to that of (T(*p*-OMe)PP)Ru(NO)Me (Fig. 3.5b). The data show the loss of the NO absorbance at 1723 cm^{-1} of the starting (T(*p*-OMe)PP)Ru(NO)Et, and a presence of the NO absorbance at 1779 cm^{-1} of oxidized product. The small NO band shift ($\Delta\nu_{NO}$ = 56 cm^{-1}) indicates that (T(*p*-OMe)PP)Ru(NO)Et also has a porphyrin-based first oxidation.

When the potential scan went further within the solvent limit, several more oxidations with weak returns (peak 2, couple 3/3', 4/4') and two daughter redox couples at -0.50 V and -1.22 V associated with those oxidations were observed (couple 5/5', 6/6' in Figure 3.4b). Interestingly, the first oxidation becomes irreversible (couple 1/1' in Figure 3.4b) in the full scan within the solvent limit. It may be caused by the interaction of the unstable second oxidation product with either the analyte, the first oxidation product, or the solvent.

As expected, the first oxidation potentials of (T(*p*-OMe)PP)Ru(NO)R (R = Me, Et) at 0.74 V are significantly lower than that of the reported (T(*p*-OMe)PP)Ru(NO)Cl compound at 0.93 V (Chapter 2).[30] Additionally, Shawn Carter, in our group, reported first oxidation potential of the (OEP)Ru(NO)(SEt) and (OEP)Ru(NO)(OEt) complexes at 0.81 V and 0.87 V, respectively.[56] The lower first oxidation potentials of the (T(*p*-OMe)PP)Ru(NO)R complexes result from the better electron donor, alkyl groups which make (T(*p*-OMe)PP)Ru(NO)R more electron rich and easier to oxidize than the (OEP)Ru(NO)(XEt) (X = S, O) and (T(*p*-OMe)PP)Ru(NO)Cl complexes. The electrochemical data are summarized in Table 3.6.

Table 3.6. Half-wave and anodic potentials in volts for the first oxidations of selected six-coordinate nitrosyl ruthenium porphyrins vs Ag/AgCl in CH_2Cl_2, 0.1 M NBu_4PF_6.

Compound	1st Oxidation	Reference
(T(*p*-OMe)PP)Ru(NO)Me	0.74	This work
(T(*p*-OMe)PP)Ru(NO)Et	0.74	This work
(OEP)Ru(NO)(SEt)	0.81	56
(OEP)Ru(NO)(OEt)	0.87	56
(T(*p*-OMe)PP)Ru(NO)Cl	0.93	30

Conclusion

In summary, new nitrosyl organoruthenium porphyrin complexes, (T(*p*-X)PP)Ru(NO)R complexes (X = OMe, CF_3; R = Me, Et), have been prepared using two alkylating agents, $Al(R)_3$ and RMgBr. The trialkyl aluminum reagents performed better than the Grignard reagents in the preparation of (T(*p*-OMe)PP)Ru(NO)Me, (T(*p*-OMe)PP)Ru(NO)Et and (T(*p*-CF_3)PP)Ru(NO)Me. However, in the case of preparation of (T(*p*-CF_3)PP)Ru(NO)Et and (T(*p*-CF_3)PP)$Ru(Me)_2$, the Grignard reagents were better alkyl donors. The ν_{NO} of these nitrosyl organoruthenium complexes and their chloro precursors support the increasing electron donating ability of chloro < aryl < alkyl groups. The (T(*p*-OMe)PP)$Ru(SO_2Me)$ compound was obtained by the reaction of SO_2 with (T(*p*-OMe)PP)Ru(NO)Me. Judging by the lack of reaction between SO_2 and (T(*p*-OMe)PP)$Ru(Me)_2$, we believe that the nitrosyl group in the (T(*p*-OMe)PP)Ru(NO)Me has a strong *trans* effect on the ruthenium-carbon bond in (T(*p*-OMe)PP)Ru(NO)Me weakening the metal-carbon bond.

The solid-state structure of (T(*p*-OMe)PP)Ru(NO)Et was obtained. An unusual bent ruthenium-nitrosyl linkage with the angle of 153.0(3)º was observed which is consistent with the previously reported bent Ru-NO conformation in (TTP)Ru(NO)(*p*-C_6H_4F)[27] and (OEP)Ru(NO)(*p*-C_6H_4F)[28]. The structure reported here is the first organometallic nitrosyl porphyrin with an alkyl group as the axial ligand.

We have also examined the redox behavior of (T(*p*-OMe)PP)Ru(NO)Et and (T(*p*-OMe)PP)Ru(NO)Me in CH_2Cl_2. The (T(*p*-OMe)PP)Ru(NO)Me compound exhibits two chemically and electrochemically reversible oxidations in the solvent limit. Similarly, the (T(*p*-OMe)PP)Ru(NO)Et compound also displays a chemically and electrochemically reversible first oxidation. In addition, the IR spectroelectrochemistry data indicate a

porphyrin-centered first oxidation for both (T(*p*-OMe)PP)Ru(NO)Et and (T(*p*-OMe)PP)Ru(NO)Me.

References

(1) Brothers, P. J.; Collman, J. P. *Acc. Chem. Res.* **1986**, *19*, 209-215.
(2) Setsune, J.-I.; Dolphin, D. *Can. J. Chem.* **1987**, *65*, 459-467.
(3) Mansuy, D. *Pure Appl. Chem.* **1987**, *59*, 759-770.
(4) Brown, K. L.; Cheng, S.; Marques, H. M. *Inorg. Chem.* **1995**, *34*, 3038-3049.
(5) Roth, J. R.; Lawrence, J. G.; Bobik, T. A. *Annu. Rev. Microbiol.* **1996**, *20*, 137-181.
(6) Augusto, O.; Kunze, K. L.; Ortiz de Montellano, P. R. *J. Biol. Chem.* **1982**, *257*, 6231-6241.
(7) Ortiz de Montellano, P. R.; Kerr, D. E. *Biochemistry* **1985**, *24*, 1147-1152.
(8) Ortiz de Montellano, P. R.; Kunze, K. L. *J. Am. Chem. Soc.* **1981**, *103*, 6534-6536.
(9) Saito, S.; Itano, H. A. *PNAS* **1981**, *78*, 5508-5512.
(10) Ortiz de Montellano, P. R.; Augusto, O.; Viola, F.; Kunze, K. L. *J. Biol. Chem.* **1983**, *258*, 8623-8629.
(11) Ortiz de Montellano, P. R.; Watanabe, M. D. *Mol. Pharmacol.* **1987**, *31*, 213-219.
(12) *Cytochrome P450 Structure, Mechanism, and Biochemistry*; Ortiz de Montellano, P. R., Ed.; Plenum Press: New York and London, 2005.
(13) Summers, J. S.; Petersen, J. L.; Stolzenberg, A. M. *J. Am. Chem. Soc.* **1994**, *116*, 7189-7195.
(14) Cocolios, P.; Lagrange, G.; Guilard, R. *J. Chem. Soc. Dalton Trans.* **1984**, 567-574.
(15) Cocolios, P.; Lagrange, G.; Guilard, R. **1983**, *253*, 65-79.
(16) Cao, Y.; Petersen, J. L.; Stolzenberg, A. M. *Inorg. Chim. Acta* **1997**, *263*, 139-148.
(17) Bill, E.; Schünemann, V.; Trautwein, A. X.; Weiss, R.; Fischer, J.; Tabard, A.; Guilard, R. *Inorg. Chim. Acta* **2002**, *339*, 420-426.
(18) Oh, Y.; Swenson, D.; Goff, H. M. *Bull. Korean. Chem. Soc.* **2003**, *24*, 167-172.
(19) Tabard, A.; Cocolios, P.; Lagrange, G.; Gerardin, R.; Hubsch, J.; Lecomte, C.; Zarembowitch, J.; Guilard, R. *Inorg. Chem.* **1988**, *27*, 110-117.
(20) Guilard, R.; Tabard, A.; Caemelbecke, E. V.; Kadish, K. M. *The Porphyrin Handbook*; Academic Press: San Diego, CA, 2000; Vol. 3.
(21) Ke, M.; Rettig, S. J.; James, B. R.; Dolphin, D. *Chem. Commun.* **1987**, 1110-1112.
(22) Ke, M.; Sishta, C.; James, B. R.; Dolphin, D.; Sparapany, J. W.; Ibers, J. A. *Inorg. Chem.* **1991**, *30*, 4766-4771.
(23) Deinum, G.; Stone, J. R.; Babcock, G. T.; Marletta, M. A. *Biochemistry* **1996**, *35*, 1540-1547.
(24) Richter-Addo, G. B.; Legzdins, P. *Metal Nitrosyls*; Oxford University Press: Oxford, 1992.
(25) Massoudipour, M.; Tewari, S. K.; Pandey, K. K. *Polyhedron* **1989**, *8*, 1447-1451.

(26) Guilard, R.; Lagrange, G.; Tabard, A.; Lancon, D.; Kadish, K. M. *Inorg. Chem.* **1985**, *24*, 3649-3656.
(27) Hodge, S. J.; Wang, L.-S.; Khan, M. A.; Young, V. G.; Richter-Addo, G. B. *Chem. Commun.* **1996**, 2283-2284.
(28) Richter-Addo, G. B.; Wheeler, R. A.; Hixson, C. A.; Chen, L.; Khan, M. A.; Ellison, M. K.; Schulz, C. E.; Scheidt, W. R. *J. Am. Chem. Soc.* **2001**, *123*, 6314-6326.
(29) Cheng, L.; Chen, L.; Chung, H.-S.; Khan, M. A.; Richter-Addo, G. B. *Organometallics* **1998**, *17*, 3853-3864.
(30) Xu, N.; Lee, J.; Powell, D. R.; Richter-Addo, G. B. *Inorganica Chimica Acta* **2005**, *358*, 2855-2860.
(31) Yang, S.-Y.; Leung, W.-H.; Lin, Z. *Organometallics* **2001**, *20*, 3198-3201.
(32) Ghosh, A. *Acc. Chem. Res.* **2005**, *38*, 943-954.
(33) Wojcicki, A. *Adv. Organomet.* **1974**, *12*, 31.
(34) Alexander, C. S.; Rettig, S. J.; James, B. *organometallics* **1994**, *13*, 2542-2544.
(35) Leung, W.-H,.; Hun, T. S. M.; Wong, K.-W.; Wong, W.-T. *J. Chem. Soc. Dalton Trans.* **1994**, 2713.
(36) Yang, S.-Y.; Leung, W.-H.; Lin, Z. *organometallics* **2001**, *20*, 3198-3201.
(37) Hansen, T.; Ovesen, H.; Svadberg, A.; Svendsen, K.; Tangen, E.; Swarts, J. C.; Ghosh, A. *Organometallics* **2004**, *23*, 3870-3872.
(38) Novozhilova, I. V.; Coppens, P.; Lee, J.; Richter-Addo, G. B.; Bagley, K. A. *J. Am. Chem. Soc.* **2006**, *128*, 2093-2104.
(39) Bohle, D. S.; Goodson, P. A.; Smith, B. D. *Polyhedron* **1996**, *15*, 3147-3150.
(40) Bohle, D. S.; Hung, C.-H.; Powell, A. K.; Smith, B. D.; Wocadlo, S. *Inorg. Chem.* **1997**, *36*, 1992-1993.
(41) Bohle, D. S.; Hung, C.-H.; Smith, B. D. *Inorg. Chem.* **1998**, *37*, 5798-5806.
(42) Chen, L.; Yi, G.-B.; Wang, L.-S.; Dharmawardana, U. R.; Dart, A. C.; Khan, M. A.; Richter-Addo, G. B. *Inorg. Chem.* **1998**, *37*, 4677-4688.
(43) Galardon, E.; Le Maux, P.; Toupet, L.; Simonneaux, G. *Organometallics* **1998**, *17*, 565-569.
(44) Harada, T.; Wada, S.; Yuge, H.; Miyamoto, T. K. *Acta Crystallogr., Sect. C* **2003**, *59*, m37–m39.
(45) Kawai, M.; Yuge, H.; Miyamoto, T. K. *Acta Crystallogr., Sect. C* **2002**, *58*, m581–m582.
(46) Lee, J.; Yi, G.-B.; Khan, M. A.; Richter-Addo, G. B. *Inorg. Chem.* **1999**, *38*, 4578-4584.
(47) Miranda, K. M.; BU, X.; Lorkovic, I.; Ford, P. C. *Inorg. Chem.* **1997**, *36*, 4838-4848.
(48) Seyler, J. W.; Fanwick, P. E.; Leidner, C. R. *Inorg. Chem.* **1990**, *29*, 2542-2544.
(49) Yi, G.-B.; Chen, L.; Khan, M. A.; Richter-Addo, G. B. *Inorg. Chem.* **1997**, *36*, 3876-3885.
(50) Yi, G.-B.; Khan, M. A.; Powell, D. R.; Richter-Addo, G. B. *Inorg. Chem.* **1998**, *37*, 208-214.
(51) Yi, G.-B.; Khan, M. A.; Richter-Addo, G. B. *Chem. Commun.* **1996**, 2045 - 2046.
(52) Evans, D. H.; M., O. C. K.; Petersen, R. A.; Kelly, M. J. *J. Chem. Ed.* **1983**, *60*, 290-293.

(53) Shaw, M. J.; Henson, R.; Houk, S. E.; Westhoff, J. W.; Jones, M. W.; Richter-Addo, G. B. *Electroanal. Chem.* **2002**, *534*, 47-53.
(54) Thomas, D. W.; Martell, A. E. *J. Am. Chem. Soc.* **1959**, *81*, 5111-5119.
(55) Kissinger, P. T.; Heineman, W. R. *J. Chem. Ed.* **1983**, *60*, 702-706.
(56) Carter, S. M.; Lee, J.; Hixson, C. A.; Powell, D. R.; Wheeler, R. A.; Shaw, M. J.; Richter-Addo, G. B. *Dalton Trans.* **2006**, *10*, 1338-1346.

Chapter 4. Interactions of nitrosamines with iron porphyrins

Introduction

Nitrosamines are well known for their potent carcinogenic properties affecting a wide variety of tissues.[1-6] Metabolic activation of nitrosamines by the enzyme cytochrome P450 is required for nitrosamines to be toxic and carcinogenic.[7,8] Oxidative dealkylation and reductive denitrosation are the two major pathways for the metabolic activation of nitrosamines (Scheme 4.1). Oxidative dealkylation begins with the

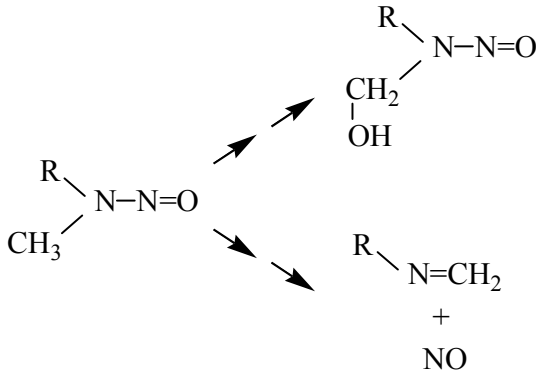

Scheme 4.1. Initial steps involved in the dealkylation and denitrosation pathways of the metabolism of nitrosamines by cytochrome P450.

hydroxylation of the α-carbon, resulting eventually in the production of an aldehyde and an alkyldiazonium ion which could then alkylate DNA. Reductive denitrosation produces nitric oxide and a secondary amine which may represent a detoxification process. Both metabolic pathways are initiated by the interactions of nitrosamines with

cytochrome P450. Two kinds of interactions of substrates with P450 are known. As seen in Figure 4.1, the first type of interaction is between the substrate (e.g. nitrosamines) and the protein distal pocket (Type 1) and the second is the direct interaction between the substrate (e.g. nitrosamines) and the iron center of the heme (Type 2). The type 1 interaction is the most studied in P450 oxygenase research. Type 2 interactions are generally associated with P450-inhibitor complexes, where the metal site is blocked by a strong-binding ligand such as CO or imidazole.

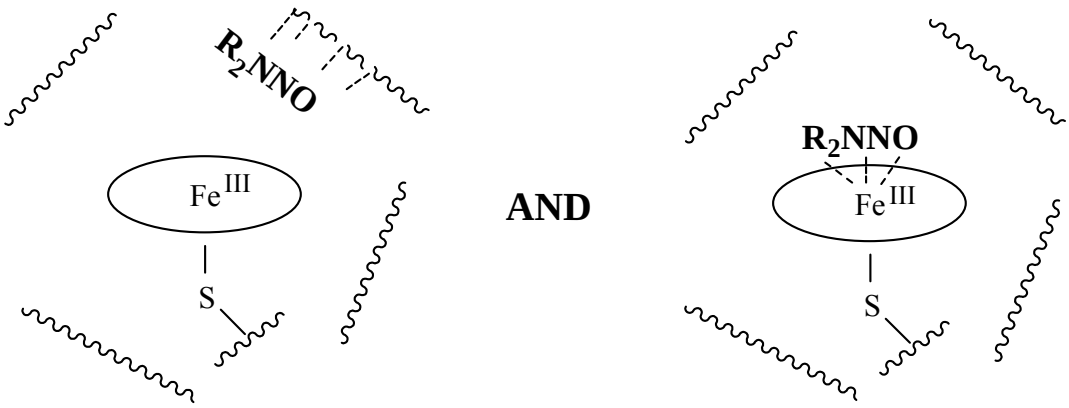

Figure 4.1. Proposed interactions of nitrosamines with the heme site of cytochrome P450.

Nitrosamines are known to react with metal complexes to form nitrosamine adducts.[9-17] Four different kinds of binding modes have been observed. For example, *N*-methyl-*N*-nitrosoaniline can coordinate to a palladium complex through the nitroso nitrogen and the *ortho*-carbon of the phenyl ring (Fig. 4.2a) .[17] *N*-nitrosodimethylamine and *N*-nitrosopiperidine can bind to two neighbouring copper atoms of a $CuCl_2$ chain

with their nitroso oxygen and nitrogen atoms (Fig. 4.2b).[9,10,16] *N*-nitrosodimethylamine also binds antimony complexes through the nitroso oxygen atom as a sole σ-O binding mode (Fig. 4.2c).[9] In addition, nitroso N-atom binding mode was observed in the primary nitrosamine iridium complexes (Fig. 4.2d) which were prepared by the reactions of the nitrosyl iridium complex, $K[IrCl_5NO]$ with primary amines.[18]

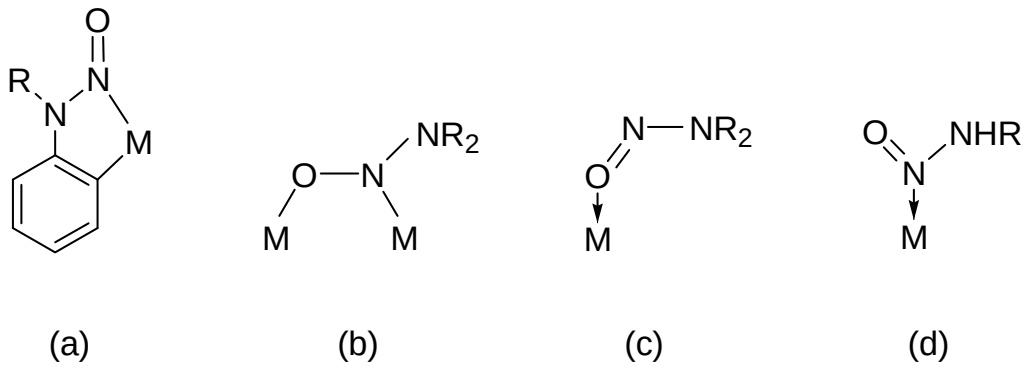

Figure 4.2. Four binding modes in metal-nitrosamine complexes

Our group reported the preparation of the first bis-nitrosamine iron heme model complex $[(TPP)Fe^{III}(Et_2NNO)_2]ClO_4$.[19] The crystal structure shows that the nitrosamine ligands are coordinated to the ferric center of the porphyrin in a σ-O binding mode. We extended such nitrosamine binding to ruthenium and osmium heme model complexes.[20,21] Despite repeated efforts, earlier workers in our group could only obtain crystals of these metalloporphyrin-nitrosamine compounds for the case of Et_2NNO. Thus, we embarked on investigating whether other nitrosamines would interact with iron

porphyrins in the same σ-O binding mode or in other modes. This chapter describes the results of our on-going work in this area.

Experimental section

All reactions were performed under an atmosphere of prepurified nitrogen using standard Schlenk glassware and/or in an Innovative Technology Labmaster 100 Dry Box. Solutions for spectral studies were also prepared under a nitrogen atmosphere. Solvents were distilled from appropriate drying agents under nitrogen just prior to use: CH_2Cl_2 (CaH_2), THF (CaH_2), hexane (CaH_2), benzene (Na), toluene (Na).

Chemicals. *N*-nitrosodimethylamine (Me_2NNO, 99%), *N*-nitrosodiethylamine (Et_2NNO, >99%), *N*-nitrosodiphenylamine (Ph_2NNO, >97.0%), tetrahydrothiophene (99%), silver perchlorate (97%), were purchased from Aldrich Chemical Company and used as received. *N*-nitrosopiperidine ((*cyclo*-$CH_2)_5NNO$, 99%), and *N*-nitrosopyrrolidine ((*cyclo*-$CH_2)_4NNO$, 99%) were purchased from Fluka. $[(TPP)Fe^{III}(THF)_2]ClO_4$[22], ferrous (TPP)Fe[23], *N*-nitrosodibenzylamine[24] ($(PhCH_2)_2NNO$, *N*-methyl-*N*-nitrosoaniline[24] (PhMeNNO) and *N*-ethyl-*N*-nitrosoaniline[24] (PhEtNNO) were prepared by published methods. Chloroform–*d* (99.8%) was obtained from Cambridge Isotope Laboratories, and purified by three freeze-pump-thaw cycles, and stored over Linde 4 Å molecular sieves. Nitric oxide (98%, Matheson Gas) was passed through KOH pellets and a cold trap (dryice/acetone) to remove higher nitrogen oxides.

Instrumentation. Infrared spectra were recorded on a Bio–Rad FT–155 FTIR spectrometer. Proton NMR spectra were obtained on Varian 300 MHz spectrometer and the signals referenced to the residual signal of the solvent employed ($CDCl_3$ at 7.24 ppm).

Preparation of [(TPP)Fe($Me_2NNO)_2$]ClO_4. To a toluene solution (20 mL) of [(TPP)Fe$(THF)_2$]ClO_4 (0.042 g, 0.048 mmol) was added Me_2NNO (0.11 mL, 1.5 mmol). The mixture was stirred for 45 min, during which time the color of the solution changed from brown-purple to red-purple. The solvent was reduced to ~10 mL and hexane (30 mL) was added to the solution. The resulting solution was placed in a freezer (-22 ºC) overnight. A violet crystalline solid that formed was collected by filtration, washed with hexane (2×15 mL), and dried in vacuo to give [(TPP)Fe$(Me_2NNO)_2$]ClO_4 (0.029g, 0.032 mmol, 66% isolated yield). The product was dissolved in a CH_2Cl_2/hexane (5 mL, 3:1), and slow evaporation of the solvent mixture under inert atmosphere gave suitable crystals for X-ray diffraction studies. IR (KBr, cm^{-1}): $\nu_{NO/NN}$ = 1256 m; also 3057 w, 1597 m, 1478 m, 1437 m, 1318 w, 1119 w, 1117 m, 1101 m, 1074 m, 1061 m, 1006 m, 802 m, 768 m, 754 m, 720 m, 703 m, 660 w, 623 m.

The other complexes were generated using similar methods.

[(TTP)Fe($Me_2NNO)_2$]ClO_4. Yield: 60%. IR (KBr, cm^{-1}): $\nu_{NO/NN}$ = 1255 m; also 3053 w, 1596 m, 1479 m, 1440 m, 1318 m, 1116 m, 1103 m, 1073 m, 1062 m, 1006 s, 802 s, 768 m, 754 m, 736 m, 720 m, 703 m, 660 w, 623 m.

[(TTP)Fe(Et_2NNO)$_2$]ClO_4. Yield: 66%. IR (KBr, cm^{-1}): $\nu_{NO/NN}$ = 1267 m; also 3023 w, 2958 w, 1596 m, 1338 m, 1334 m, 1202 m, 1184 m, 1136 m, 1123 m, 1106 s, 1092 m, 999 m, 846 w, 799 s, 722 m, 632 w, 626 m, 524 w, 420 w.

[(TPP)Fe((*cyclo*-CH_2)$_4$NNO)$_2$]ClO_4. Yield: 72%. X-ray suitable crystals were grown at room temperature from a CH_2Cl_2/hexane (3:1) mixture by slow evaporation. IR (KBr, cm^{-1}): ν_{NO} = 1267 m, ν_{NN} = 1239 m; also 3057 w, 2960 w, 1597 m, 1442 m, 1337 m, 1332 w, 1200 m, 1179 w, 1114 m, 1098 s, 1073 m, 1006 s, 802 s, 756 m, 722 m, 702 m, 660 w, 623 m, 535 w.

[(TPP)Fe((*cyclo*-CH_2)$_5$NNO)$_2$]ClO_4. Yield: 57%. X-ray suitable crystals were grown at room temperature from a CH_2Cl_2/hexane (3:1) mixture by slow evaporation. IR (KBr, cm^{-1}): ν_{NO} = 1274 m, ν_{NN} = 1242 m; also 3058 w, 2946 w, 2856 w, 1597 m, 1477 m, 1443 m, 1313 w, 1200 m, 1178 w, 1102 m, 1096 s, 1072 m, 1007 s, 802 m, 754 m, 754 w, 719 m, 703 m, 660 w, 623 m, 569 w.

[(TPP)Fe(($PhCH_2$)$_2$NNO)$_2$]ClO_4. Yield: 61%. X-ray suitable crystals were grown at room temperature from a CH_2Cl_2/hexane (3:1) mixture by slow evaporation. IR (KBr, cm^{-1}): ν_{NO} = 1285 m, ν_{NN} = 1260 m; also 3056 m, 3056 w, 3028 w, 1597 m, 1477 m, 1340 w, 1110 m, 1140 m, 1070 m, 1008 s, 903 w, 803 m, 753 m, 701 m, 659 w, 623 w, 612 w.

Attempted Preparation of [(TPP)Fe(THT)(Me_2NNO)]ClO_4. To a CH_2Cl_2 solution (20 mL) of [(TPP)Fe(THF)$_2$]ClO_4 (0.042 g, 0.048 mmol) was added THT (0.052 mL, 0.058 mmol). The mixture was stirred for 45 min, during which time the color of

the solution changed from brown-purple to red-purple. The solvent was reduced to ~10 mL. To this solution was added Me_2NNO (0.036 g, 0.048 mmol) and the solution was stirred for an additional hour. The resulting product appeared to be a mixture of $[(TPP)Fe(THT)(Me_2NNO)]ClO_4$ and $[(TPP)Fe(Me_2NNO)]_2ClO_4$ (by IR spectroscopy). Attempts to obtain spectroscopically pure $[(TPP)Fe(THT)(Me_2NNO)]ClO_4$ were unsuccessful. IR (KBr, cm^{-1}): $\nu_{NO/NN}$ = 1289 m.

Preparation of $[(TPP)Fe(NO)(Me_2NNO)]ClO_4$. Method I. Nitric oxide was bubbled through a CH_2Cl_2 solution (15 mL) of $[(TPP)Fe(Me_2NNO)_2]ClO_4$ (50 mg, 0.055 mmol) for 2 min. During this time, the color of the mixture changed from red-purple to bright-red. The volume of solution was reduced to *ca.* 5 mL, and hexane (20 mL) was added slowly. A dark purple crystalline solid that formed was collected by filtration, washed with hexane (2×15 mL), and dried in vacuo to give $[(TPP)Fe(NO)(Me_2NNO)]ClO_4$ (0.023g, 0.028 mmol, 56% isolated yield). IR (KBr, cm^{-1}): ν_{NO} = 1910 s, $\nu_{NO/NN}$ = 1254 m; also 3056 m, 3028 w, 1596 m, 1480 m, 1440 m, 1400 w, 1318 m, 1198 m, 1116 m, 1101 s, 1070 m, 1006 s, 802 m, 767 m, 754 m, 736 w, 702 m, 660 w, 622 m.

Method II. Crystals of $[(TPP)Fe(Me_2NNO)_2]ClO_4$ under N_2 were exposed to NO gas. After 5h of exposure to NO, the gas was removed from the vial by purging with N_2. The $[(TPP)Fe(NO)(Me_2NNO)]ClO_4$ compound was obtained as bright red crystals.

Caution: (i) Due to the toxicity of nitrosamines (R_2NNO), they were handled with extreme care in a drybox or in standard Schlenk glassware. (ii) Due to the fire and explosion hazard, the perchlorate compounds were used or prepared in a small amount and carefully handled.

Results and discussion

Synthesis and characterization. Our research group reported the first nitrosamine complex of an iron porphyrin $[(TPP)Fe(Et_2NNO)_2]ClO_4$.[19] We found that a convenient preparative method involved the displacement of weakly bound THF ligands in the precursor $[(TPP)Fe(THF)_2]ClO_4$ complex by Et_2NNO. A similar synthetic method was used in the preparation of the iron porphyrin derivatives in this chapter. The reaction of $[(por)Fe(THF)_2]ClO_4$ (por = TPP, TTP) with five different nitrosamines (*N*-nitrosodimethylamine, *N*-nitrosodiethylamine, *N*-nitrosodibenzylamine, *N*-nitrosopiperidine, and *N*-nitrosopyrrolidine) in toluene generates, after workup, the dark purple products in 57-72% isolated yields (Eq. 4.1). Because of the weak

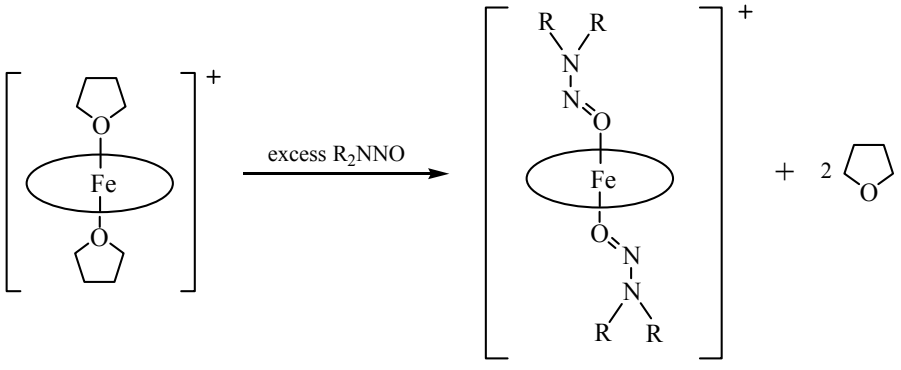

(4.1)

R_2 = Me_2, Et_2, $(PhCH_2)_2$, (*cyclo*-$CH_2)_4$, (*cyclo*-$CH_2)_5$

interaction between the iron center and the nitrosamine ligands, the nitrosamine ligands easily dissociate from the iron center in the absence of excess nitrosamine. Thus, the presence of excess nitrosamine maintains bis-nitrosamine coordination in these complexes. In addition, these complexes convert to the bis-aquo derivatives in the presence of moisture (Eq. 4.2). The ferric μ-oxo dimer porphyrin complex (i.e.

$$[(por)Fe(R_2NNO)_2]ClO_4 + 2\,H_2O \longrightarrow [(por)Fe(H_2O)_2]ClO_4 + 2\,R_2NNO \qquad (4.2)$$

$[(por)Fe]_2(\mu\text{-}O)$) is produced when air/oxygen is present. In the solid state, the bis-nitrosamine compounds are fairly air stable. The reactions of $[(TPP)Fe(THF)_2]ClO_4$ with three aryl nitrosamines (PhMeNNO, PhEtNNO, Ph_2NNO) were also attempted. However, formation of the expected compounds did not occur. Nitrosamines can be written in two main forms shown in Figure 4.3. Structure B represents a 1,3-dipolar form with a formal N=N double bond.[25] It is likely that the phenyl groups weaken the dipolar contribution of the aryl nitrosamines, reducing the affinity of the terminal O-atoms for the "hard" ferric center.

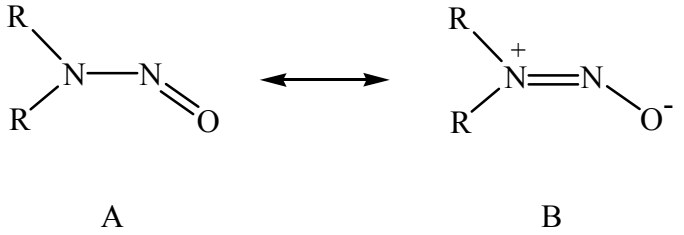

Figure 4.3. Resonance structures of nitrosamines.

The IR spectrum (KBr) shows either one or two new bands in the range from 1200 cm^{-1} to 1300 cm^{-1} which are assigned as ν_{NO} and ν_{NN} for the coordinated nitrosamines (Table 4.1). Two new bands at around 1100 and 622 cm^{-1} were also

Table 4.1. IR data for ν_{NO} and ν_{NN} in nitrosamine iron porphyrin complexes.

Compound	ν_{NO} (cm^{-1})	ν_{NN} (cm^{-1})	Ref
$[(TPP)Fe(Me_2NNO)_2]ClO_4$	1256		This work
$[(TTP)Fe(Me_2NNO)_2]ClO_4$	1255		This work
$[(TPP)Fe(Et_2NNO)_2]ClO_4$	1270		19
$[(TTP)Fe(Et_2NNO)_2]ClO_4$	1267		This work
$[(TTP)Fe(Et_2NNO)_2]SbF_6$	1271	1256	21
$[(TPP)Fe((cyclo\text{-}CH_2)_4NNO)_2]ClO_4$	1267	1239	This work
$[(TPP)Fe((cyclo\text{-}CH_2)_5NNO)_2]ClO_4$	1274	1242	This work
$[(TPP)Fe((PhCH_2)_2NNO)_2]ClO_4$	1285	1260	This work

observed for the uncoordinated perchlorate anion.[26] Previous isotope-labeling studies in our group have aided in the assignments of the ν_{NO} and ν_{NN} bands.[21] For example, the use of $Et_2N^{15}NO$ in $[(TPP)Fe(Et_2NNO)]^+$ resulted in an isotopic shift of -16 cm^{-1} for the coincident ν_{NO}/ν_{NN} bands, whereas the use of $Et_2NN^{18}O$ shifted only the ν_{NO} band in $(OEP)Ru(CO)(Et_2NN^{18}O)$ by -17 cm^{-1}.[21] Free aliphatic secondary nitrosamines

generally display bands in the 1425-1460 and 1030-1150 cm^{-1} ranges due to ν_{NO} and $\nu_{NN,}$ respectively.[27] The ν_{NO}s and ν_{NN}s of the coordinated nitrosamines are much closer to each other compared to those of the free nitrosamines, which indicates that the coordinated nitrosamines are best represented by a resonance hybrid having a significant contribution from structure B in Figure 4.3. Furthermore, the ν_{NO} and ν_{NN} infrared bands are distinguishable in $[(TTP)Fe(Et_2NNO)_2]SbF_6$, while the $[(TTP)Fe(Et_2NNO)_2]ClO_4$ compound only shows one band for both ν_{NO} and ν_{NN} in IR spectrum. These two compounds have the same cation but different anions which indicates that the anions may affect the infrared absorption of the coordinated nitrosamines. Additionally, the ν_{NO} and ν_{NN} bands of the coordinated nitrosamines do not show a clear trend with R group substitution on the nitrosamines.

The preparation of mixed ligated nitrosamine Fe^{III} porphyrin was attempted. The reaction of $[(TPP)Fe(THT)_2]ClO_4$ with Me_2NNO resulted in a mixture of $[(TPP)Fe(THT)(Me_2NNO)]ClO_4$ and $[(TPP)Fe(Me_2NNO)_2]ClO_4$ based on IR spectroscopy. A new band of $\nu_{NO/NN}$ shows at 1289 cm^{-1} and its intensity is about a half of the $\nu_{NO/NN}$ band of $[(TPP)Fe(Me_2NNO)_2]ClO_4$. Unfortunately, the isolation of the spectroscopically pure $[(TPP)Fe(THT)(Me_2NNO)]ClO_4$ compound was unsuccessful because of its instability.

Besides the interaction of nitrosamines with ferric Fe^{III} porphyrin complexes, we are interested in determining the nature of nitrosamine binding to ferrous (por)Fe^{II} complexes. For example, reaction of $[(TPP)Fe^{III}(Me_2NNO)_2]ClO_4$ with NO gas results

in the formation of a compound formulated as $[(TPP)Fe^{II}(NO)(Me_2NNO)]ClO_4$ based on its IR spectrum (Eq. 4.3). A new band at 1910 cm^{-1} is assigned to the ν_{NO} band of a

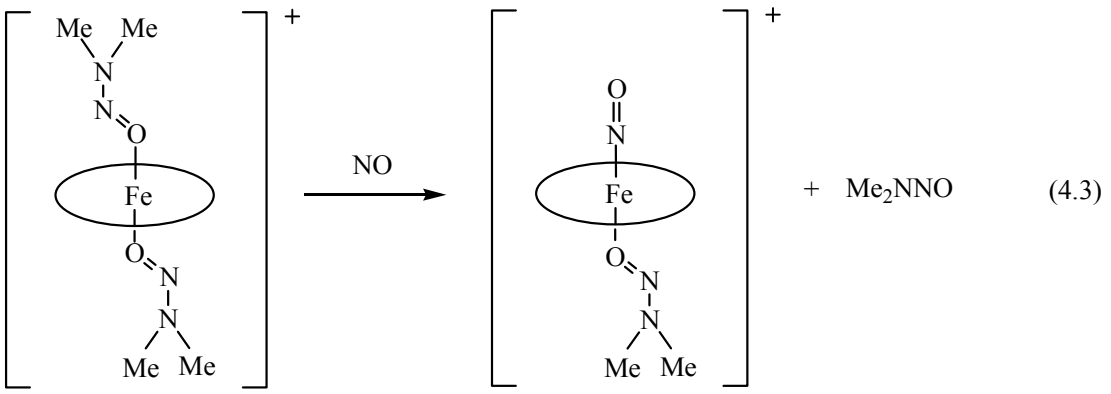

(4.3)

nitrosyl group, whereas the 1254 cm^{-1} band is assigned to the $\nu_{NO/NN}$ bands (overlapped) of coordinated *N*-nitrosodimethylamine. It is well known that ferric nitrosyl porphyrins with *trans* water, alcohol, imidazole, indazole, and pyrazine donors have ν_{NO} bands of >1900 cm^{-1} and linear or near linear FeNO moieties.[28-31] Thus, the ν_{NO} of nitrosyl group at 1910 cm^{-1} of $[(TPP)Fe^{II}(NO)(Me_2NNO)]ClO_4$ suggests a linear FeNO conformation. In addition, the similar $\nu_{NO/NN}$ band(s) of $[(TPP)Fe(Me_2NNO)_2]ClO_4$ and $[(TPP)Fe(NO)(Me_2NNO)]ClO_4$ indicate that the η^1-O binding mode is also present in the nitrosyl derivative. However, we have not been able to isolate it in pure form because of its instability even in inert atmosphere. Attempts were also made to investigate the direct interaction of nitrosamines with $(por)Fe^{II}$ complexes. Interestingly, the nitrosamines which coordinate to the $iron^{III}$ center of the porphyrins do not, at least in our hands, form adducts with the reduced four-coordinate Fe^{II} porphyrin. On the

contrary, the other three nitrosamines with at least one phenyl group react with the four-coordinate Fe^{II} porphyrin to produce five-coordinate nitrosyl iron porphyrin derivatives. For example, the reaction of $(TPP)Fe^{II}$ with *N*-nitrosodiphenylamine in CH_2Cl_2 produces (TPP)Fe(NO) in 38% isolated yield (Eq. 4.4). In addition, diphenylamine (Ph_2NH) was identified by NMR spectroscopy in 35% yield. This

$$(TPP)Fe^{II} + Ph_2NNO \longrightarrow (TPP)Fe(NO) + Ph_2NH \qquad (4.4)$$

denitrosation process is consistent with the metabolic mechanism of *N*-nitrosodiphenylamine in physiological media.[32]

N-nitrosodiphenylamine serves as a nitrosylating agent in the reaction of *N*-nitrosodiphenylamine with $(TPP)Fe^{II}$ (Eq. 4.4). It is a common feature of other organic nitroso compounds such as alkyl nitrites (RONO), alkyl thionitrites (RSNO), Diazald, and NONOates which are also used as nitrosylating agents to generate metal-NO moieties (Fig. 4.4).[29,33-44]

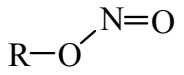

Alkyl nitrites

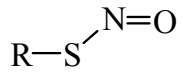

Alkyl thionitrites

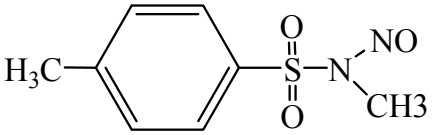

Diazald

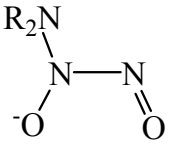

NONOates

Figure 4.4. Structural diagrams of alkyl nitrites, alkyl thionitrites, Diazald and NONOate compounds.

Molecular structures. Four crystal structures of iron-porphyrin nitrosamine complexes were obtained. Suitable crystals of $[(TPP)Fe(Me_2NNO)_2]ClO_4$, $[(TPP)Fe((PhCH_2)_2NNO)_2]ClO_4$, $[(TPP)Fe((cyclo\text{-}CH_2)_4NNO)_2]ClO_4$, and $[(TPP)Fe((cyclo\text{-}CH_2)_5NNO)_2]ClO_4$ were grown from their CH_2Cl_2/hexane (2:1) solutions with the presence of excess corresponding nitrosamines by slow evaporation of the solvent under N_2. The crystal structures of the compounds are shown in Figure 4.5-4.8 with a focus on the cations. Selected bond lengths, bond angles, and torsion angles are also listed in Table 4.2. The average Fe-N(por) and Fe-O(axial) bond lengths of the four bis-nitrosamine complexes are 2.044 Å and 2.112 Å, respectively. These

values are similar to those of high-spin ferric compounds such as $[(TPP)Fe(H_2O)_2]^+$ and $[(TPP)Fe((CH_2)_4SO)_2]^+$, indicating that these bis-nitrosamine complexes belong to a high-spin ferric porphyrin catalog.[45-47] Additionally, the μ_{eff} of 5.9 (C_6D_6) of $[(TPP)Fe(Et_2NNO)_2]ClO_4$[21] and 6.0 ($C_6D_6$) of $[(TPP)Fe(Et_2NNO)_2]SbF_6$[21] also support the high-spin formulation for these nitrosamine complexes. The most interesting feature of the structure is that all the nitrosamine ligands are attached to the ferric center via a η^1-O bonding mode. Prior to this work, our research group reported the first iron-porphyrin nitrosamine complex with a η^1-O fashion.[19] Therefore, the crystal structures of the nitrosamine ferric porphyrin complexes remain the only transition metal complexes to date, showing the sole η^1-O bonding mode.

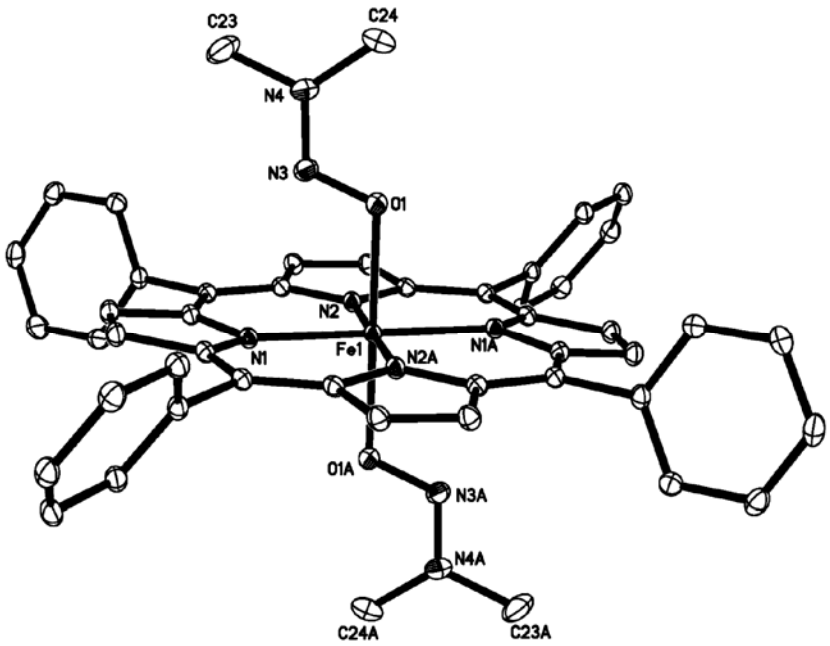

Figure 4.5. Molecular structure of the cation of $[(TPP)Fe(Me_2NNO)_2]^+ClO_4^-$.

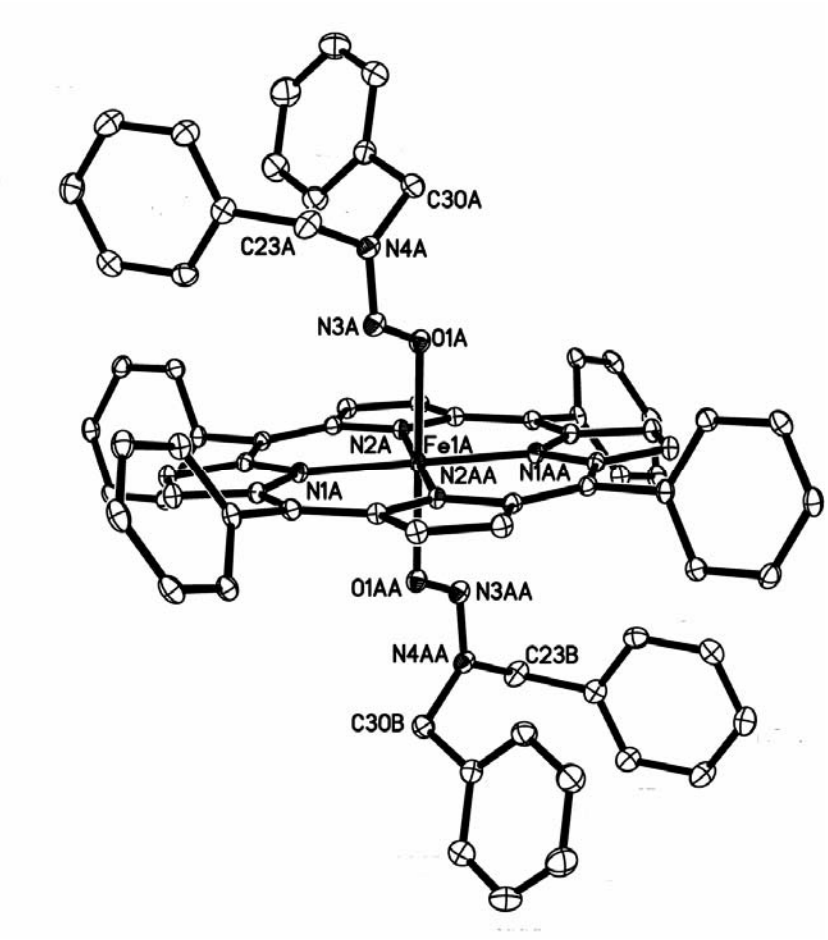

Figure 4.6. Molecular structure of the cation of $[(TPP)Fe((PhCH_2)_2NNO)_2]^+ClO_4^-$.

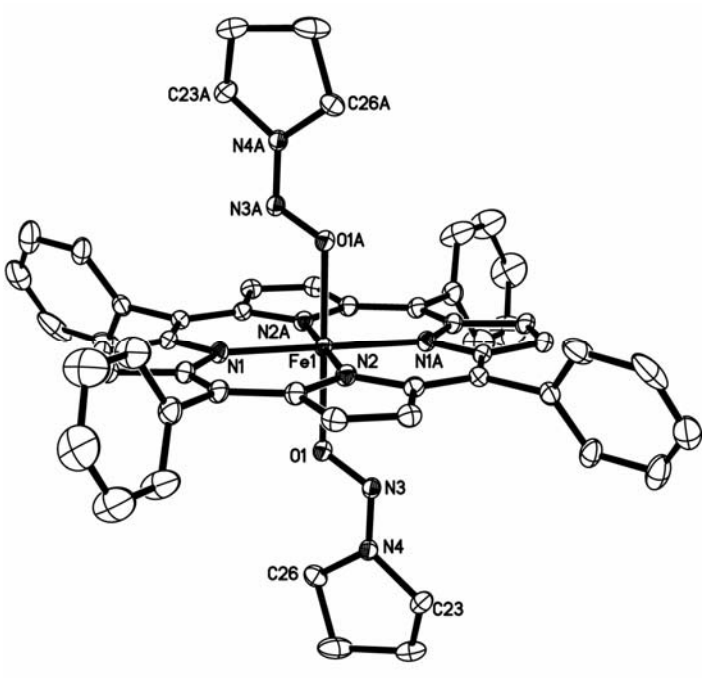

Figure 4.7. Molecular structure of the cation of $[(TPP)Fe((cyclo\text{-}CH_2)_4NNO)_2]^+ClO_4^-$.

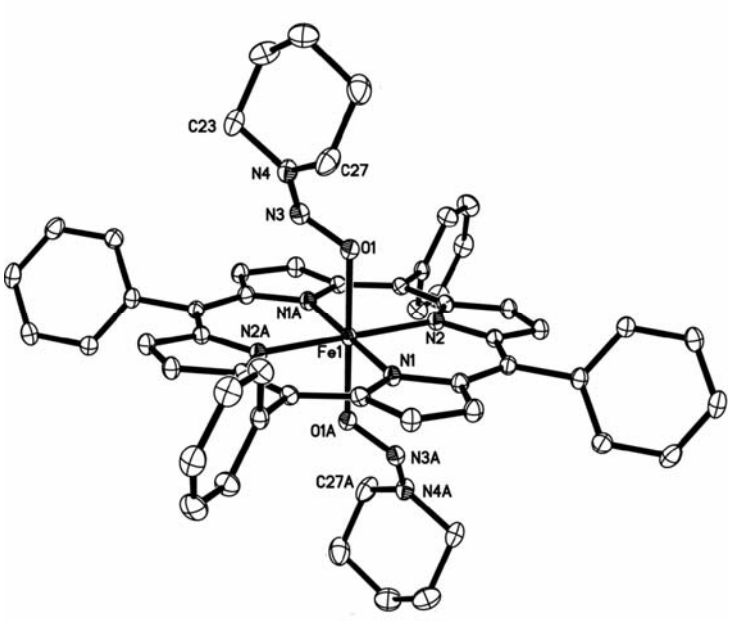

Figure 4.8. Molecular structure of the cation of $[(TPP)Fe((cyclo\text{-}CH_2)_5NNO)_2]^+ClO_4^-$.

Table 4.2. Selected bond lengths (Å), angles (°) and torsion angles (°) for nitrosamine metal complexes.

Compound	Bond length				Bond angle		Torsion angle		Ref
	Fe-N(por)	M-O	O-N	N-N	∠ M-O-N	∠ O-N-N	ONNC[1]	ONNC[2]	
$[(TPP)Fe(Me_2NNO)_2]ClO_4$	2.040	2.136(1)	1.271(1)	1.284(1)	111.5(1)	114.2(1)	-175.0	-0.8	This work
$[(TPP)Fe((PhCH_2)_2NNO)_2]ClO_4$	2.040	2.124(1)	1.271(2)	1.288(2)	112.7(1)	114.5(1)	174.8	-2.7	This work
$[(TPP)Fe((cyclo\text{-}CH_2)_4NNO)_2]ClO_4$	2.050	2.101(1)	1.271(2)	1.270(1)	115.6(1)	113.7(1)	179.0	0.7	This work
$[(TPP)Fe((cyclo\text{-}CH_2)_5NNO)_2]ClO_4$	2.048	2.086(1)	1.275(2)	1.281(2)	115.7(1)	114.2(2)	173.7	0.5	This work
$[(TPP)Fe(Et_2NNO)_2]ClO_4$	2.044	2.107(6)	1.260(9)	1.276(10)	116.3 (3)	113.9(7)	177.7	1.1	18
$(Me_2NNO)SbCl_5$		2.113(3)	1.310(5)	1.262(5)	115.7(2)	112.0(3)	-179.8	0.6	9
$(Me_2NNO)CuCl_2$		2.29(1)	1.22(2)	1.29(2)	115.5(1)	115.9(1)	180.0	0	9
$((cyclo\text{-}CH_2)_5NNO)CuCl_2$		2.010(2)	1.279(3)	1.288(3)	117.2(2)	114.9(2)	-177.3	-1.7	9

In the nitrosamine iron porphyrin complexes, the average O-N distance of the bound nitrosamines is 1.270 Å, and the average N-N bond distance is 1.280 Å. The individual bond distances of N-O and N-N of these nitrosamine complexes are listed in Table 4.2. Compared to the related distances in free *N*-nitrosodimethylamine of 1.260(6) Å (N-O) and 1.320(6) Å (N-N) as determined by low-temperature X-ray diffraction[48] and in free *N*-nitrosopiperidine of 1.252 Å (N-O) and 1.315 Å (N-N)[49], the O-N and N-N bond distances in bound nitrosamines are much closer to each other which suggests that the complexed nitrosamines are best represented by a resonance hybrid having a significant contribution from the dipolar structure (Fig.4.3B) which also supported by previously described IR data. In addition, other two nitrosamines, namely *N*-nitrosodiphenylamine[50] and *N*-methyl-*N*-nitrosoaniline[51], have also been structurally characterized with N-O bond distances at 1.206 Å and 1.226 Å and N-N bond distances at 1.344 Å and 1.304 Å respectively. The N-O bond lengths in these nitrosamines are shorter in the free (unbound) state than in the complexes, and the N-N bond lengths are longer in the free (unbound) state. These bond length trends indicate the presence of a substantial contribution from the dipolar resonance structure that makes it easier to form the η^1-O binding nitrosamine complexes with the Fe^{III} porphyrins. Furthermore, in the $[(TPP)Fe(Me_2NNO)_2]^+$ cation, the nitrosamine atoms O1, N3, N4, C23, and C24 are found basically in one plane. The O1-N3-N4-C23 and O1-N3-N4-C24 torsion angles in $[(TPP)Fe(Me_2NNO)_2]^+$ are -175.0° and -0.8°, respectively, with a mean deviation of 0.02 Å from the $ONNC_2$ plane. The similar planarity of the five atoms ($ONNC_2$) is observed

in other four nitrosamine Fe^{III} porphyrin complexes which also supports that the coordinated nitrosamines have significant contribution from the dipolar structures.

Lastly, to the best of our knowledge, the crystal structures of free *N*-nitrosopyrrolidine and *N*-nitrosodibenzylamine have not been reported. Therefore, the crystal structures of $[(TPP)Fe((PhCH_2)_2NNO)_2]ClO_4$ and $[(TPP)Fe((cyclo\text{-}CH_2)_4NNO)_2]ClO_4$ also provide valuable information for the related structural study of *N*-nitrosopyrrolidine and *N*-nitrosodibenzylamine.

Conclusion

In summary, new bis-nitrosamine iron porphyrin complexes have been prepared from the reactions of precursor $[(por)Fe(THF)_2]ClO_4$ with nitrosamines (Me_2NNO, Et_2NNO, $(cyclo\text{-}CH_2)_4NNO$, $(cyclo\text{-}CH_2)_5NNO$, $(PhCH_2)_2NNO$). These iron nitrosamine complexes have been characterized by infrared spectroscopy and X-ray structure determination. Not all nitrosamines are able to form adducts with iron porphyrins using this method. The nitrosamines with phenyl group attached to the amido N atom (PhMeNNO, PhEtNNO, and Ph_2NNO) did not form adducts with $[(por)Fe(THF)_2]ClO_4$. However, these aryl nitrosamines react with four-coordinate iron(II) porphyrin compounds to produce five-coordinate nitrosyl iron porphyrins and the corresponding amines, while the other nitrosamines with alkyl groups do not have any noticeable interactions with iron(II) porphyrins. This implies that the contribution of the dipolar resonance form in free nitrosamine compounds plays a key role in their chemical

reactivities. In this work, we have expanded the set of nitrosamines that can form Type 2 adducts (Fig. 4.1) with heme models. Importantly, a sole η^1-O binding mode for nitrosamine iron(III) complexes has been determined by single-crystal X-ray crystallography. With the great interest in the study of nitrosamine carcinogenicity, the reactivities and structural information on the nitrosamines and their metal complexes could potentially provide chemical insight on the metabolic pathways of nitrosamine activation.

References

(1) Magee, P. N.; Barnes, J. M. *Br. J. Cancer* **1956**, *10*, 114-122.
(2) Stiborova, M.; Hansikova, H.; Frei, E. *Gen. Physiol. Biophys.* **1996**, *15*, 211-223.
(3) Stiborova, M.; Hansikova, H.; Frei, E. *Cancer Letters* **1996**, *110*, 11-17.
(4) Smith, T. J.; Liao, A.; Wang, L.-D.; Yang, G.-y.; Starcic, S.; Philbert, M. A.; Yang, C. S. *Carcinogenesis* **1998**, *19*, 667-672.
(5) Hill, M. J. *Nitrosamines: Toxicology and Microbiology*; VCH Ellis Horwood Ltd.: Chichester, England, 1988.
(6) Cadogan, J. I. G. *Acc. Chem. Res.* **1971**, *4*, 186-192.
(7) Magee, P. N.; Barnes, J. M. *Adv. Cancer Res.* **1967**, *10*, 163-246.
(8) Guttenplan, J. B. *Mutat. Res.* **1987**, *186*, 81-134.
(9) Schmidpeter, A.; Nöth, H. *Inorg. Chim. Acta* **1998**, *269*, 7-12.
(10) Asaji, T.; Sakai, H.; Nakamura, D. *Inorg. Chem.* **1983**, *22*, 202-206.
(11) Schmidpeter, A. *Chem. Ber.* **1963**, *96*, 3275-3279.
(12) Klement, U.; Schmidpeter, A. *Angew. Chem. Int. Ed.* **1968**, *7*, 470.
(13) Klement, V. U. *Acta Cryst.* **1969**, *V25*, 2460-2465.
(14) Brown, R. D.; Coates, G. E. *J. Chem. Soc.* **1962**, 4723-4724.
(15) Willett, R. D. *Acta Crystallogr., Sec. B* **1988**, *B44*, 503-508.
(16) Asaji, T.; Ikeda, R.; Indue, M.; Nakamura, D. *J. Mol. Struct.* **1980**, *58*, 315-322.
(17) Constable, A. G.; McDonald, W. S.; Shaw, B. L. *J. Chem. Soc., Dalton Trans.* **1980**, 2282-2287.

(18) Doctorovich, F.; Di Salvo, F.; Escola, N.; Trápani, C.; Shimon, L. *Organometallics* **2005**, *24*, 4707-4709.
(19) Yi, G.-B.; Khan, M. A.; Richter-Addo, G. B. *J. Am. Chem. Soc.* **1995**, *117*, 7850-7851.
(20) Yi, G.-B.; Khan, M. A.; Reed, C. A. *Inorg. Chem.* **1996**, *35*, 3453-3454.
(21) Chen, L.; Yi, G.-B.; wang, L.-S.; Dharmawardana, U. R.; Dart, A. C.; Khan, M. A.; Richter-Addo, G. B. *Inorg. Chem.* **1998**, *37*, 4677-4688.
(22) Landrum, J. T.; Hatano, K.; Scheidt, W. R.; Reed, C. A. *J. Am. Chem. Soc.* **1980**, *102*, 6729-6735.
(23) Reed, C. A.; Mashiko, T.; Bentley, S. P.; Kastner, M. E.; Scheidt, W. R.; Spartalian, K.; Lang, G. *J. Am. Chem. Soc.* **1979**, *101*, 2948-2958.
(24) Zolfigol, M. A. *Synth. commun.* **1999**, *29*, 905-910.
(25) Lee, J.; Chen, L.; West, A. H.; Richter-Addo, G. B. *Chem. Rev.* **2002**, *102*, 1019-1065.
(26) Gowda, N. M. N.; Naikar, S. B.; Reddy, G. K. N. *Adv. Inorg. Chem. Radiochem.* **1984**, *28*, 255-299.
(27) Williams, R. L.; Pace, R. J.; Jeacocke, G. J. *Spectrochim. Acta* **1964**, *20*, 225-236.
(28) Scheidt, W. R.; Lee, Y., J.; Hatano, K. *J. Am. Chem. Soc.* **1984**, *106*, 3191-3198.
(29) Yi, G.-B.; Chen, L.; Khan, M. A.; Richter-Addo, G. B. *Inorg. Chem.* **1997**, *36*, 3876-3885.
(30) Ellison, M. K.; Schulz, C. E.; Scheidt, W. R. *J. Am. Chem. Soc.* **2002**, *124*, 13833-13841.
(31) Ellison, M. K.; Scheidt, W. R. *J. Am. Chem. Soc.* **1999**, *121*, 5210-5219.
(32) McGregor, D. *Mutat. Res.* **1994**, *317*, 195-211.
(33) Robinson, S. D.; Uttley, M. F. *Dalton Trans.* **1972**, 1-5.
(34) Chen, L.; Khan, M. A.; Richter-Addo, G. B. *Inorg. Chem.* **1998**, *37*, 533-540.
(35) Yi, G.-B.; Khan, M. A.; Powell, D. R.; Richter-Addo, G. B. *Inorg. Chem.* **1998**, *37*, 208-214.
(36) Cheng, L.; Powell, D. R.; Khan, M. A.; Richter-Addo, G. B. *Inorg. Chem.* **2001**, *40*, 125-133.
(37) Lee, J.; Yi, G.-B.; Khan, M. A.; Richter-Addo, G. B. *Inorg. Chem.* **1999**, *38*, 4578-4584.
(38) Lee, J.; Yi, G.-B.; Powell, D. R.; Khan, M. A.; Richter-Addo, G. B. *Can. J. Chem.* **2001**, *79*, 830-840.
(39) Yi, G.-B.; Khan, M. A.; Richter-Addo, G. B. *Chem. Commun.* **1996**, 2045-2046.
(40) Carter, S. M.; Lee, J.; Hixson, C. A.; Powell, D. R.; Wheeler, R. A.; Shaw, M. J.; Richter-Addo, G. B. *Dalton Trans.* **2006**, *10*, 1338-1346.
(41) Andreasen, L. V.; Lorkovic, I. M.; Richter-Addo, G. B.; Ford, P. C. *Nitric Oxide* **2002**, *6*, 228-235.
(42) Legzdins, P.; Reina, R.; Shaw, M. J.; Batchelor, R. J.; Einstein, F. W. B. *Organometallics* **1993**, *12*, 1029-1037.

(43) Keefer, L. K.; Christodoulou, D.; Dunams, T. M.; Hrabie, J. A.; Maragos, C. M.; Saavedra, J. E.; Wink, D. A. In *Nitrosamines and Related N-Nitroso Compounds: Chemistry and Biochemistry*; Loeppky, R. N., Michejda, C. J., Eds.; American Chemical Society: Washington, DC, 1994.
(44) Drago, R. S.; Karstetter, B. R. *J. Am. Chem. Soc.* **1961**, *83*, 1819-1822.
(45) Mashiko, T.; Kastner, M. E.; Spartalian, K.; Scheidt, W. R.; Reed, C. A. *J. Am. Chem. Soc.* **1978**, *100*, 6354-6362.
(46) Scheidt, W. R.; Cohen, I. A.; Kastner, M. E. *Biochemistry* **1979**, *18*, 1546-1552.
(47) Scheidt, W. R.; Reed, C. A. *Chem. Rev.* **1981**, *81*, 543-555.
(48) Krebs, B.; Mandt, J. *Chem. Ber* **1975**, *108*, 1130-1137.
(49) Gdaniec, M.; Milewska, M. J.; Polonski, T. *Angew. Chem. Int. Ed.* **1999**, *38*, 392-395.
(50) Banerjee, A.; Brown, C. J.; Lewis, J. F. P. *Acta Cryst.* **1982**, *B38*, 2744-2745.
(51) Szyrszyng, M.; Nowak, E.; Gdaniec, M.; Milewska, M. J.; Herman, A.; Polonski, T. *J. Org. Chem.* **2001**, *66*, 7380-7384.

Chapter 5. The synthesis, characterization and structures of nitrosyl heme(III) model complexes for thiolate and alkoxide heme proteins*

Introduction

Heme proteins containing the (por)Fe(SR) and (por)Fe(OR) moieties (por = porphyrinato dianion; SR = cysteinate, OR = tyrosinate) display rich and diverse reactivities that include nitric oxide (NO) biosynthesis, NO reduction, hydroxylation, detoxification of xenobiotics, and disproportionation of hydrogen peroxide.[1-3] The thiolate and alkoxide groups in these proteins serve as axial ligands that influence the reactivities of the iron centers. In the case of thiolate heme proteins, crystal structures of the cytochromes P450 reveal stabilization of the Fe-SR linkage via hydrogen bonding between the sulfur atom and neighboring peptide NH groups; in NO synthase (NOS), one of these hydrogen bonds is provided by the indole NH group of a conserved tryptophan (Trp) residue.[4]

It is well known that NO interacts readily with thiolate heme proteins. NO binds to the iron center in P450 and inhibits the enzyme.[5] Interestingly, the NO adduct of ferric NOS is an observable intermediate in the catalytic cycle of NOS.[6] In the case of fungal

---

* Reproduced in part with permission from "The First Structurally Characterized Nitrosyl Heme Thiolate Model complex" Xu, N.; Powell, D. R.; Cheng L.; Richter-Addo, G. B. *Chem. Commun.* **2006**, *2030-2032. Copyright © RSCPublishing.*
http://www.rsc.org/AboutUs/Copyright/RightsRetainedbyJournalsauthors.asp

P450nor (nor = nitric oxide reductase), NO binds to the ferric center and is reduced by NADH.[3] NO reacts with the ferric heme thiolate protein *Cimex nitrophorin* not only by nitrosylation of the iron center, but also by nitrosation of the axial thiolate sulfur atom (Fig. 5.1).[7] A related nitrosylation/nitrosation double reaction has been proposed as a

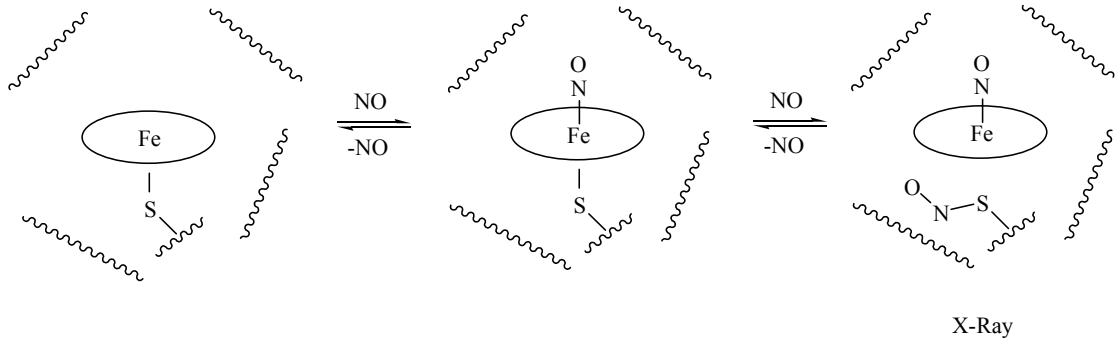

Figure 5.1. Proposed mechanism for the nitrosation of heme and axial thiolate in P450.

mechanism of deactivation of liver microsomal P450 by NO;[5] such processes have been proposed to occur with some ferric thiolate porphyrins based on result of kinetics.[8]

NO has been shown to bind reversibly to synthetic ferric thiolate porphyrins,[8,9] but no X-ray structural studies of synthetic iron nitrosyl heme thiolate compounds were reported prior to this study. Our group reported the preparation of nitrosyl thiolate porphyrins of Ru and Os by the *trans* addition reaction of alkyl thionitrites (RSNO) with a metalloporphyrin carbonyl compound (Eq. 5.1).[10-16] Several of these were characterized

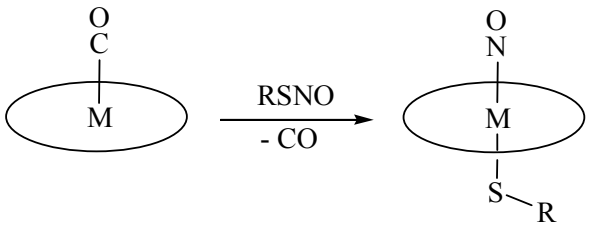

(5.1)

M = Ru, Os;

by X-ray crystallography. As shown in Table 5.1, the near linear Ru(Os)-N-O bond angles are dominant in these complexes.

Table 5.1. Bond angles for Ru(Os)-N-O (°) in six-coordinate nitrosyl thiolate metalloporphyrins.

Compound	∠ Ru(Os)–N–O	Reference
(OEP)Ru(NO)(SCH_2CF_3)	162.8	10
(OEP)Ru(NO)($SC(Me)_2CH_2NHC(O)Me$)	172.8(3)	12
(OEP)Ru(NO)(*S*-NACysMe)[a]	174.8(6)	11,13
(OEP)Ru(NO)(SCH_2CH_2SH)	170.9(9)	15
(TTP)Os(NO)(S-*i*-C_5H_{11})	172.0(9)	13
(OEP)Os(NO)($SC(Me)_2CH_2NHC(O)Me$)	176.8(5)	14
(OEP)Os(NO)(SEt)	172.7(8)	16

[a] *S*-NACysMe = *N*-acetyl-*S*-nitroso-L-cysteinate methyl ester

Surprisingly, the Fe-N-O angles in the two structural reports on the NO adducts of ferric heme thiolate proteins range from 100° to 165°.[3,17] Distal pocket residues are

known to affect the bent FeNO bond geometry in "ferrous" $\{FeNO\}^7$ nitrosyl heme proteins, but it is not clear to what extent distal residues influence the FeNO geometry in the formally "ferric" $\{FeNO\}^6$ derivatives.[18] For example, Hu and Kincaid have shown that the FeNO moiety in the NO adduct of ferric P450cam is linear in the absence of substrates, whereas it is slightly bent in the presence of substrates.[19] Further, Scherlis et al. have reported results of Density-Functional Theoretical (DFT) calculations on a [Fe(porphine)(NO)(cysteinate)] model, which show that the ground state structure possesses a linear FeNO geometry (178.7°), and that higher energy states of this model may contain bent FeNO geometries.[20]

Besides the ferric thiolate proteins above, NO also interacts with tyrosinate ferric metal center of heme enzyme catalase (Cat) which catalyzes the disproportionation of hydrogen peroxide to water and dioxygen.[21,22] Most catalases have porphyrin-type heme *b* as the prosthetic group. However, a number of fungal and bacterial catalases containing chlorin-type heme *d* have been reported.[23-25] Chlorins are reduced porphyrins which contain a partially saturated porphyrin macrocycle which is shown in Fig. 5.2. NO binds to the iron center in catalase and inhibits the enzyme reversiblly.[21] Ford and coworkers reported the formation of $Cat^{III}NO$ compound by the addition of NO into an aqueous solution of Cat^{III}.[22] In addition, NO-catalase complexes can be formed by the reactions of NH_2OH, azide and hyroxyurea with catalase.[26-29] As far as we know, no protein crystal structure of NO-catalase has been reported. The only structurally characterized synthetic

ferric porphyrin model complex with a *O*-bound ligand (other than water) *trans* to the

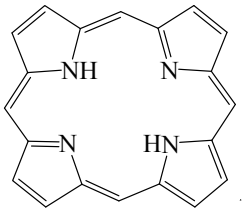

porphine

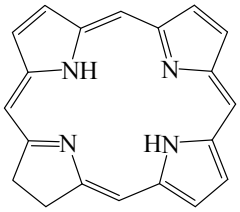

chlorin

Figure 5.2. Structural diagrams of porphine and chlorin.

nitrosyl was prepared in our group by the reaction of $[(TPP)Fe(THF)_2]ClO_4$ with *i*-$C_5H_{11}ONO$.[13] The crystal structure of the resulting cationic $[(TPP)Fe(NO)(HO\text{-}i\text{-}C_5H_{11})]^+$ compound reveals a linear FeNO geometry.

We were thus interested in structurally characterizing ferric heme model complexes containing mutually *trans* NO and *S*-bound or *O*-bound ligands. Octaethylporphyrin, tetraphenylporphyrin and tetraphenylchlorin were used in this study. Our major intent was to examine (i) the FeNO bond geometry in the absence of distal amino acid residues that could influence this geometry, and (ii) the effect of the bound NO group on the *trans* Fe-S(C), Fe-O(C) bonds.

Experimental section

All reactions were performed under an atmosphere of prepurified nitrogen using standard Schlenk glassware and/or in an Innovative Technology Labmaster 100 Dry Box. Solutions for spectral studies were also prepared under a nitrogen atmosphere. Solvents

were distilled from appropriate drying agents under nitrogen just prior to use: CH_2Cl_2 (CaH_2), THF (CaH_2), hexane (CaH_2), benzene (Na), toluene (Na).

Chemicals. Compounds (TPP)FeCl[30], [(por)Fe]$_2$O (por = TPP, OEP)[31-33] and (OEP)Fe(SPh)[34] were prepared by published procedures. CF_3COOH used in the preparation of (TPC)Fe($OCOCF_3$) was produced by the reaction of 2-aminothiophenol with trifluoroacetic anhydride. (OEP)FeCl was purchased from Mid-Century Chemical Inc. 2-Aminophenyl disulfide (97%), hydrazine hydrate ($H_2NNH_2 \cdot H_2O$, 50-60%), hypophosphorous acid (50%), 6-nitrobenzothiazole (99%), nitrosylsulphuric acid (40%), pyridine (anhydrous, 99.8%), sodium hydroxide (97%), thiophenol (97%), tin chloride dihydrate (98%), *p*-toluenesulfonyl chloride ($CH_3C_6H_4SO_2Cl$, 98%), trifluoroacetic anhydride (99%) were purchased from Aldrich Chemical Company. Acetic acid (99.8%), ammonia hydroxide (28-30%), hydrogen peroxide (30%), sodium bicarbonate (99%), sulfuric acid (95-98%) were purchased from EM Science. Sodium nitrite (97%) was purchased from J. T. Baker Chemical Company. Hydrochloric acid (36.5-38.0%), sodium chloride (99%), sodium sulfate (anhydrous, 99%) were purchased from EMD Chemical Inc. Chloroform–*d* (99.8%) was obtained from Cambridge Isotope Laboratories, and purified by three freeze-pump-thaw cycles, and stored over Linde 4 Å molecular sieves. Nitric oxide (98%, Matheson Gas) was passed through KOH pellets and a cold trap (dry ice/acetone) to remove higher nitrogen oxides. Elemental analyses were performed by Atlantic Microlab, Norcross, Georgia.

Instrumentation. Infrared spectra were recorded on a Bio–Rad FT–155 FTIR spectrometer. Proton NMR spectra were obtained on Varian 300 MHz spectrometer and the signals referenced to the residual signal of the solvent employed ($CHCl_3$ at 7.24 ppm). ESI mass spectra were obtained on a Micromass Q-TOF mass spectrometer.

Preparation of bis[2,6-bis(trifluoroacetylamino)phenyl]disulfide. The synthesis of [S-2,6-$(CF_3CONH)_2C_6H_3]_2$ was previously reported[35], however, the detailed procedure of the ligand preparation was not included in the paper. Thus, the 8-step preparation of [S-2,6-$(CF_3CONH)_2C_6H_3]_2$ is described in detail below.

Step 1. Preparation of 6-aminobenzothiazole: 6-Nitrobenzothiazole (13 g, 0.072 mol) was added to a stirred warm solution (55 ^oC) of stannous chloride (60 g, 0.26 mol) in concentrated hydrochloric acid (120 mL), and the mixture was kept at 65-70 ^oC in a water bath for 30 min. The mixture was cooled to 5 ^oC in an ice bath, and kept at 5 ^oC for 5 h. The precipitate was collected, dissolved in hot water (100 mL), and 40% aqueous solution of sodium hydroxide was added dropwise until the solution achieved a pH of 7-8. The solution was extracted with $CHCl_3$ (2×200 mL) and dried with anhydrous Na_2SO_4. Evaporation of the solvent gave 6-aminobenzothiazole as a light yellow solid (10 g, 0.067 mol, 93% yield). ^1H NMR ($CDCl_3$, ppm): δ 8.68 (s, 1H, H-1), 7.87 (d, 1H, H-7), 7.15 (d, 1H, H-4), 6.85 (dd, 1H, H-5), 3.84 (s, 2H, NH_2).

Step 2. Preparation of 6-toluene-*p*-sulfonamido-benzothiazole: A solution of 6-aminobenzothiazole (10 g, 0.067 mmol) and *p*-toluenesulfonyl chloride (15 g, 0.080

mol) in pyridine (10 mL) was refluxed for 1 h. The solution was cooled, and added to 6 N HCl (400 mL) and stirred for 2 h. A tar resulted, which was washed with water. The solid was extracted of 5% warm aqueous NaOH (2×400 mL), and the extract was added dropwise to a stirred solution of 15% HCl (200 mL). The precipitate was collected, washed with water, and dried in vacuo to give 6-toluene-*p*-sulfonamido-benzothiazole (10 g, 0.034 mol, 51% yield). ^{1}H NMR ($CDCl_3$, ppm): δ 8.92 (s, 1H, H-1), 7.95 (d, 1H, H-4), 7.79 (d, 1H, H-7), 7.63 (d, 2H, *m,m'-H* of Ph), 7.20 (d, 2H, *o,o'-H* of Ph), 7.09 (dd, 1H, H-5), 6.79 (s, 1H, N*H*), 2.35 (s, 3H of CH_3).

Step 3. Preparation of 7-nitro-6-toluene-*p*-sulfonamido-benzothiazole: 6-Toluene-*p*-sulfonamido-benzothiazole (9.2 g, 0.030 mol) was dissolved in the minimum amount of acetic acid at 60 ^{o}C (180 mL) with stirring. Solid $NaNO_2$ (ca. 0.10 g) was added, followed by a mixture of concentrated nitric acid (1.6 mL) and glacial acetic acid (2.0 mL). The stirred solution was heated to 90 ^{o}C and kept at this temperature overnight. After cooling to room temperature, the solution was poured over ice. The resulting precipitate was collected by filtration, washed with water, and dried in vacuo to give 7-nitro-6-toluene-*p*-sulfonamido-benzothiazole as a yellow solid (8.2 g, 0.023 mol, 77% yield). ^{1}H NMR ($CDCl_3$, ppm): δ 10.65 (s, 1H, N*H*), 9.02 (s, 1H, H-1), 8.29 (d, 1H, H-4), 8.05 (d, 1H, H-7), 7.81 (d, 2H, *m,m'-H* of Ph), 7.27 (d, 2H, *o,o'-H* of Ph), 2.36 (s, 3H of CH_3).

Step 4. Preparation of 7-nitro-6-aminobenzothiazole: 7-Nitro-6-toluene-*p*-sulfonamido-benzothiazole (4.6 g, 0.013 mol) was added to concentrated sulphuric acid (50 mL) and the solution was heated at 40°C for 10 min. After cooling to room temperature, the solution was poured on ice and neutralized with aqueous NH_4OH. The product was extracted with $CHCl_3$ (2×200 mL), and the combined $CHCl_3$ extracts were dried with anhydrous Na_2SO_4. Evaporation of the solvent gave solid 7-nitro-6-aminobenzothiazole (2.4 g, 0.012 mol, 93% yield). ^{1}H NMR data is not available because of the low solubility of the product in $CDCl_3$. This product was used directly for the next step.

Step 5. Preparation of 7-nitrobenzothiazole: 7-Nitro-6-aminobenzothiazole (2.4 g, 0.012 mol) was added to 2% nitrosylsulphuric acid (50 mL) at 0 ^{o}C. After stirring the solution for 15 min, 50% hypophosphorous acid (25 mL) was added, and the mixture was kept at 0 ^{o}C for 30 min and left at room temperature overnight. The solution was poured on ice (100 g) and excess aqueous ammonia was added. The brown precipitate was collected, dried in vacuo, and extracted with benzene (3×250 mL). After removal of the solvent, 7-nitrobenzothiazole was obtained (1.7 g, 9.4 mmol, 76% yield). ^{1}H NMR ($CDCl_3$, ppm): δ 9.17 (s, 1H, H-1), 8.45 (dd, 2H, H-5,7), 7.69(t, 1H, H-6).

Step 6. Preparation of 7-aminobenzothiazole: 7-Nitrobenzothiazole (1.0 g, 5.5 mmol) was added to a warm (55 ^{o}C) stirred solution of stannous chloride ($SnCl_2 \cdot 2H_2O$, 6.0 g) in concentrated HCl (20 mL). The mixture was heated and kept at 65-70 ^{o}C for 30 min. The mixture was then cooled to 5 ^{o}C in an ice bath and kept at this temperature for 5

h. The precipitate was collected and dissolved in hot water (20 mL). A 40% aqueous sodium hydroxide was added dropwise until the solution reached a pH of 7-8. The solution was extracted with $CHCl_3$ (2×50 mL). The solution was removed from the extracts in vacuo to give 7-aminobenzothiazole (0.75 g, 5.0 mmol, 91% yield) as a white solid. ^{1}H NMR ($CDCl_3$, ppm): δ 8.93 (s, 1H, H-1), 7.62 (d, 1H, H-7), 7.33 (t, 1H, H-6), 6.74 (d, 1H, H-5), 3.79 (s, 2H of NH_2).

Step 7. Preparation of bis(2,6-diaminophenyl)disulfide: Hydrazine hydrate ($H_2NNH_2 \cdot H_2O$, 1.5 mL) was added to a stirred ethanol solution (10 mL) of 7-aminobenzothiazole (0.44 g, 2.9 mmol). The solution was refluxed for 3 h and then cooled to 5 ^oC in an ice bath. Hydrogen peroxide (30%, 2 mL) was added, and the solution immediately solidified. Recrystallization of this solid from ethanol gave bis(2,6-diaminophenyl)disulfide as needle-shaped crystals (0.32 g, 1.2 mmol, 79% yield). ^{1}H NMR ($CDCl_3$/d_6-acetone = 3:7, ppm): δ 6.10 (t, 2H), 5.32 (d, 4H), 4.15 (s, 8H of NH_2).

Step 8. Preparation of bis[2,6-bis(trifluoroacetylamino)phenyl]disulfide, [S-2,6-$(CF_3CONH)_2C_6H_3]_2$: To a stirred THF solution (10 mL) of bis(2,6-diaminophenyl)disulfide (0.20 g, 0.72 mmol) was added trifluoroacetic anhydride (1.5 mL) at 0 ^oC. The solution was stirred overnight at room temperature. Water (10 mL) was added, and the resulting solution was concentrated then redissolved in a mixture of ethyl acetate (100 mL) and water (25 mL). The organic layer was washed with 2% HCl aqueous solution, saturated NaCl aqueous solution, 4% $NaHCO_3$ aqueous solution,

and saturated NaCl aqueous solution successively, dried over Na_2SO_4, and concentrated to dryness. The crude product was recrystallized from diethyl ether to give pale yellow crystals of bis[2,6-bis(trifluoroacetylamino)phenyl]disulfide (0.30 g, 0.49 mmol, 68% yield). ^{1}H NMR ($CDCl_3$, ppm): δ 8.60 (s, 4H of N*H*), 8.20 (d, 4H), 7.62 (t, 2H). IR (CH_2Cl_2, cm^{-1}): ν_{CO} = 1743.

Preparation of bis[(2-trifluoroacetylamino)phenyl]disulfide, [S-2-($CF_3CONH)C_6H_4]_2$. [S-2-($CF_3CONH)C_6H_4]_2$ was prepared using methods similar to those described for the preparation of [S-2,6-($CF_3CONH)_2C_6H_3]_2$; however, bis(2-aminophenyl)disulfide was used instead of bis(2,6-diaminophenyl)disulfide as starting material in step 8. Yield: 72%. ^{1}H NMR ($CDCl_3$, ppm): δ 8.78 (s, 2H of N*H*), 8.34 (dd, 2H), 7.49 (td, 2H), 7.35 (dd, 2H), 7.13 (td, 2H). IR (CH_2Cl_2, cm^{-1}): ν_{CO} = 1743.

Preparation of (OEP)Fe[S-2,6-($CF_3CONH)_2C_6H_3$] (1). The compound was prepared from the reaction of (OEP)Fe(SPh) with [S-2,6-($CF_3CONH)_2C_6H_3]_2$ by modified literature method[36-38].

A mixture of (OEP)Fe(SPh) (0.19 g, 0.28 mmol) and [S-2,6-($CF_3CONH)_2$-$C_6H_3]_2$ (0.11 mg, 0.17 mmol) in toluene (12 mL) was stirred for 1 h at 60 °C using an oil bath. The color changed from dark purple to reddish purple. The solution was reduced to 4 mL in vacuo, and then hexane (30 mL) was added. This solution mixture was kept at -20 °C overnight. The precipitate was collected by filtration, and dried in vacuo to give

black microcrystals (0.14 g, 0.11 mmol, 56% yield). X-ray diffraction-quality crystals were grown at room temperature from a CH_2Cl_2/hexane (3:1) mixture by slow evaporation. Anal. Calcd for $C_{46}H_{49}F_6N_6O_2SFe \cdot 0.6C_6H_{14}$: C, 61.32; H, 5.95; N, 8.65; S, 3.30. Found: C, 60.07; H, 5.37; N, 9.14; S, 3.49. IR (CH_2Cl_2, cm^{-1}): ν_{CO} = 1720; IR (KBr, cm^{-1}): ν_{CO} = 1728; also 2969 s, 2935m, 2873 m, 1583 m, 1512 m, 1466 m, 1450 w 1374 w, 1265 s, 1190 s, 1164 m, 1057 w, 1010 w, 961 m, 841 w.

Preparation of (OEP)Fe[S-2-($CF_3CONH)C_6H_4$] (2). (OEP)Fe[S-2-($CF_3CONH)C_6H_4$] was prepared in a simliar method which was described for the preparation of compound **1** except [S-2-($CF_3CONH)C_6H_4]_2$ was used instead of [S-2,6-($CF_3CONH)_2C_6H_3]_2$. The product was obtained in 56% isolated yield. Suitable crystals were grown at room temperature from a CH_2Cl_2/hexane (3:1) mixture by slow evaporation. Anal. Calcd for $C_{44}H_{49}F_3N_5OSFe \cdot 0.2C_6H_{14}$: C, 65.72; H, 6.32; N, 8.48; S, 3.88. Found: C, 68.31; H, 6.11; N, 8.66; S, 3.96. IR (CH_2Cl_2, cm^{-1}): ν_{CO} = 1720; IR (KBr, cm^{-1}): ν_{CO} = 1722, also 2967 s, 2933m, 2873 m, 1735 m, 1577 w, 1534 m, 1458 w, 1278 s, 1187 s, 1161 m, 1056 m, 1016 s, 958 m, 752 w.

Preparation of (TPP)Fe[S-2,6-($CF_3CONH)_2C_6H_3$] (3). The (TPP)Fe[S-2,6-($CF_3CONH)_2C_6H_3$] complex was prepared using the reported literature method.[38] Suitable crystals were grown at room temperature from a CH_2Cl_2/acetonitrile (3:1) mixture by slow evaporation.

Preparation of (TPC)Fe[S-2,6-$(CF_3CONH)_2C_6H_3$] (4). To a toluene solution (10 mL) of $[(TPC)Fe]_2O$ (25 mg, 0.018 mmol) was added diphenyl disulfide (40 mg, 0.18 mmol) and 0.02 mL (0.20 mmol) thiophenol. The solution was stirred overnight at 60 ^oC. The solution was reduced to 2 mL in vacuo, and then hexane (20 mL) was added. The precipitate was collected and redissolved in 10 mL toluene. $[S\text{-}2,6\text{-}(CF_3CONH)_2C_6H_3]_2$ (12 mg, 0.018 mmol) was added at 60 °C and the solution was stirred overnight. No obvious color change was observed. The solution was reduced to 2 mL in vacuo, and then hexane (20 mL) was added. This solution mixture was kept at -20 °C overnight resulting in the formation of a black precipitate. The precipitate was collected by filtration, and dried in vacuo to give black microcrystals (12 mg, 0.012 mmol, 33% yield). Suitable crystals for X-ray crystallography were grown at room temperature from a CH_2Cl_2/hexane (2:1) mixture by slow evaporation. IR (CH_2Cl_2, cm^{-1}): ν_{CO} = 1733; IR (KBr, cm^{-1}): ν_{CO} = 1720; also 3294 s, 1583 m, 1510 m, 1465 m, 1441 w, 1411 w, 1331 m, 1265 s, 1190 s, 1065 w, 1018 w, 1003 m, 992 s, 967 m, 800 m, 752 m, 702 s.

Preparation of (TPC)Fe($OCOCF_3$) (5). To a stirred CH_2Cl_2 solution (5 mL) of $[(TPC)Fe]_2O$ (20 mg 0.015 mmol) was added excess trifluoroacetic acid at room temperature. After the solution was stirred for 8 hours, the solvent was reduced to approximately 2 mL and then hexane (20 mL) was added. This mixture was kept at -20 °C overnight. The precipitate that formed was collected by filtration and dried in vacuo to give black microcrystals (12 mg, 0.015 mmol, 51% yield). Suitable crystals for X-ray

crystallography were grown at room temperature from a CH_2Cl_2/hexane (1:1) mixture by slow evaporation. IR (KBr, cm^{-1}): ν_{CO} = 1717; also 1585 m, 1542 m, 1509 s, 1441 m, 1387 m, 1333 m, 1197 s, 1174 s, 1145 s, 1069 m, 1019 m, 1003 s, 992 s, 800 m, 752 m, 719 m, 701 s, 660 w, 613 w, 522 w. ESI mass spectrum: *m/z* 670 $[(TPC)Fe]^+$ (100%)

Preparation of (por)Fe(NO)(X) and (chlorin)Fe(NO)(X) compounds (por = OEP, TPP; chlorin = TPC; X = S-2-$(CF_3CONH)C_6H_4$, S-2,6-$(CF_3CONH)_2C_6H_3$, $OCOCF_3$). These nitrosyl compounds were prepared from the reaction of 5-coordinate (por)Fe(X) with NO gas. The following reaction is representative:

A Schlenk flask was charged with hand-picked crystals of (OEP)Fe[S-2,6-$(CF_3CONH)_2C_6H_3$], and placed under an atmosphere of NO gas for 12 hours, during which time the color of the crystals turned from dark brown to slightly dark red. A suitable crystal was then picked for X-ray diffraction studies. The bulk product was a mixture of the desired six-coordinate nitrosyl complex and the side-product five-coordinate nitrosyl complex based on IR spectroscopy.

(OEP)Fe(NO)[S-2,6-$(CF_3CONH)_2C_6H_3$] (6). IR (KBr, cm^{-1}): ν_{NO} = 1830. Also present was a band at 1672 cm^{-1} due to ν_{NO} of (OEP)Fe(NO).

(TPP)Fe(NO)[S-2,6-$(CF_3CONH)_2C_6H_3$] (7). IR (KBr, cm^{-1}): ν_{NO} = 1847. Also present was a band at 1686 cm^{-1} due to ν_{NO} of (TPP)Fe(NO).

(TPC)Fe(NO)[S-2,6-$(CF_3CONH)_2C_6H_3$] (8). IR (KBr, cm^{-1}): ν_{NO} = 1831. Also present was a band at 1685 cm^{-1} due to ν_{NO} of (TPC)Fe(NO).

(OEP)Fe(NO)[S-2-$(CF_3CONH)C_6H_4$] (9). The (OEP)Fe(NO)[S-2-$(CF_3CONH)C_6H_4$] compound was generated similarly in powder form. IR (KBr, cm^{-1}): ν_{NO} = 1859. Also present was a band at 1672 cm^{-1} due to ν_{NO} of (OEP)Fe(NO).

(TPC)Fe(NO)$(OCOCF_3)$ (10). IR (KBr, cm^{-1}): ν_{NO} = 1899, ν_{CO} = 1717; also 2923 s, 2848 m, 1588 s, 1560 m, 1542 m, 1522 m, 1508 m, 1441 m, 1335 m, 1175 s, 1143 s, 1070 m, 1004 s, 834 w, 800 w, 752 m, 721 w, 702 m, 660 w.

Attempted preparation of (OEP)Fe(NO)[S-2,6-$(CF_3CONH)_2C_6H_3$] in CH_2Cl_2. (OEP)Fe[S-2,6-$(CF_3CONH)_2C_6H_3$] (0.010g, 0.011 mmol) was dissolved in CH_2Cl_2 (20 mL) and NO gas was bubbled through the solution at room temperature for 5 min. The reaction was monitored by IR spectroscopy. The resulting product appeared to be a mixture of (OEP)Fe(NO) and [S-2,6-$(CF_3CONH)_2C_6H_3]_2$ (by IR spectroscopy).

Results and discussion

The synthesis of [S-2,6-$(CF_3CONH)_2C_6H_3]_2$ was previously reported,[35] however, the synthetic procedures from the commercially available starting material (6-nitrobenzothiazole) were not described in the paper. After much effort, we successfully prepared the desired compound. The scheme of this 8-step preparation of [S-2,6-$(CF_3CONH)_2C_6H_3]_2$ is shown in Figure 5.3.

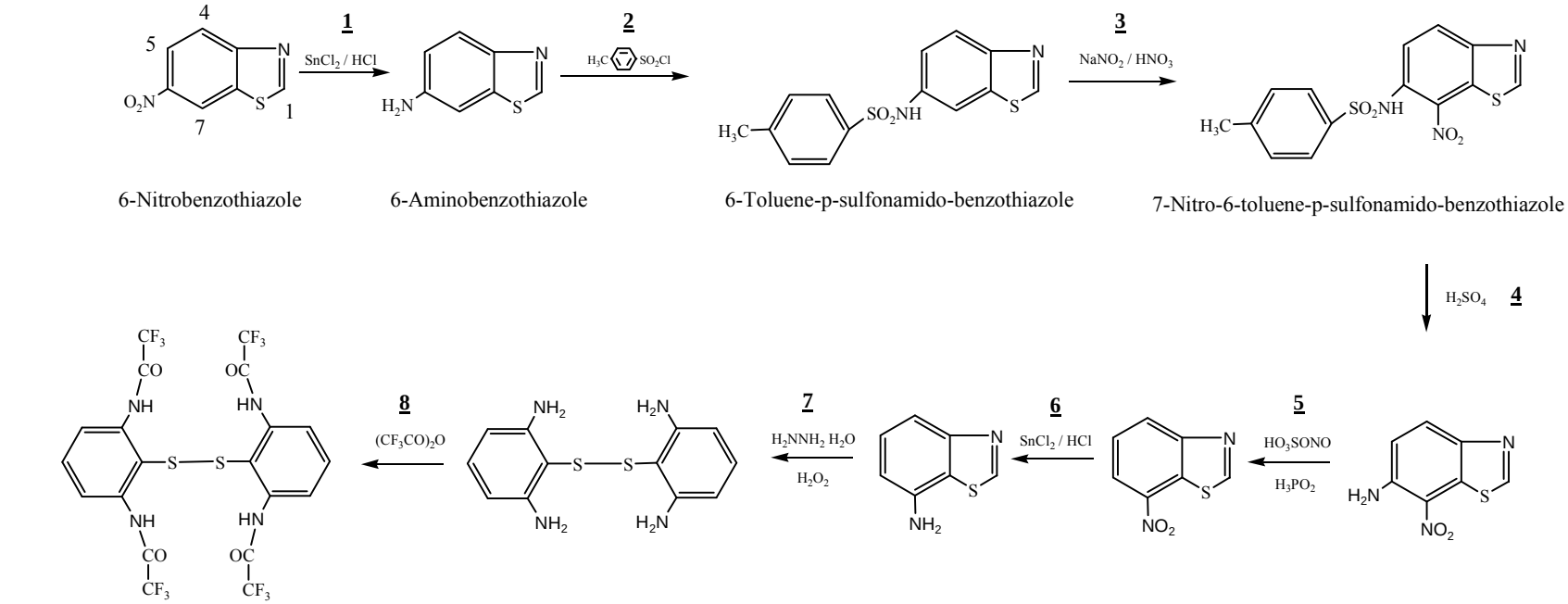

Figure 5.3. Synthesis of bis[2,6-bis(trifluoroacetylamino)phenyl]disulfide.

The five-coordinate thiolate iron porphyrin compounds used in this study have been reported previously,[36-38] and the new chlorin derivative, (TPC)Fe[S-2,6-$(CF_3CONH)_2C_6H_3$] was prepared using similar procedures for the porphyrin derivatives which is shown schematically (for compounds **1**, **3** and **4**) in equation 5.2. The

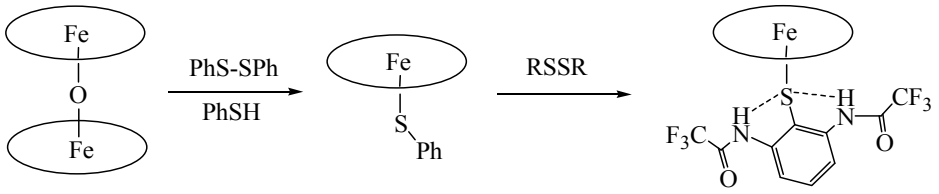

(5.2)

(TPC)Fe[S-2,6-$(CF_3CONH)_2C_6H_3$] complex was synthesized in 33% isolated yield from the reaction of μ-oxo dimer iron chlorin with thiophenol and then [S-2,6-$(CF_3CONH)_2C_6H_3]_2$. The structural diagrams of the compounds prepared during this study are shown in Figure 5.4. The model complexes **(1-4)** possess 1 or 2 hydrogen bonds between the sulfur atom and NH groups which imitate the hydrogen bonding environment around the bound S atom from the proximal cysteinate ligands in the thiolate-ligated hemeproteins. Compared to many other model complexes of ferric thiolate proteins, these complexes are fairly stable in air or moisture due to these hydrogen bonds.

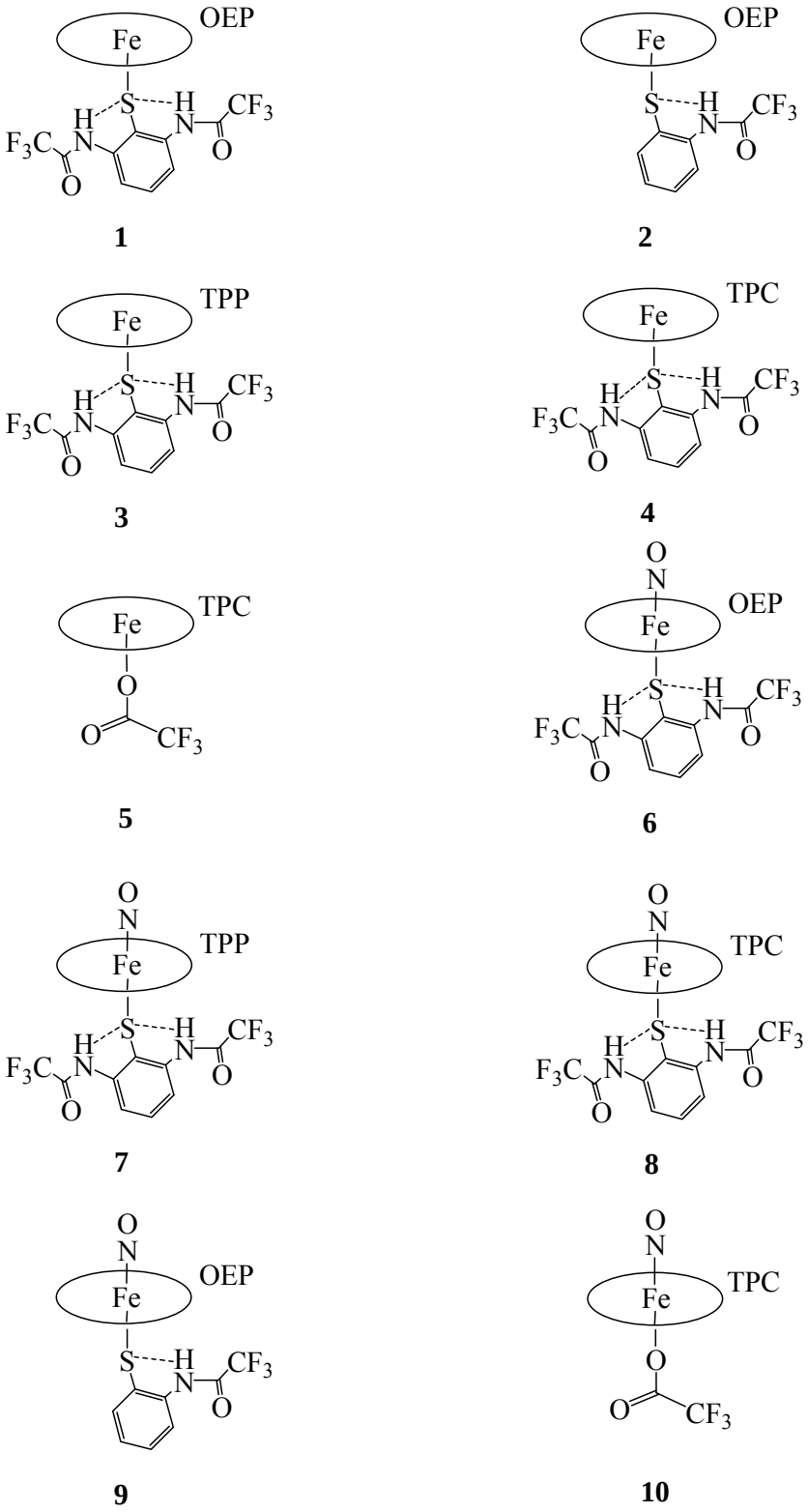

Figure 5.4. Structural diagrams of compounds **1-10**.

The reactions of the five-coordinate iron porphyrin thiolate complexes with NO in CH_2Cl_2 were attempted (Eq. 5.3), and the resulting six-coordinate nitrosyl thiolate iron

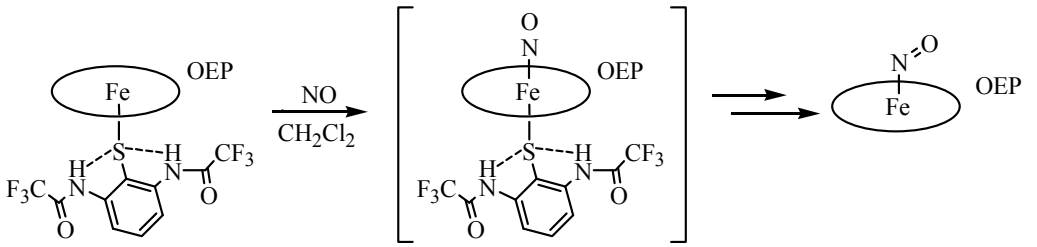

(5.3)

1

porphyrin decomposed to the five-coordinate nitrosyl porphyrin rapidly. To illustrate this, the reaction of the five-coordinate iron porphyrin thiolate complex $(OEP)Fe^{III}[S\text{-}2,6\text{-}(CF_3CONH)_2C_6H_3]$ **(1)** with NO in CH_2Cl_2 was monitored by IR spectroscopy. The resulting spectra recorded at different times after NO addition are shown in Figure 5.5. A new band at ~1850 cm^{-1} formed immediately after NO addition assigned to ν_{NO} of the six-coordinate intermediate in equation 5.3. (*c.f.*, free NO at 1875 cm^{-1}).[39] However, this band was quickly consumed with the resulting formation of the ν_{NO} band at 1667 cm^{-1} due to the final five-coordinate (OEP)Fe(NO) compound. Also observed was the reduction in intensity of the band at 1720 cm^{-1} due to the ν_{CO} (of the thiolate ligand) of $(OEP)Fe^{III}[S\text{-}2,6\text{-}(CF_3CONH)_2C_6H_3]$ and the generation of a new band at 1743 cm^{-1} which is coincident with the ν_{CO} of the organic disulfide (We verified this ν_{CO} assignment by preparing the organic disulfide and recording its IR spectrum; Experimental section). We thus assign the new band at ~1850 cm^{-1} to the ν_{NO} of the target six-coordinate compound $(OEP)Fe(NO)[S\text{-}2,6\text{-}(CF_3CONH)_2C_6H_3]$. The disappearance of

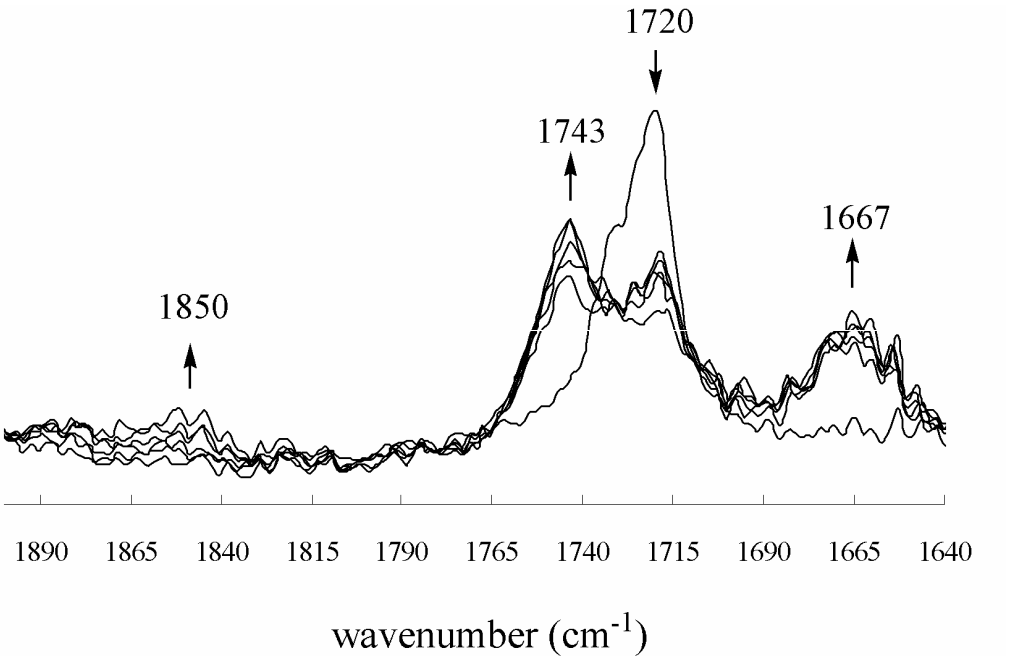

Figure 5.5. Infrared spectral monitoring of the reaction of **1** with NO in CH_2Cl_2; Intervals are 0 s, 10 s, 20 s, 35 s, 60 s, and 120 s.

the initial 1720 cm^{-1} band appears to occur in two phases; an initial rapid loss from 0-10 seconds, and a slower phase after 10 seconds. Further work is needed to determine the nature of this reaction.

All our attempts, to date, at crystallizing six-coordinate nitrosyl thiolate iron porphyrins/chlorin from their reaction mixtures have not been successful; only the five-coordinate nitrosyl derivatives were obtained, consistent with the readily lost thiolate ligands from the six-coordinate compounds in solution.

Due to the fact that the decomposition of the desired six-coordinate species is very fast in solution, we hypothesized that a heterogeneous (solid-gas) reaction without solvent may slow down the decomposition, allowing for stabilization and isolation of the six-coordinate compounds. Indeed, the reactions of the iron porphyrin/chlorin thiolate compounds (**1-4**, as powders) with NO gas in a solvent-free environment produced corresponding nitrosyl derivatives with ν_{NO} bands in the 1830-1859 cm^{-1} range (KBr) (Table 5.2). The five-coordinate nitrosyl side-products were also formed as judged by the

Table 5.2. Infrared spectral data for six-coordinate nitrosyl thiolate iron porphyrins.

Compound	ν_{NO} (cm^{-1})		Reference
	KBr	CH_2Cl_2	
(OEP)Fe(NO)[S-2,6-$(CF_3CONH)_2C_6H_3$] **(6)**	1830	1850	This work
(OEP)Fe(NO)[S-2-$(CF_3CONH)C_6H_4$] **(9)**	1859		This work
(TPP)Fe(NO)[S-2,6-$(CF_3CONH)_2C_6H_3$] **(7)**	1847		This work
(TPC)Fe(NO)[S-2,6-$(CF_3CONH)_2C_6H_3$] **(8)**	1831		This work
SRFe-NO [a]		1826	9

[a] The structural diagram of **SR**Fe-NO is shown in Figure 5.6.

presence of the characteristic bands at ~1680 cm^{-1} in the IR spectra. These products were stable as solids under an atmosphere of NO for several days in the dark. However, attempted dissolution and crystallization of the nitrosyl products resulted only in the

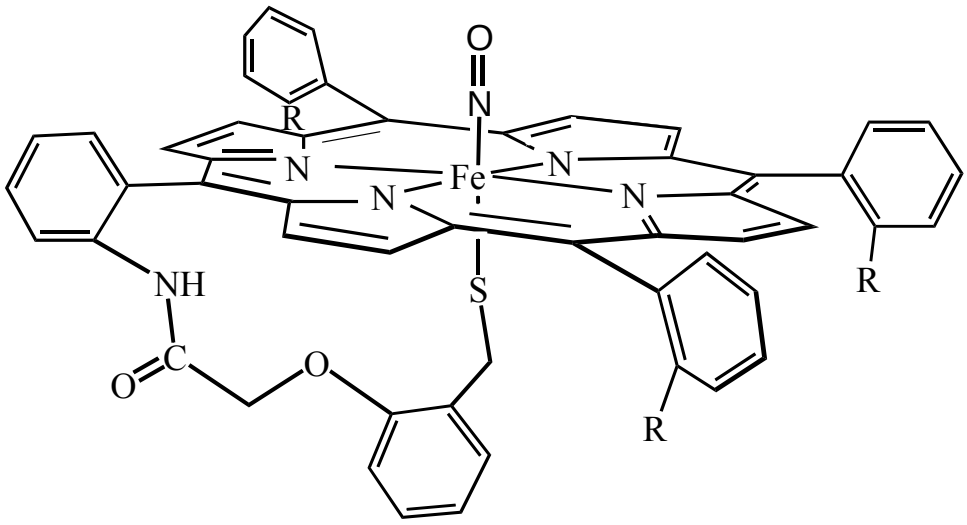

Figure 5.6. Structural diagram of SR(Fe^{III})-NO (R = $NHCOC(CH_3)_3$).

generation of the precursor compounds and five-coordinate nitrosyl compounds. For example, the solid product (OEP)Fe(NO)[S-2,6-$(CF_3CONH)_2C_6H_3$] rapidly decomposed to (OEP)Fe[S-2,6-$(CF_3CONH)_2C_6H_3$] and (OEP)Fe(NO) after dissolution in CH_2Cl_2.

We then explored the possibility of the heterogeneous reaction of crystals of these five-coordinate thiolate compounds with NO gas with the hope that products formation would not be accompanied by extensive crystal fragmentation. Crystals of (OEP)Fe[S-2,6-$(CF_3CONH)_2C_6H_3$] **(1)** which were grown from CH_2Cl_2/hexane (2:1)[36] were first tried using this method. The molecular structure of **1** is shown in Figure 5.7. Several purple crystals of **1** were hand-picked and exposed to NO gas at room temperature for several hours to allow for NO diffusion into the crystal lattice. The crystal was mounted immediately after removal of the NO atmosphere. The structure of the

six-coordinate nitrosyl product (OEP)Fe(NO)[S-2,6-$(CF_3CONH)_2C_6H_3$] **(6)** was obtained successfully and its molecular structure is shown in Figure 5.8. Interestingly, the volume of the crystal lattice increased from 2266.3(6) $Å^3$ for the crystal of **1** to 2360(2) $Å^3$ for the crystal of its nitrosyl derivative **6**. Selected structural data of **6** are presented in Table 5.3, and are compared with the related data from starting complex **1**.

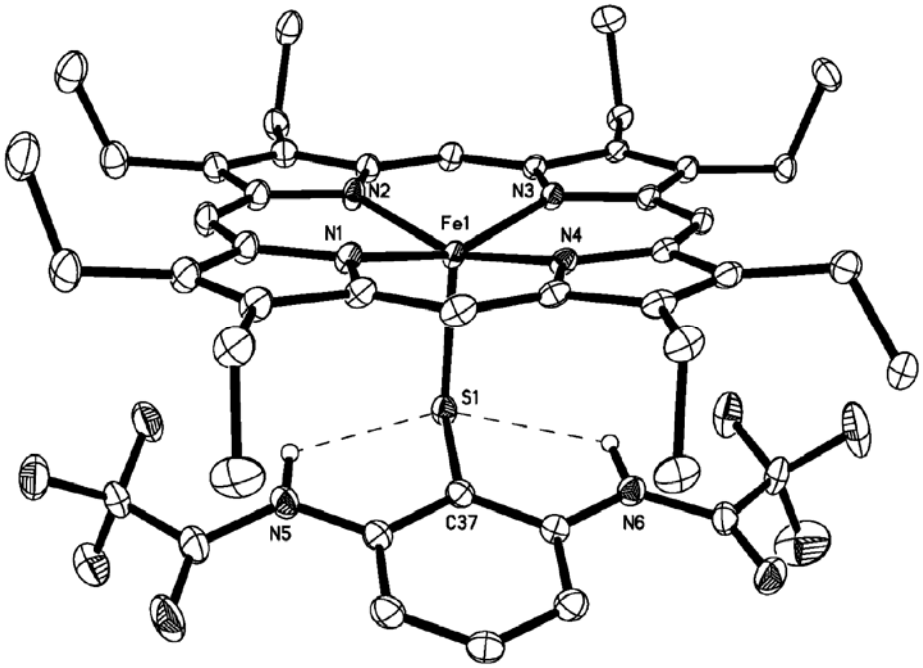

Figure 5.7. Molecular structure of (OEP)Fe[S-2,6-$(CF_3CONH)_2C_6H_3$] **(1)**.

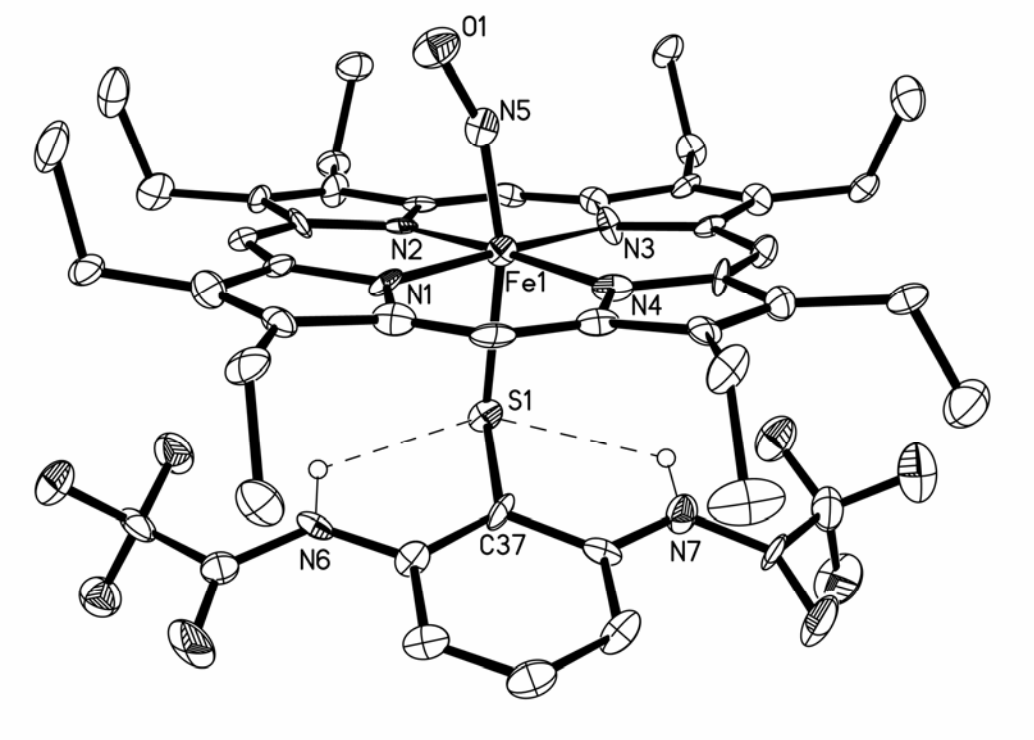

Figure 5.8. Molecular structure of (OEP)Fe(NO)[S-2,6-$(CF_3CONH)_2C_6H_3$] **(6)**.

Table 5.3. Selected structural data (in Å and °) for (OEP)Fe[S-2,6-$(CF_3CONH)_2C_6H_3$] (**1)** and (OEP)Fe(NO)[S-2,6-$(CF_3CONH)_2C_6H_3$] (**6).**

	1	**6**
Fe–N(O)		1.671(9)
N–O		1.187(9)
Fe–N_{por}	2.054(2)- 2.064(2)	2.003(8)- 2.017(7)
Fe–S	2.359(1)	2.356(3)
∠Fe–N–O		159.6(8)
∠S–Fe–N		165.5(3)
∠C37–S1–Fe1	104.22(11)	110.6(3)
S tilt [a]	3.4 [4.3]	6.3 [6.7]

[a] Tilt of the S atom from the normal to the porphyrin 4N [24-atom] plane.

The five-coordinate O-bound ferric chlorin compound, (TPC)Fe($OCOCF_3$) **(5)**, was prepared by the reaction of [(TPC)Fe]$_2$O with CF_3COOH. This synthetic method is similar to that of (OEP)Fe($OCOCCl_3$).[40] An X-ray suitable crystal of (TPC)Fe($OCOCF_3$) was grown from a CH_2Cl_2/hexane mixture by slow evaporation of the solvent under inert atmosphere. The molecular structure is displayed in Fig. 5.9.

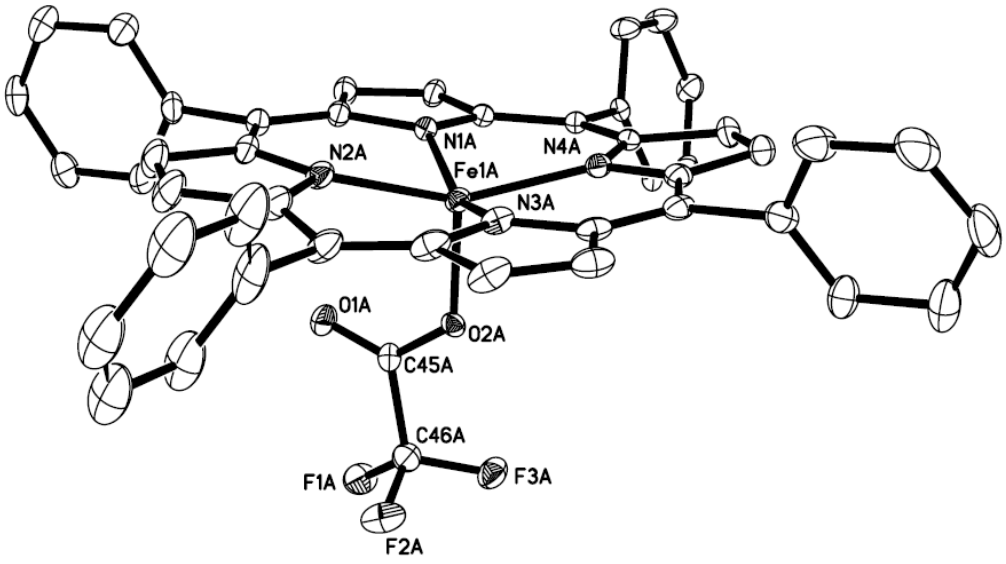

Figure 5.9. Molecular structure of (TPC)Fe($OCOCF_3$) **(5)**.

The preparation and isolation of model complexes of nitrosyl ferric tyrosinate heme proteins are also very difficult because of the well known high lability of the nitrosyl group in $\{FeNO\}^6$ porphyrin complexes.[41] For example, the nitrosyl alcohol iron porphyrin complex, $[(TPP)Fe(NO)(i\text{-}C_5H_{11}OH)]ClO_4$, is air-sensitive in both the solid state and organic solvent and it is also thermally unstable, readily losing the nitrosyl group.[13] In addition, $\{FeNO\}^6$ porphyrin complexes are readily reduced to $\{FeNO\}^7$ complexes under the conditions of excess NO with the presence of NO^+ acceptors such as H_2O or ROH in solution. Because of these synthetic difficulties, the solid-gas reaction method was again used to prepare the nitrosyl derivative of **5.** The desired $(TPC)Fe(NO)(OCOCF_3)$ **(10)** product was prepared successfully by the reaction of the iron chlorin compound **5** with NO gas in a solvent-free environment. Further, we were able to obtain the crystal structure of **10** using hand-picked crystals to react with NO gas (Figure 5.10). Selected structural data of **10** are presented in Table 5.4 and are compared with the related data from **5**.

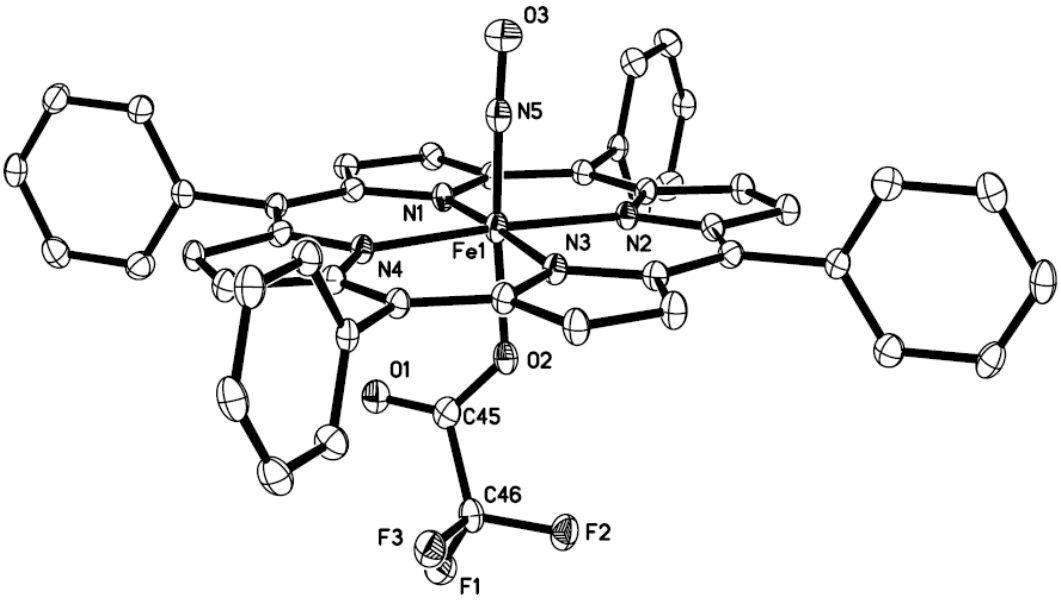

Figure 5.10. Molecular structure of (TPC)Fe(NO)($OCOCF_3$) **(10)**.

Table 5.4. Selected structural data (in Å and °) for (TPC)Fe($OCOCF_3$) **(5)** and (TPC)Fe(NO)($OCOCF_3$) **(10)**.

	5	**10**
Fe1–N5		1.635(5)
N5–O1		1.153(5)
Fe1–N_{por}	2.052(4)- 2.086(4)	2.012(3)- 2.020(4)
Fe1–O2	1.939(4)	1.902(4)
∠Fe1–N5–O3		177.0(4)
∠O2–Fe1–N5		173.0(2)
∠C45–O2–Fe1	127.8(7)	131.7(3)
O tilt	4.0 [5.0]	4.7 [5.0]

[a] Tilt of the S atom from the normal to the porphyrin 4N [24-atom] plane.

There are several interesting features about the structures of the six-coordinate nitrosyl ferric complexes **6** and **10**. The selected structural data for **6, 10** and corresponding five-coordinate precursors **1, 5** are listed in Table 5.3 and 5.4. First, the FeNO moiety in **6** is bent with an angle of 159.6(8)° (β), and in **10** is near linear with an angle of 177.0(4)° (β') in these two formally $\{FeNO\}^6$ compounds which are expected to have a linear FeNO linkage. The nitrosyl N-atom in **6** is tilted 9.1° (α) from the normal to 24-atom porphyrin plane (α' = 1.9° in **10)**. The S atom in **6** and O atom in **10** are also titled 6.7° (γ) and 5.0° (γ'), respectively. The corresponding angles are shown in Figure

5.11. The bent NO geometry in **6** is not the result of any close intermolecular contacts; the shortest intermolecular distances are between the nitrosyl O-atom and a thiolate F atom of another molecule, and between the nitrosyl N-atom and another porphyrin ethyl carbon atom (both distances are ≥ 3.3 Å). Recently, Paulat et al. studied the electronic structure of **6** by Density Functional Theory (DFT) using our X-ray derived coordinates and revealed that the intrinsic bending of the FeNO moiety was due to an additional Fe-N(O) σ interaction that is mediated by the d_{z^2}/d_{xz} orbital of Fe and a σ*-type orbital of NO.[42] On the other hand, the near linear conformation of FeNO moiety in **10** is consistent with those of $\{FeNO\}^6$ complexes.

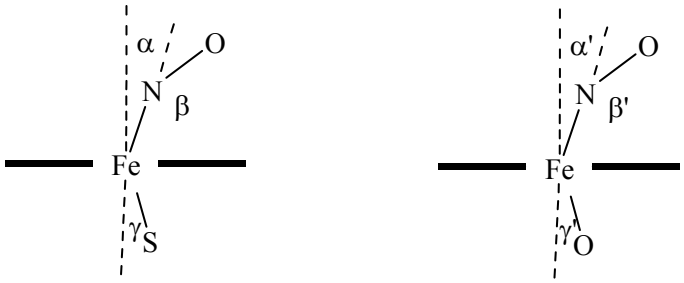

6 **10**

Fig 5.11. Selected bond angles and tilting angles of (OEP)Fe(NO)[S-2,6-$(CF_3CONH)_2C_6H_3$] **(6)**, and (TPC)Fe(NO)($OCOCF_3$) **(10)**.

Second, both the Fe atoms in **6** and **10** are situated almost coincident with the 24-atom mean planes of the porphyrin or chlorin, with upward displacements of 0.01 Å and 0.07 Å, respectively, towards the NO ligands (Figure 5.12b, 5.13b). Concurrent with these upward movements of the Fe atoms upon formation of **6** and **10** are the shortening of

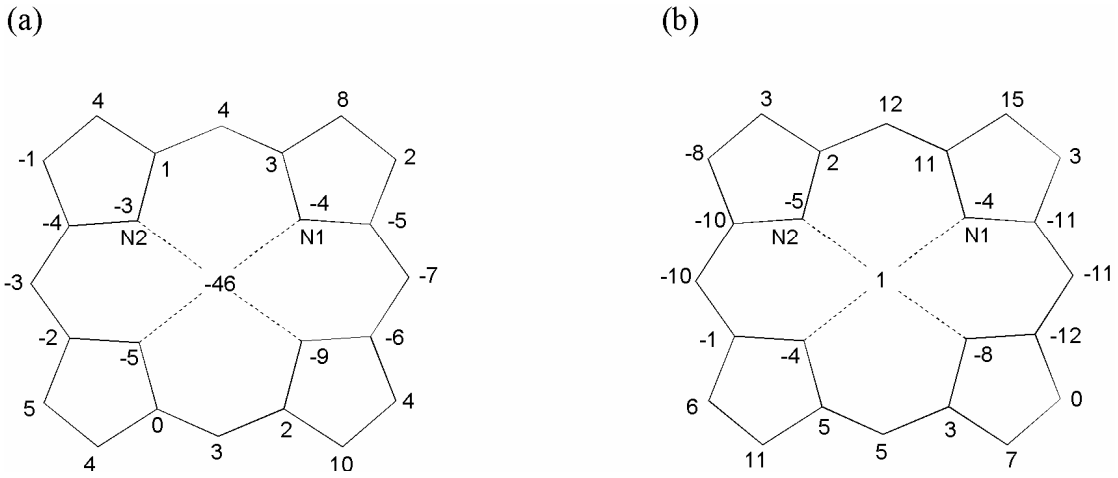

Figure 5.12. Perpendicular atom displacements (in units of 0.01 Å) of the porphyrin core from the 24-atom mean porphyrin planes of (a) (OEP)Fe[S-2,6-$(CF_3CONH)_2C_6H_3$] **(1)** and (b) (OEP)Fe(NO)[S-2,6-$(CF_3CONH)_2C_6H_3$] **(6)**.

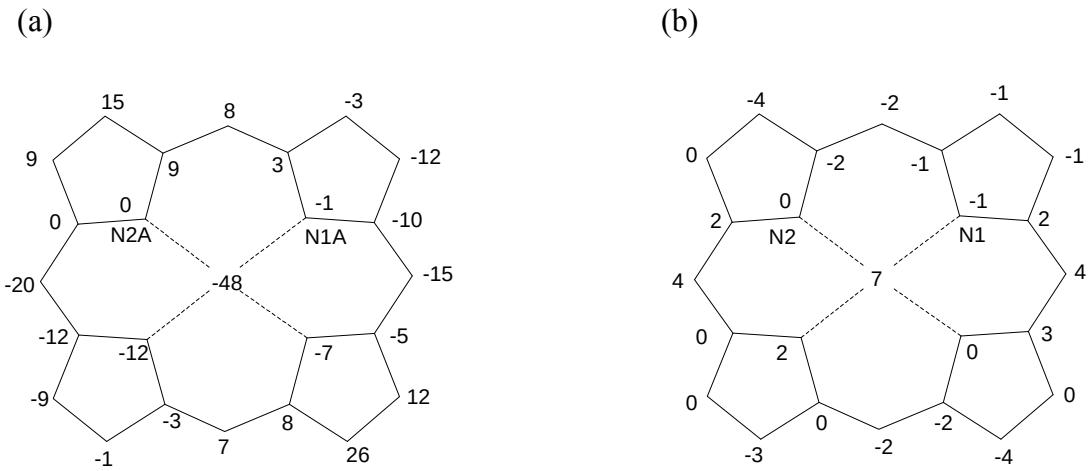

Figure 5.13. Perpendicular atom displacements (in units of 0.01 Å) of the porphyrin core from the 24-atom mean porphyrin planes of (a) (TPC)Fe($OCOCF_3$) **(5)** and (b) (TPC)Fe(NO)($OCOCF_3$) **(10)**.

the Fe–N_{por} bond lengths by ~0.05 Å. Considering that the Fe atoms were displaced 0.46 Å and 0.48 Å towards the S and O atoms in the precursor **1** and **5** (Figure 5.12a, 5.13a), these represent a remarkable ~0.47 Å and 0.55 Å apical movements of the Fe atoms in these solid-state reactions of **1** and **5** with NO gas! Also, the distance between the two closest porphyrin planes in **6** increases from around 4.7 Å to 5.2 Å which is consistent with the increased volume of crystal lattice of **6**. Even more striking is that the *trans* Fe–S bond length does not change in going from the five-coordinate **1** to the six-coordinate **6**, implying that there is no significant structural *trans* effect of NO in this six-coordinate iron nitrosyl thiolate porphyrin when prepared from the five-coordinate crystals. However, in the case of compound **10**, the slightly shortening (~0.04 Å) of the *trans* Fe-O bond length reveals a possible small *trans* effect of nitrosyl group.

Third, the FeNO and FeSC(thiolate) planes in **6** are essentially mutually perpendicular, and these two planes straddle the Fe–N1 bond; the C37–S1–Fe1–N1 torsion angle is –55.6(4)°, and that of O1–N5–Fe1–N1 is 43(2)°. In addition, there is a slight opening of the Fe1-S1-C37 angle (from 104° to 111°) upon NO binding and subsequent movement of the S-atom toward the mean porphyrin in **6**. A similar opening of Fe-O-C was observed in the compound **10** (128° to 132°).

Attempts to get structural information of other six-coordinate nitrosyl thiolate iron porphyrin derivatives have been tried using this method. The crystals of (TPP)Fe[S-2,6-$(CF_3CONH)_2C_6H_3$] **(3)** and (TPC)Fe[S-2,6-$(CF_3CONH)_2C_6H_3$] **(4)** were

obtained and used to react with NO gas. The corresponding six-coordinate nitrosyl complexes were formed based on the IR spectroscopy (Table 5.2). Unfortunately, the quality of the crystals after these reactions was not good enough for X-ray diffraction. It is surprising that the reaction of crystalline solid of (OEP)Fe[S-2-($CF_3CONH)C_6H_4$] **(2)** with NO gas only yielded a five-coordinate nitrosyl iron porphyrin. However, when the powder-form was used, the characteristic NO band (1859 cm^{-1}) of the six-coordinate complex was observed. We believe that the different reactivities of the compound **1** and **2** with NO gas is due to the packing arrangements of the molecules in crystalline solid. As shown in Figure 5.14a, one molecule of **1** with Fe1 as the metal center is stacked with another molecule. From the side view we can observe that there is a large distance between the two macrocycles, the distance between these two planes is around 4.7 Å. In addition, based on the top view in Figure 5.14b, the molecules are staggered and leave the area above the Fe1 wide open which allows small molecules such as nitric oxide to come in and coordinate to the iron center. On the contrary, the packing arrangement of the compound **2** is more compact than that of the compound **1**. As shown in Figure 5.15a, the distance between the two planes is much shorter (around 3.4 Å) and the top view (Figure 5.15b) shows that the two molecules are significantly eclipsed, leaving insufficient space for nitric oxide to coordinate to the iron centers. Thus, NO attacks the more accessible S atoms of thiolate ligands, replacing the thiolate ligands to afford 5-coordinate nitrosyl iron porphyrin.

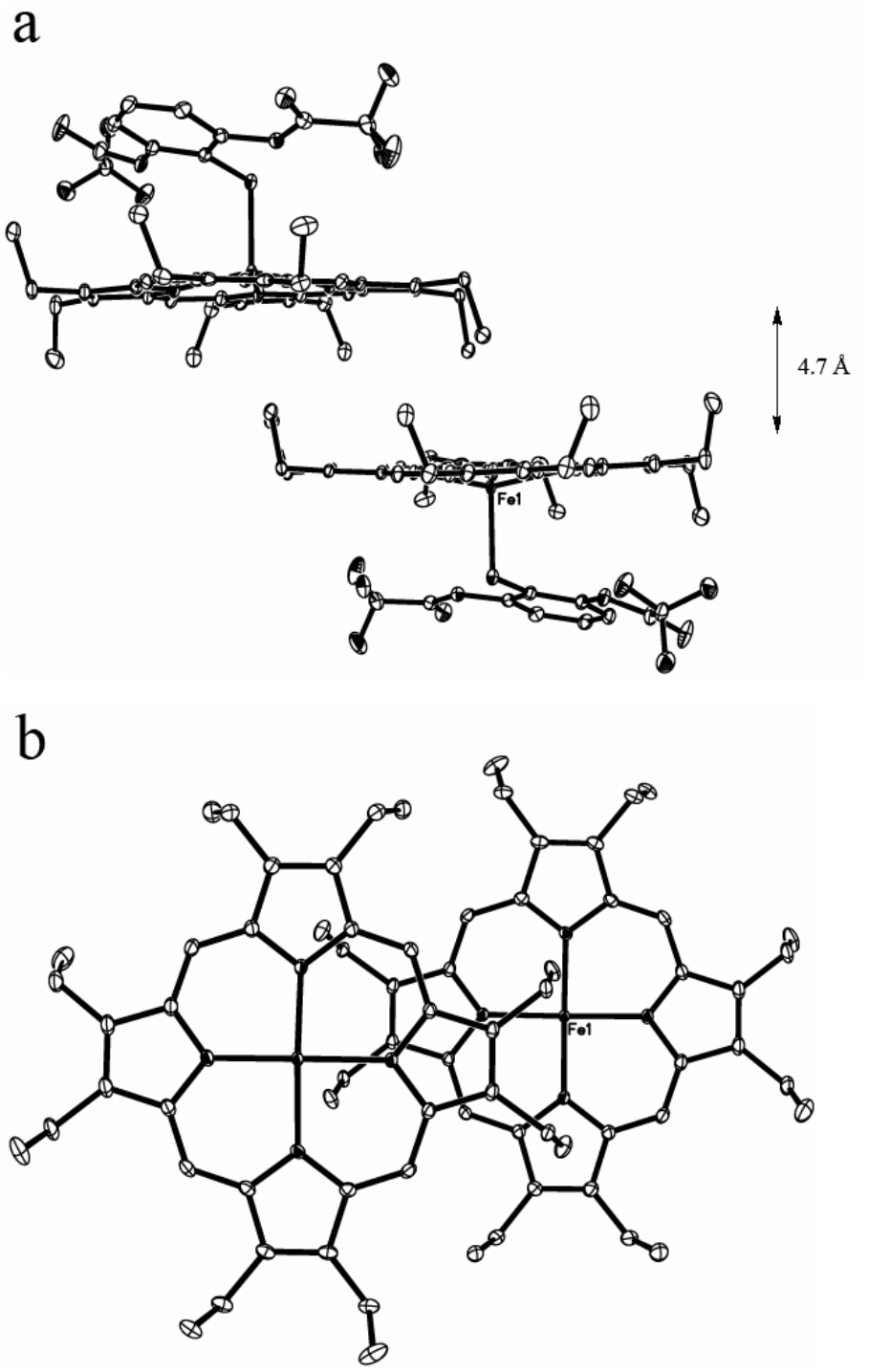

Figure 5.14. (a) Side view and (b) top view of two neighboring porphyrin molecules of **1** in a unit cell. The thiolate ligands in the two molecules have been omitted for clarity in the bottom figure.

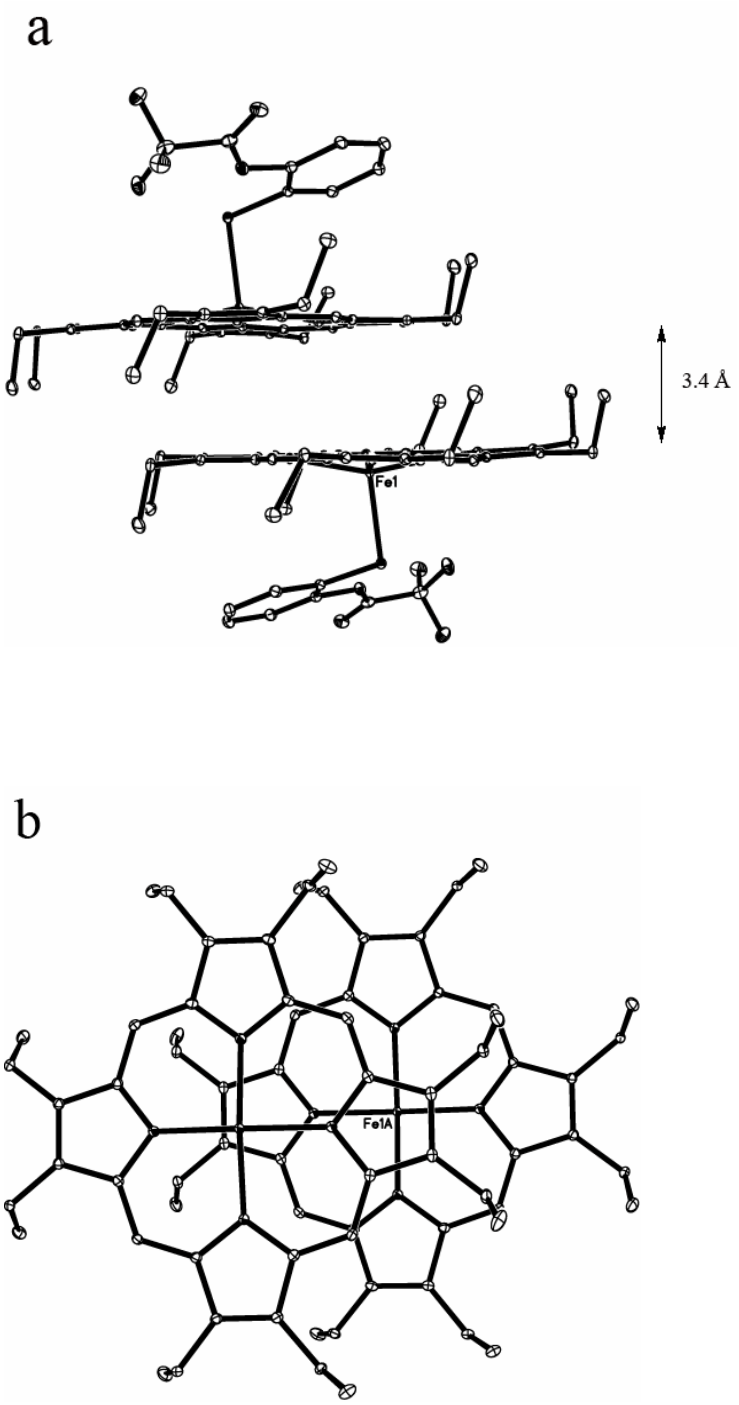

Figure 5.15. (a) Side view and (b) top view of two neighboring porphyrin molecules of **2** in a unit cell. The thiolate ligands in the two molecules have been omitted for clarity in the bottom figure.

On the other hand, the molecules in powder form do not have well-organized packing arrangements and nitric oxide molecules react with either iron centers or thiolate ligands of compound **2** to produce a mixture of desired six-coordinate complex and as a side product, the five-coordinate nitrosyl compound. We are still working on growing suitable crystals of **3** and **4** for the solid-gas phase reaction. Based on the IR data, we predict that less bent angles of FeNO moieties should be found in nitrosyl derivatives of **7** and **8**.

When placed in a broader context, the crystal structure of **5** reveals an intrinsic tilting (of the nitrosyl N-atom from the porphyrin normal) and bending of the NO group in this formally $\{FeNO\}^6$ species. We have previously reported that such tilting and bending features represent a low energy conformation in the related $\{FeNO\}^6$ compound $(OEP)Fe(NO)(C_6H_4F)$.[43] Our results suggest that such a tilting and bending of the NO group may be a common feature in the NO adducts of ferric heme thiolate proteins. The crystal structure of **10** exhibits a linear Fe-N-O conformation which is consistent with those of most $\{FeNO\}^6$ species. It also reveals that the more electron rich chlorin ring does not have a significant effect on the conformation of the FeNO group.

The unique solid-gas method employed in this work allows the NO gas to diffuse into the crystals and coordinate to the iron center of thiolate porphyrin to afford the six-coordinate nitrosyl complexes which are extremely difficult to be obtained in solution.

This new method could be used in preparations and structure determinations of many other previously inaccessible complexes.

Conclusion

We have prepared a series of iron porphyrin/chlorin complexes containing axial S-bound and O-bound ligands *trans* to nitric oxide using a unique heterogenous solid-gas method which allows the NO gas to diffuse into the crystals and coordinate to the iron center in a solvent-free environment. This method overcomes synthetic difficulties of $\{FeNO\}^6$ complexes such as the lability of the Fe-NO linkage, the easy reduction of $\{FeNO\}^6$ complexes and possible fast decomposition in organic solvents. This new method could be used in preparations and structure determinations of many other previously inaccessible complexes.

Solid-state structures were obtained for the six-coordinate (OEP)Fe(NO)[S-2,6-$(CF_3CONH)_2C_6H_3$] and (TPC)Fe(NO)($OCOCF_3$) compounds. Interestingly, the (OEP)Fe(NO)[S-2,6-$(CF_3CONH)_2C_6H_3$] compound displays an unusual bent metal-nitrosyl linkage (159.6(8)°), while the (TPC)Fe(NO)($OCOCF_3$) compound exhibits the typical linear metal-nitrosyl linkage of $\{FeNO\}^6$ complexes. No significant *trans* effect of NO was observed in (OEP)Fe(NO)[S-2,6-$(CF_3CONH)_2C_6H_3$] based on the Fe-S bond length change from the five-coordinate precursor to the six-coordinate nitrosyl compounds. In the case of (TPC)Fe(NO)($OCOCF_3$), a small trans effect of NO was observed. Additionally, both of the Fe atoms in these two-phase reactions were pulled

upwards to nitrosyl groups with remarkable movements of ~0.46 Å and ~0.55 Å in solid state respectively.

The structure of (OEP)Fe(NO)[S-2,6-$(CF_3CONH)_2C_6H_3$] is the first reported structure of model complexes of nitrosyl cysteinate heme proteins. The bent FeNO geometry in (OEP)Fe(NO)[S-2,6-$(CF_3CONH)_2C_6H_3$] suggests that the bending of the NO group may be a common feature in the NO adducts of ferric heme thiolate proteins. The (TPC)Fe(NO)($OCOCF_3$) compound is also the first structural characterized neutral model complex of nitrosyl tyrosinate heme proteins. The structure displays a typical linear Fe-NO linkage of $\{FeNO\}^6$ complexes.

References

(1) Mansuy, D.; Battioni, P. *Diversity of Reactions Catalyzed by Heme-Thiolate Proteins*, In *The Porphyrin Handbook*; Kadish, K. M., Smith, K. M., Guilard, R., Eds.; Academic Press: San Diego, 2000; Vol. 4, p 1-15.

(2) Andersson, L. A.; Dawson, J. H. *Structure and Bonding* **1991**, *64*, 1-40.

(3) Shimizu, H.; Obayashi, E.; Gomi, Y.; Arakawa, H.; Park, S.-Y.; Nakamura, H.; Adachi, S.-i.; Shoun, H.; Shiro, Y. *J. Biol. Chem.* **2000**, *275*, 4816-4826.

(4) Poulos, T. L.; Johnson, E. F. *Cytochrome P450: Structure, Mechanism, and Biochemistry*; 3rd ed.; Plenum: New York, 2005.

(5) Minamiyama, Y.; Takemura, S.; Imaoka, S.; Funae, Y.; Tanimoto, Y.; Inoue, M. *J. Pharmacol. Exp. Ther.* **1997**, *283*, 1479-1485.

(6) Abu-Soud, H. M.; Ichimori, K.; Nakazawa, H.; Stuehr, D. J. *Biochemistry* **2001**, *40*, 6876-6881.

(7) Weichsel, A.; Maes, E. M.; Andersen, J. F.; Valenzuela, J. G.; Shokhireva, T. K.; Walker, F. A.; Montfort, W. R. *Proc. Natl. Acad. Sci., USA* **2005**, *102*, 594-599.

(8) Franke, A.; Stochel, G.; Suzuki, N.; Higuchi, T.; Okuzono, K.; Van Eldik, R. *J. Am. Chem. Soc.* **2005**, *127*, 5360-5375.

(9) Suzuki, N.; Higuchi, T.; Urano, Y.; Kikuchi, K.; Uchida, T.; Mukai, M.; Kitagawa, T.; Nagano, T. *J. Am. Chem. Soc.* **2000**, *122*, 12059-12060.
(10) Fomitchev, D. V.; Coppens, P.; Li, T.; Bagley, K. A.; Chen, L.; Richter-Addo, G. B. *Chem. Commun.* **1999**, 2013-2014.
(11) Yi, G.-B.; Khan, M. A.; Richter-Addo, G. B. *Chem. Commun.* **1996**, 2045-2046.
(12) Yi, G.-B.; Khan, M. A.; Powell, D. R.; Richter-Addo, G. B. *Inorg. Chem.* **1998**, *37*, 208-214.
(13) Yi, G.-B.; Chen, L.; Khan, M. A.; Richter-Addo, G. B. *Inorg. Chem.* **1997**, *36*, 3876-3885.
(14) Lee, J.; Yi, G.-B.; Powell, D. R.; Khan, M. A.; Richter-Addo, D. G. B. *Can. J. Chem.* **2001**, *79*, 830-840.
(15) Lee, J.; Yi, G.-B.; Khan, M. A.; Richter-Addo, G. B. *Inorg. Chem.* **1999**, *38*, 4578-4584.
(16) Carter, S. M. Ph.D. Thesis, *Syntheses, molecular structures, and fiber-optic infrared spectroelectrochemistry of nitrosyl metalloporphyrins containing axially bound alkoxide thiolate, imidazole, and imidazolate,* **2006**, *University of Oklahoma*.
(17) Pant, K.; Crane, B. R. *Biochemistry* **2006**, *45*, 2537-2544.
(18) Enemark, J. H.; Feltham, R. D. *Coord. Chem. Soc.* **1974**, *13*, 339-406.
(19) Hu, S.; Kincaid, J. R. *J. Am. Chem. Soc.* **1991**, *113*, 2843-2853.
(20) Scherlis, D. A.; Cymeryng, C. B.; Estrin, D. A. *Inorg. Chem.* **2000**, *39*, 2352-2359.
(21) Brown, G. C. *Eur. J. Biochem.* **1995**, *232*, 188-191.
(22) Hoshino, M.; Ozawa, K.; Seki, H.; Ford, P. C. *J. Am. Chem. Soc.* **1993**, *115*, 9568-9575.
(23) Murshudov, G. N.; Grebenko, A. I.; Barynin, V.; Dauter, Z.; Wilson, K. S.; Vainshtein, B. K.; Melik-Adamyan, W.; Bravo, J.; Ferrán, J. M.; Ferrer, J. C.; Switala, J.; Loewen, P. C.; Fita, I. *J. Biol. Chem.* **1996**, *271*, 8863-8868.
(24) Chiu, J. T.; Loewen, P. C.; Switala, J.; Gennis, R. B.; Timkovich, R. *J. Am. Chem. Soc.* **1989**, *111*, 7046-7050.
(25) Jacob, G. S.; Orme-Johnson, W. H. *Biochemistry* **1979**, *18*, 2975-2980.
(26) Craven, P. A.; DeRubertis, F. R.; Pratt, D. W. *J. Biol. Chem.* **1979**, *254*, 8213-8222.
(27) Kalyanaraman, B.; Janzen, E. G.; Mason, R. P. *J. Biol. Chem.* **1985**, *260*, 4003-4006.
(28) Deisseroth, A.; Dounce, A. L. *Physiol. Rev.* **1970**, *50*, 319-375.
(29) Huang, J.; Kim-Shapiro, D. B.; King, S. B. *J. Med. Chem.* **2004**, *47*, 3495-3501.
(30) Adler, A. D.; Longo, F. R.; Kampas, F.; Kim, J. *J. Inorg. Nucl. Chem* **1970**, *32*, 2443-2448.
(31) Mar, G. N. L.; Eaton, G. R.; Holm, R. H.; Walker, F. A. *J. Am. Chem. Soc.* **1973**, *95*, 63-75.
(32) Cheng, B.; Hobbs, J. D.; Debrunner, P. G.; Erlebacher, J.; Shelnutt, J. A.; Scheidt, W. R. *Inorg. Chem.* **1995**, *34*, 102-110.

(33) Helms, J. H.; Haar, L. W. T.; Hatfield, W. E.; Harris, D. L.; Jayaraj, K.; Toney, G. E.; Gold, A.; Mewborn, T. D.; Pemberton, J. E. *Inorg. Chem.* **1986**, *25*, 2334-2337.
(34) Tang, S. C.; Koch, S.; Papaefthymiou, G. C.; Foner, S.; Frankel, R. B.; Ibers, J. A.; Holm, R. H. *J. Am. Chem. Soc.* **1976**, *98*, 2414-2434.
(35) Ueyama, N.; Okamura, T.; Yamada, Y. *J. Org. Chem* **1995**, *60*, 4893-4899.
(36) Ueyama, N.; Nishikawa, N.; Yamada, Y.; Okamura, T.; Oka, S. S., H.; Nakamura, A. *Inorg. Chem.* **1998**, *37*, 2415-2421.
(37) Ueyama, N.; Nishikawa, N.; Yamada, Y.; Okamura, T.; Nakamura, A. *J. Am. Chem. Soc.* **1996**, *118*, 12826-12827.
(38) Ueyama, N.; Nishikawa, N.; Yamada, Y.; Okamura, T.; Nakamura, A. *Inorg. Chim. Acta* **1998**, *283*, 91-97.
(39) Richter-Addo, G. B.; Legzdins, P. *Metal Nitrosyls*; Oxford University Press: New York, 1992.
(40) Neal, T. J.; Cheng, B.; Ma, J.-G.; Shelnutt, J. A.; Schulz, C. E.; Scheidt, W. R. *Inorg. Chim. Acta* **1999**, *291*, 49-59.
(41) Ellison, M. K.; Scheidt, W. R. *J. Am. Chem. Soc.* **1999**, *121*, 5210-5219.
(42) Paulat, F.; Lehnert, N. *Inorg. Chem.* **2007**, *46*, 1547-1549.
(43) Richter-Addo, G. B.; Wheeler, R. A.; Hixson, C. A.; Chen, L.; Khan, M. A.; Ellison, M. K.; Schulz, C. E.; Scheidt, W. R. *J. Am. Chem. Soc.* **2001**, *123*, 6314-6326.